IOP Publishing Phys. Med. Biol. 65 (2020) 05TR02 (43pp) https://doi.org/10.1088/1361-6560/ab4f29

Physics in Medicine & Biology

IPEM Institute of Physics and Engineering in Medicine

RECEIVED
5 June 2019

REVISED
6 September 2019

ACCEPTED FOR PUBLICATION
18 October 2019

PUBLISHED
2 March 2020

TOPICAL REVIEW

Absorbed dose calorimetry

J Renaud[1,2,6], H Palmans[3,4], A Sarfehnia[2,5] and J Seuntjens[2]

[1] Metrology Research Centre, National Research Council Canada, Ottawa, Canada
[2] Medical Physics Unit, McGill University, Montréal, Canada
[3] EBG MedAustron GmbH, Medical Physics, Wiener Neustadt, Austria
[4] National Physical Laboratory, Acoustics and Ionising Radiation Division, Teddington, United Kingdom
[5] Department of Radiation Oncology, University of Toronto, Toronto, Canada
[6] Author to whom any correspondence should be addressed.

E-mail: james.renaud@nrc-cnrc.gc.ca

Keywords: dosimetry, calorimetry, primary dose standards, absolute dosimetry, reference dosimetry, beam quality conversion factors, Monte Carlo

Abstract

This article reviews the development and summarizes the state-of-the-art in absorbed dose calorimetry for all the common clinical beam modalities covered in reference dosimetry codes of practice, as well as for small and nonstandard fields, and brachytherapy. It focuses primarily on work performed in the last ten years by national laboratories and research institutions and is not restricted to primary standard instruments. The most recent absorbed dose calorimetry review article was published over twenty years ago by Ross and Klassen (1996 *Phys. Med. Biol.* **41** 1–29), and even then, its scope was limited to water calorimeters. Since the application of calorimetry to the measurement of radiation has a long and often overlooked history, a brief introduction into its origins is provided, along with a summary of some of the landmark research that have shaped the current landscape of absorbed dose calorimeters. Technical descriptions of water and graphite calorimetry are kept general, as these have been detailed extensively in relatively recent review articles (e.g. McEwen and DuSautoy (2009 *Metrologia* **46** S59–79) and Seuntjens and Duane (2009 *Metrologia* **46** S39–58). The review categorizes calorimeters by the radiation type for which they are applied; from the widely established standards for Co-60 and high-energy x-rays, to the prototype calorimeters used in high-energy electrons and hadron therapy. In each case, focus is placed on the issues and constraints affecting dose measurement in that beam type, and the innovations developed to meet these requirements. For photons, electrons, proton and carbon ion beams, a summary of the ionization chamber beam quality conversion factors (k_Q) determined using said calorimeters is also provided. The article closes with a look forward to some of the most promising new techniques and areas of research and speculates about the future clinical role of absorbed dose calorimetry.

1. Introduction

Calorimetry was originally the science of measuring changes in the state functions of a sample due to chemical reactions, physical changes, or phased transitions, to derive the heat transfer associated with changes of state (Laidler 1995). There are numerous approaches to quantifying heat, and since calorimetry's advent in the late 18th century, many measurement techniques have been developed. The first calorimeters, such as the ice calorimeter developed by Antoine de Lavoisier and Pierre-Simon Laplace in 1780, relied on the phase transition of melting ice to measure the specific heat capacities of solids and liquids, as well as the heats of combustion and the production of heat by small animals present in a thermally-insulated chamber (de Lavoisier and Laplace 1920). Initial calorimetric techniques were based on thermometric methods, but more recently, advances in electronics and control have added a new dimension to calorimetry, enabling users to collect data and maintain samples under conditions that were previously not possible. Calorimetric study has grown to include applications involving any physical process (i.e. not strictly due to changes of state) that results in heat being generated and exchanged with the environment, among which measuring absorbed dose. As early as 1903, Marie Curie, Pierre

Curie, Albert Laborde, and Sir James Dewar had observed radium's remarkable property of liberating heat spontaneously and continuously (Curie and Laborde 1903, Curie 1904, Dewar and Curie 1904, Dewar 1905). Hence, it is not surprising that within 15 years of the discoveries of x-rays and radioactivity, calorimetry saw its first application to the dosimetry of ionizing radiation.

British physicist and resistance thermometry pioneer, Hugh Longbourne Callendar, was among the earliest investigators to apply calorimetry to radiation dosimetry. In 1910, he proposed and demonstrated the use of the Peltier effect in the operation of a radio-calorimetric balance employed to compare samples of radon sealed in glass containers, which had been given to him by Ernest Rutherford. The radio-balance comprised of two twin discs in which a quantity of heat generated in one disc could be measured by balancing it either against the cooling of a Peltier element or against incident radiant heat in the opposite disc (Callendar 1910). Despite it failing to generate any significant interest at the time, Callendar's design was revived and adapted nearly a half-century later by Wilfrid B. Mann of the then National Bureau of Standards (NBS), now the National Institute of Standards and Technology (NIST), for radioactivity measurements of radium (Mann 1954). Other notable examples of early radiation calorimeters were developed in late 1920s Europe by Walther Otto Rump, Charles Drummond Ellis, William Wooster, and Ernst Stahel. In 1927, Rump, a German physicist, used mercury contained in a thin-walled glass vessel to absorb x-rays produced by generators with peak voltages ranging from 43 kV to 150 kV. Attached to this vessel was a long capillary tube, which served to display changes in the temperature of the mercury absorber (Rump 1927). That same year in England, Ellis and Wooster used a total absorption lead calorimeter (also known as a bolometer) to measure the heating due to the disintegration of a radium source contained within, and thus the average energy of beta emission (Ellis and Wooster 1927). Two years later, Stahel, a Swiss-born physicist, employed a similar calorimetry method to measure the energy absorbed by water exposed to x-rays and γ-rays. The measured doses were then related to the occurrence of skin erythema in humans, in what was likely the first calorimetric-radiobiology experiment (Stahel 1929).

In the twenty years that followed, relatively little advancement was achieved in the field of radiation calorimetry, largely due to inadequate thermometric sensitivity. This would change in the years following World War II, when Joseph Becker, a research physicist with the Bell Telephone Laboratories in New York City, developed and patented the bolometric thermistor, a metal-oxide semiconductor with a highly temperature-dependent resistance (Becker *et al* 1946). Bell had long been seeking a device that would regulate repeaters on transcontinental cables more sensitively to eliminate the clicking noises often heard during long distance telephone calls. In comparison to platinum resistance thermometers, which have a room temperature coefficient of about 0.4%, thermistors commonly have a negative temperature coefficient as large as 4% per degree. The first reported use of thermistors in a radiation calorimeter came from the NBS, where in 1955, Sebastian Genna and John S. Laughlin developed a total absorption lead calorimeter to measure the energy fluence of a teletherapy Co-60 source (Genna and Laughlin 1955). This work was a significant achievement as cobalt radiotherapy had been first introduced to the world only 3 years prior. That very same month (September 1955), an absorbed dose calorimeter also employing thermistors was reportedly used in Co-60 γ-radiation by Canadian physicist, Johns, to experimentally determine the value of W_{air}, the mean energy expended in air per ion pair formed (Johns *et al* 1955, Bernier *et al* 1956). This was not, however, the first application of calorimetry to the measurement of absorbed dose. Earlier efforts using an adiabatic calorimeter in 1953 by Hochanadel and Ghormley of the Oak Ridge National Laboratory were made in the first determinations of $G_{Fe^{3+}}$, the radiation chemical yield of ferric ions in the Fricke chemical dosimeter (Hochanadel and Ghormley 1953). Notably, their work also represents one of the very first absorbed dose water calorimeters. This was the same year that the International Commission on Radiation Units and Measurements, ICRU, established absorbed dose as a new quantity (ICRU 1954).

By the mid-1960s, significant efforts to refine the design and modernize the operation of the solid body absorbed dose calorimeters had been made by university researchers and national metrology institutes (NMIs) alike (Skarsgard *et al* 1957, Petree 1958, Milvy *et al* 1958, 1960, Reid and Johns 1961, Myers *et al* 1961, Cole *et al* 1962, Bewley 1963, Genna *et al* 1963, Geisselsoder *et al* 1963, Bradshaw 1965). Long viewed as a cumbersome instrument confined to a handful of dosimetry laboratories, graphite calorimeters would be widely established as portable field instruments used in international comparisons of high-energy photon absorbed dose standards by the early 1990s (Henry 1977, Pruit *et al* 1981, Boutillon 1989, Owen and DuSautoy 1991, Shortt *et al* 1993, Boutillon *et al* 1994, DuSautoy 1995). While lead was often preferred for total absorption calorimetry (Laughlin and Genna 1956, McElhinney *et al* 1957, Goodwin 1959), graphite had emerged as an absorber of choice for the measurement of absorbed dose over water. Graphite is a preferable choice of material given its low atomic number and radiological similarities to water, substantially lower specific heat capacity, high purity, relatively low cost, and good machinability. Moreover, the high thermal conductivity of graphite lends itself well to calorimetry applications involving heat compensation; the temperature of a graphite body can be effectively modulated through localized and embedded ohmic heating (e.g. thermistors or wires that act as quasi-point and line-sources, respectively). The development of a small (~2 cm) spherical graphite calorimeter was described by Ben Petree and George Ward of the NBS (Petree and Ward 1962, Petree and Lamperti 1967). Most notably, their design consisted

of two nested graphite bodies, a sensitive volume (i.e. the core) and a surrounding shield, each containing electrical heaters. In the core, the heater served to inject accurate amounts of electrical energy for calibrating the calorimeter's response, and in the shield, the heater permitted a degree of temperature modulation necessary to mitigate heat transfer in the core. These design principles were further developed at NBS over the course of a decade, culminating in a landmark paper in 1974 by Steve Domen and Paul Lamperti.

Often referred to as the father of absorbed dose calorimetry for his highly influential contributions to both graphite and water calorimetry, Steve Domen described in detail the theory and operation of a graphite calorimeter designed around the concept of quickly bringing its four nested graphite bodies to a state of thermal equilibrium and maintaining it long enough for an accurate measurement to be made (Domen and Lamperti 1974). This type of absorbed dose calorimeter, which would eventually bear the moniker of the once Pennsylvania steel mill worker, 'Domen-type', emerged as the metrology world's most widely duplicated, and thus most vetted design. Prior to their adoption of the Domen-type design in the early 1980s, the UK's National Physical Laboratory (NPL) had spent a decade developing a unique graphite calorimeter system in which the constituent pyrolytic graphite was used as its own electrical resistor (Kemp *et al* 1971). This NPL calorimeter operated in a so-called 'dynamic-equilibrium' mode; a precursor to what would eventually be referred to as isothermal mode. Another novel calorimeter design to emerge from this period is the Shonka A-150 tissue-equivalent portable calorimeter developed at Memorial Sloan Kettering by MacDonald *et al* (1976) While the uncertainties in this work were relatively large (~5%), the A-150 calorimeter found a niche in neutron dosimetry for radioprotection purposes and was heavily used for the next ten years. In 1984, an Austrian-based group led by Witzani demonstrated an alternative mode of operating a Domen-type calorimeter. In contrast to the then well-known quasi-adiabatic operation, which entails the measurement of core temperature rises during irradiation, the quasi-isothermal mode is characterized by an electrical power compensation principle in which the temperatures of the graphite bodies remain constant throughout the measurement. In this mode, the electrical power necessary to maintain an isothermal state is used to determine via substitution the rate of energy imparted by the ionizing radiation (Witzani *et al* 1984). These and other related developments have been extensively covered by major review articles by Laughlin and Genna (1956), by Stuart Gunn (1976), and by Domen (1987).

In the 1980s, primary absorbed dose to water standards were not widely available, so dosimeters were typically calibrated using an indirect method. Most commonly, ionization chambers were calibrated in terms of air kerma in Co-60, and then converted to an absorbed dose to water calibration using an established protocol (e.g. the American Association of Physicists in Medicine Task Group (AAPM TG) 21 (Schulz *et al* 1983) and the International Atomic Energy Agency Technical Report (IAEA TRS) 277 (Andreo *et al* 1987). The uncertainty in this approach was estimated to be as large as 4%, a significant contribution to the overall uncertainty in the radiotherapy treatment process. Several NMIs were operating dose standards based on the Domen-type calorimeter, however the dose conversion process from graphite was, and still is, a limiting factor on the overall uncertainty on the determination of dose to water, the clinical parameter of interest (Reich 1979). For this reason, as of the late 70s, focus began to be placed on developing absorbed dose water calorimetry. A comprehensive review of water calorimetry and its use in determining absorbed dose to water by Ross and Klassen of the National Research Council of Canada (NRC) was published in the mid-90s (Ross and Klassen 1996).

Up until 1980, performing water calorimetry in a large continuous volume of water was considered infeasible. Domen was the first to demonstrate that the thermal diffusivity of water is so low that radiation-induced thermal distributions remain in place to permit accurate point measurements. In his view, the major obstacles were the insulation of the thermistor and its electrical leads from water. In 1979, he performed a set of experiments that proved that the necessary isolation could be accomplished by enclosing the thermistor in a polyethylene membrane (Kase 1996). He constructed and operated a large water calorimeter capable of absorbed dose measurement, however his initial results were systematically high (Domen 1980, 1982, 1988, Mattsson 1984, Kubo 1983) compared to doses obtained using graphite calorimeters and ionization chambers. Radiation-induced exothermic chemical reactions in the water, the dissolved impurities, and perhaps also convection in the water were at least partly to cause. To more easily compare heat defect modeled using knowledge of the radiolysis of water with calorimetry, Ross *et al* constructed a small, sealed water calorimeter at the NRC in 1984 (Ross *et al* 1984, 1988). The volume of water was small, and the calorimeter sealed from the atmosphere, thus it was relatively easy to saturate the water with various gas mixtures. Their group was the first to show that impurities present in water can serve as scavengers for reactive species, such as hydroxyl radicals, created in the radiolysis of water leading to a potentially non-zero and stable heat defect which could be accounted for. Conversely, if all impurities are consumed with accumulated radiation dose, a potential zero heat defect is achievable. Another early effort to develop water calorimetry was made in 1987 at Yale (Schulz *et al* 1987, 1988). In their design, water purity was carefully controlled using a commercial ion exchange system, and for the first time, the entire calorimeter was operated at 4 °C to successfully eliminate the effects of convection. By the early 1990s, Domen updated the design of his original water calorimeter by introducing a sealed glass vessel inside the larger volume of water, in which the water quality could be carefully controlled (Domen 1994). The vessel was designed to contain the thermistors as well

as act as a convective barrier. Based in part on this revised design, Seuntjens *et al* developed their own water calorimeter in Ghent to measure the dose due to medium-energy x-rays using different aqueous systems (Seuntjens 1991, 1993, 1994). The main difference in their design was the use of a Perspex vessel, an AC Wheatstone bridge circuit to sense the changes in thermistor resistance, as well as air-circulated thermal control. At the time of the review by Ross and Klassen, primary absorbed dose standards based on water calorimetry had yet to be fully developed. By the end of the millennium, the NRC-constructed water calorimeter, which shared aspects of the later Domen and Seuntjens designs, began serving as the basis of the Canadian standard for absorbed dose to water for Co-60 γ-rays and high-energy x-rays (Ross *et al* 1999). In parallel, a rebuilt Ghent calorimeter including glass vessel was described and used to determine absorbed dose to water and beam quality correction factors in high-energy photon beams (Seuntjens and Palmans 1999, Palmans *et al* 1999) Since then, similar absorbed dose to water standards based on water calorimetry have been established in Germany (Physikalisch-Technische Bundesanstalt; PTB (Krauss 2006a)), the Netherlands (Van Swinden Laboratory; VSL (Pieksma *et al* 2002)), Switzerland (Federal Institute of Metrology; METAS (Medin *et al* 2004)) (Seuntjens and DuSautoy 2003) and China (National Institute of Metrology; NIM (Wang *et al* 2014). In comparison, at least seven other countries, including Australia (Australian Radiation Protection and Nuclear Safety Agency; ARPANSA (Huntley *et al* 1999)), Austria (Bundesamt für Eich- und Vermessungswesen; BEV (Baumgartner *et al* 2010)), France (Laboratoire National Henri Becquerel; LNE-LNHB (Picard *et al* 2009)), Hungary (National Office of Measures; MKEH (Csete *et al* 2010)), Japan (National Metrology Institute of Japan; NMIJ AIST (Morishita *et al* 2012)), Russian Federation (Institute of Physical Technical and Radiotechnical Measurements, Rosstandart; VNIIFTRI (Berlyand and Bregadze 1985), and the United Kingdom (NPL (DuSautoy 1996)), currently operate graphite calorimeter-based absorbed dose standards. In addition to Co-60 and high-energy x-rays, calorimetry-based absorbed dose standards (dose to air, graphite, tissue, etc) have been developed for use in high-energy electrons, low- and medium-energy x-rays, Cs-137, Sr-90/Y-90, and Ru-106 (BIPM 2018).

In the mid-1980s, it had been recognized that the combined standard uncertainty on the dose delivered to the treatment volume in radiotherapy should not exceed 5% (Brahme 1984). To achieve this therapeutic goal, absorbed dose to water as determined under reference conditions could not exceed (0.5–1)%, a figure that was not likely achievable with air kerma-based approaches (Ross and Klassen 1996). Hence, the shift in emphasis in NMIs from exposure and air kerma standards to those for absorbed dose to water was principally motivated by the desire to improve the uncertainty of clinical reference dosimetry. Furthermore, all the air kerma-based standards in the world used the same basic approach (i.e. a graphite-walled cavity ionization chamber), thus intercomparisons could not resolve systematic uncertainties (Rogers 1996). The relative diversity of absorbed dose standards (e.g. graphite calorimetry, water calorimetry, Fricke, ionometry) on the other hand, each having different systematic uncertainties, has resulted in a network of standards that is robust against large systematic errors affecting all standards. The mechanism by which primary dose measurements are transferred to the clinical community is by the calibration of secondary dose standards against the appropriate primary dose standard and the subsequent use of this secondary dose standard to calibrate tertiary and ultimately user instruments (e.g. air-filled ionization chambers). This process renders user instruments traceable to a primary dose standard, which is usually a national standard that must itself be verified internationally. Meaningful comparisons of the outcome of radiotherapy treatments require a degree of uniformity in the entire radiotherapy process, from treatment prescription to delivery, so that common criteria are applied throughout. A key step in the radiotherapy process is the requirement for harmonized reference dosimetry procedures. Following the development of national dosimetry protocols pioneered by Germany (Deutsches Institut für Normung e.V., DIN 6800, Hohlfeld 1988), Russia (Izdatelstvo standartov RD-50-691-89, Berland *et al* 1990), and the United Kingdom (Institute of Physical Sciences in Medicine, IPSM 1990, Burns *et al* 1988), two major international protocol committees, the AAPM TG-51 and the IAEA TRS 398, drew up guidelines to permit the dissemination of the absorbed dose to water standards and to further harmonize radiotherapy deliveries among institutions. Thus, since 1999, clinical reference dosimetry of high-energy photons and other radiation types has largely been performed using ionization chamber calibrated in terms of absorbed dose to water produced by a reference radiation quality, Q_0, conventionally Co-60, at a reference point under specific setup conditions. Both protocols make use of chamber dependent absorbed dose beam quality correction factors, k_Q, defined as the scaling factor used in conjunction with the absorbed dose calibration coefficient at a reference beam quality to arrive at the absorbed dose calibration coefficient in the beam quality of interest, Q. One major application of absorbed dose calorimetry since the conception of these protocols has been the direct measurement of k_Q factors for different models of ionization chambers. To date, most of these measurements have been performed in high-energy x-rays (Vatnitsky *et al* 1995, Palmans *et al* 1999, Seuntjens *et al* 2000a, McEwen 2010), though a handful of experimental studies have been done in electrons (McEwen and Ross 2007, Renaud *et al* 2015), and proton beams (Medin *et al* 2006, 2010, Gagnebin *et al* 2010, Sarfehnia *et al* 2010, Rossomme *et al* 2014b). Most of the present-day numerical values for k_Q come from Monte Carlo (MC) studies where the overall standard uncertainty is estimated to be 0.4% or less. In their 2004 topical review paper of chamber-based clinical reference photon and electron beam dosimetry, Saiful Huq and

Pedro Andreo noted that for the few chambers where experimentally derived data are available, measured and calculated k_Q factors generally agree within the uncertainties estimated for each method (Huq and Andreo 2004).

Over the last two decades, clinical advances in non-conformal radiation delivery and the emergence of specialized radiotherapy modalities (e.g. linear accelerator-magnetic resonance imaging (MR-linac) hybrids, Gamma Knife®, Cyberknife®, TomoTherapy®) incapable of producing standard reference conditions have prompted the development of methodologies to adapt reference dosimetry traceability to non-standard conditions (Alfonso *et al* 2008, ICRU 2014). In this approach, a suitable ionization chamber with a calibration traceable to a primary absorbed dose standard is used under non-standard conditions. Correction factors must then be applied to the chamber readings to account for all the effects (e.g. volume averaging, fluence perturbation) which cause the detector response to vary between reference and non-reference conditions. Most recently, this correction-based technique has been extended to include the effects due to the presence of a magnetic field (O'Brien *et al* 2016). As a more direct alternative method to realize absorbed dose in non-standard fields, calorimeters based on transportable designs have been developed to permit operation at the user's facility (Hofmeester 1980, McEwen and Duane 2000, Palmans *et al* 2004, Duane *et al* 2012, de Prez *et al* 2016, Renaud *et al* 2016, 2018). Thus, calorimetry-based dose measurements can form the basis of a direct dose calibration of an ionization chamber in the clinically-relevant field, or a derivation of their correction factors for those beams. ICRU (2007) and (2014), which provide prescribing, recording and reporting guidelines for proton therapy and small photon beams, respectively, recommend the direct use of absorbed dose calorimetry in the user's beam where possible. Direct use of absorbed dose calorimetry has been extended in the past to include therapy-range photon (section 3) and electron (section 4) beams, medium-energy x-rays (section 5), protons (section 6), heavy-ions (section 7), and high dose rate (HDR) brachytherapy sources (section 9).

2. Methods

2.1. Theory

Human tissue is mostly composed of water, as such, absorbed dose to water has become the quantity of interest in radiotherapy. Consequently, dose conversion coefficients are normally used in radiation dosimetry to convert dose in the detector medium into dose to water. The general form describing the conversion of a detector signal measurement, M_{det}, into absorbed dose to water, D_w, can be expressed as:

$$D_w = M_{\mathrm{det}} \cdot N_{D,\mathrm{det},Q} \cdot f_{\mathrm{med,\,det},Q}^{D_{\mathrm{det}} \to D_w} \cdot \prod_i k_i \tag{1}$$

where, $N_{D,\mathrm{det},Q}$ is the detector coefficient that converts the measured quantity into absorbed dose to the detector medium, and $f_{\mathrm{med},\mathrm{det},Q}^{D_{\mathrm{det}} \to D_{\mathrm{med}}}$ is the coefficient that converts absorbed dose to the detector to absorbed dose to water. Several correction factors, k_i, are usually applied to account for non-ideal measurement conditions.

The most prevalent effect of radiation-induced energy absorption in a medium is temperature rise. For absorbed dose calorimeters, dose to the sensitive volume, most commonly water or graphite, is determined by converting from measured temperature change using the specific heat capacity of the medium, $c_{p,\mathrm{med}}$. Absorbed dose to water determination in calorimetry can be summarized as:

$$D_w = \Delta T \cdot c_{p,\mathrm{med}} \cdot f_{w,\mathrm{det},Q}^{D_{\mathrm{med}} \to D_w} \cdot \prod_i k_i \tag{2}$$

where,

$$M_{\mathrm{det}} \;\to \Delta T \tag{2a}$$

$$N_{D,\mathrm{det},Q} \to c_{p,\mathrm{med}}. \tag{2b}$$

For water calorimetry, absorbed dose to water is measured at a point in water, and $f_{w,\mathrm{det},Q}^{D_{\mathrm{med}} \to D_w}$ is taken as unity, while for graphite, a dose conversion process is required (see section 2.3). In general, it is assumed that all the absorbed energy contributes to a temperature rise in the medium. If some fraction of the energy is in fact absorbed or released by radiation-induced physical or chemical reactions, then there is said to be a heat defect. Furthermore, heat transfer occurring in the sensitive volume, which can be strongly radiation field dependent, must be quantified to ensure accurate dose to water measurements. Absorbed dose calorimetry is unique in that calibration can be achieved entirely in terms of temperature and electrical standards, independent of radiation. It is for this reason that calorimetry can be considered the most absolute dosimetry technique. In contrast, absorbed dose standards based on ionometry and Fricke solutions require a characterized radiation field to accurately determine W_{air} and $G_{\mathrm{Fe}^{3+}}$, respectively, since, at present, it has not been possible to determine these quantities with adequate accuracy from first principles.

The accurate measurement of temperature rises at a point is possible in stagnant water calorimeters due to the relatively low thermal diffusivity of water. Conceptually, water calorimetry is relatively straight forward: the calorimeter is used to measure the temperature rise at a point, ΔT_w, which is then converted by the specific heat capacity of water, $c_{p,w}$, to yield absorbed dose to water at a point (Osborne *et al* 1939). In practice, this process is complicated by fundamental effects that potentially disturb the energy balanced between absorbed dose and energy appearing as a temperature rise, and technical effects that complicate the accurate measurement of the temperature rise. Both fundamental and technical effects are handled as correction factors, as shown in the following expression:

$$D_w = c_{p,w} \cdot \Delta T_w \cdot k_{hd} \cdot k_{ht} \cdot k_p \cdot k_{dd} \cdot k_\rho \tag{3}$$

where k_{hd} is the correction factor for the heat defect, h; k_{ht} is a general correction factor for heat transfer due to conduction and convection; k_p is the radiation field perturbation factor due to the presence of non-water materials in the beam; k_{dd} corrects for a non-uniform dose profile at the point of measurement; and k_ρ accounts for the difference in density between the calorimeter operating temperature and the temperature at which another detector is calibrated. The accuracy of the disseminated quantity absorbed dose to water critically depends on the determination of these correction factors. An expanded description of these corrections is provided in section 2.3.

Within the context of absorbed dose calorimetry, graphite differs from water in three important respects as an absorbing medium: (i) its specific heat is approximately six times smaller, (ii) its thermal diffusivity is about six hundred times larger, and (iii) it is a rigid elemental solid rather than a liquid chemical compound. As a technique, graphite calorimetry holds several advantages and disadvantages over water calorimetry. For one, its smaller specific heat capacity results in signal to noise ratio that is six times larger than water. Unlike water, no radiation-induced chemical reactions that would otherwise contribute to a heat defect occur in graphite (radiation-induced heat defect due lattice absorption is generally considered to be negligible). As a machinable solid with a high thermal diffusivity, the effective measurement becomes one of absorbed dose averaged over the entire absorbing graphite core (i.e. the sensitive volume), rather than dose at a point in water. The major downside of using graphite is the need to convert the measured dose to absorbed dose to water. While the conversion itself is not strongly energy dependent, it does nevertheless introduce an uncertainty not present in water calorimetry. The effects of heat transfer are minimized by nesting the core within one or more graphite layers, referred to as jackets, each separated by insulating gaps (often evacuated). The high thermal diffusivity of graphite permits the use of electrical heating as an integral part of the dose measurement.

From the definition of absorbed dose, the dose to graphite, D_{gr} is obtained from:

$$D_{gr} = \frac{E_{\text{rad}}}{m_{\text{core}}} \cdot \prod_i k_i \tag{4}$$

where E_{rad} is the energy imparted to the core by radiation, m_{core} is the core mass, and k_i are the correction factors. When neglecting heat defect, the total change in thermal energy in the core, $\Delta E_{\text{tot,thermal}}$, can be expressed both as the sum of contributing sources (i.e. from radiation, E_{rad}, from electrical heating, E_{elect}, and from heat transfer, E_{transfer}), and as the product of the core mass, m_{core}, specific heat capacity,$c_{p,\text{core}}$, and change in core temperature, ΔT_{core}:

$$\Delta E_{\text{tot,thermal}} = m_{\text{core}} \cdot c_{p,\text{core}} \cdot \Delta T_{\text{core}} = E_{\text{rad}} + \Delta E_{\text{elec}} + \Delta E_{\text{transfer}}. \tag{5}$$

Absorbed dose graphite calorimeters are typically operated in one of three modes: (i) Quasi-adiabatic radiation mode, (ii) quasi-adiabatic electrical mode, and (iii) isothermal mode. In quasi-adiabatic radiation mode, the sensed core temperature is measured over time in the absence of electrical heating (i.e. $\Delta E_{\text{elec}} = 0$). Provided that the core temperature is adequately stable, the calorimeter is irradiated. Independent fits are made to the pre- and post-irradiation temperature curve, and the rise in temperature is obtained by extrapolating these fits to the mid-heating time. This temperature rise may be multiplied by the specific heat capacity to determine the dose, or alternatively, the calorimeter response may be quantified through the quasi-adiabatic electrical mode. By dissipating an accurately known amount of electrical energy into the calorimeter and measuring its response in the absence of radiation (i.e. $E_{\text{rad}} = 0$), an effective specific heat capacity for the system (e.g. $m_{\text{core}} \cdot c_{p,\text{core}} = \sum_i m_i \cdot c_{p,i}$; where i are the individual impurities in the core and a portion of the impurities outside of the core) can be experimentally measured and serve as a calibration coefficient. The main advantage of the quasi-adiabatic electrical mode is that absolute temperatures are not measured, rather the ratio of responses during irradiation and electrical calibration is used to determine the absorbed dose. Finally, in the isothermal mode, electrical dissipation is controlled such that the temperature distribution inside the calorimeter remains constant throughout operation. The quantity of interest is the change in electrical power necessary to maintain this state during irradiation, which then by substitution, provides a measure of the rate of energy imparted by the radiation. The energy from electrical heating of the core is obtained by integrating the core electrical power with respect to time.

2.2. Technical considerations and heat transfer

All absorbed dose calorimeters operated as standards at primary standards dosimetry laboratories (PSDLs) use negative temperature coefficient (NTC) thermistors to quantify the temperature increase in absolute terms. Thermistors are calibrated against primary standard thermometers over a temperature range that encompasses the prospective operating temperature typically by several degrees to reduce the sensitivity to limited readout of the temperature standard. The calibration process links the fractional resistance change that is proportional to a temperature difference in absolute terms, by quantifying the thermistor material constant, β (Seuntjens and Duane 2009). For graphite calorimeters calibrated electrically, temperature calibration of the sensing thermistors is not needed. By dissipating a known amount of electrical energy via Joule heating in a thermistor heating network, the response of the calorimeter under irradiation may be measured provided that the heat transfers under both scenarios (electrical calibration and irradiation) are identical (Daures *et al* 2005). The accuracy of an absorbed dose determination hinges on the long-term stability of the thermistors, which has been shown to be within a few tenths of a percent (Domen 1994, Seuntjens *et al* 1999, Krauss 2006b). A change in thermistor material constant can only be quantified by recalibration of the thermistors outside of the context of the calorimeter. However, Domen (1994) demonstrated that this type of change leads to a change in the nominal resistance value of the thermistor, which in turn leads to a change in Wheatstone bridge setting; therefore, monitoring bridge setting as a function of operating temperature is a good way to detect anomalies with the material constant of the thermistors used. In a measurement circuit, thermistors form part of a Wheatstone bridge setup, where their fractional resistance change leads to a voltage change of the bridge (Kubo and Brown 1984). There is a tendency for AC bridges to be less sensitive to noise than DC equivalents, but a clear disadvantage is that capacitive components from cables and all components in the bridge need to be balanced as well, and this leads to some additional complexity. The stability of the Wheatstone bridge and voltage amplifier is verified by switching high-accuracy reference resistors in the circuit and measuring the response of the bridge. The response of the bridge can be improved by increasing the power dissipation in the thermistors; however, high power dissipations lead to other non-linearities, such as the change in thermistor excess temperature and the subsequent signal change. For typical low power dissipation (25 μW or less) this effect is usually ignored.

The parameters that affect the accuracy of the dose determination are the specific heat capacity and the correction factors, which are dependent on the physical characteristics of the measurement (e.g. pre-drift time, irradiation time, post-drift time, power, operating temperature, dose rate, field size, depth, etc). All these parameters need to be carefully taken into consideration for accurate work and a calorimeter's characterization entails determination of these factors for the beam and setup in which the calorimeter is intended to be used. The specific heat capacity typically used for water calorimetry in PSDLs is the one determined by Saul and Wagner (1989), with a value of 4206.8 J kg^{-1} K^{-1} at 4 °C and an uncertainty of 0.1% specified over the complete range of applicability of the Helmholtz equation. A more reasonable uncertainty estimate on these data for the narrower temperature operating range in water calorimetry is 0.03% (Krauss 2006a). The specific heat capacity of graphite, in all it is commercially-available forms, is generally taken to be build-specific (e.g. Picard *et al* (2007)).

In the case of graphite calorimeters, heat transfer may occur via conduction or radiative processes. Conduction and convection between adjacent graphite bodies are mitigated using evacuated gaps to separate the bodies (figure 1). Some conduction through the electrical leads and graphite supports is unavoidable, though the use of fine gauge wire and silk threads under tension, respectively, minimizes these effects to generally negligible levels. Radiative transfer is also reduced by coating the surfaces of the graphite jackets in aluminized Mylar. The effectiveness of thermal isolation can be ascertained by measuring the time constant for the core temperature to relax towards its equilibrium value, given a constant jacket temperature and constant core heating power. This time constant is the ratio of the relevant heat capacity and heat transfer coefficient and may range from ~30 s for older portable calorimeters using air gaps, to ~1800 s for modern primary standard calorimeters (McEwen and Duane 2000, Seuntjens and Duane 2009). Isolation of the core from the ambient temperature is achieved by introducing multiple nested jackets, often referred to as the shield and mantle. These extra layers may be temperature controlled at a set point above ambient through means of electrical dissipation. The downside to this strategy is the radiation field perturbation caused by the relatively low-density gaps.

Thermal equilibrium within water calorimeter phantoms is usually achieved through the circulation of a thermally controlled fluid (figure 2). In some instances, a coolant flowing through a network of pipes in direct contact with a conductive layer (e.g. copper plate) enclosing the water phantom on all sides is used (figure 2b). The conductive layer becomes a quasi-isothermal surface, which effectively isolates the calorimeter from thermal fluctuations in the surrounding environment. The isothermal surface is often sandwiched by additional insulating layers (e.g. expanded polystyrene) to further dampen changes in ambient temperature. In other instances, the fluid is circulated through a radiator inside the calorimeter phantom (figure 2a). Attached fans force the enclosed air mass through the radiator, which eventually thermally stabilizes. In both types of designs, the fluid is circulated by a programmable chiller.

Heat transfer in absorbed dose calorimeters occurs because of temperature heterogeneities caused by: (i) non-graphite and non-water materials (e.g. glass vessel, thermistors, etc), respectively, with specific heat capacities differing from graphite or water; (ii) thermistor power dissipation leading typically to (1–2) mK of excess temperature per microwatt of power dissipated; (iii) non-homogeneities in the initial dose (and temperature) distribution during irradiation. In most water calorimeter designs, convection is eliminated by choosing 4 °C as the operating temperature, since the density of water is maximal and the driving force for convection is removed. For most calorimeters (especially in broad high energy photon beams), the handling of heat transfer thus boils down to correcting for conductive heat loss or gain. This is typically modelled using finite element analysis software packages that require the details of the geometry, material properties, initial temperature non-uniformity and timing of the irradiation as input (Choi *et al* 2019). The correction procedure can then amount to a linearization of the measured temperature trace using the calculated excess temperature curve, or by expressing the measured excess temperature curve in terms of corrections on a mid-run extrapolation procedure (Seuntjens and Duane 2009). More complex procedures account for sequences of calorimeter runs and the effect of non-linearities of excess temperature drifts of the previous run on the accuracy of the next run (Krauss 2006b, Sarfehnia 2010). For graphite calorimeters, sensing of the temperatures and electrical powers in each of the graphite bodies (in addition to that of the core) can provide accurate estimates of the heat transfer between graphite components. The assessment of heat transfer coefficients between bodies permits the estimation or simulation of heat transfer under different temperature and power configurations.

2.3. Other correction factors and dose conversion

The heat defect, h, quantifies the relative difference between energy absorbed E_a and energy appearing as heat E_h; and is defined as:

$$h = \frac{E_a - E_h}{E_a} \rightarrow E_a = E_h \frac{1}{1-h} \tag{6}$$

therefore, the correction for the heat defect is given as $k_{HD} = \frac{1}{1-h}$. The heat defect is positive for an endothermic process and negative for an exothermic process in the calorimeter. While it is generally assumed that the heat defect is a negligible quantity in graphite calorimetry, it has been shown to be of considerable importance in water calorimetry. Even though several other processes could contribute to a heat defect (e.g. energy transferred to Cherenkov radiation or to acoustic modes), it has been shown that the most significant portion of the heat defect is due to radiation-induced chemical reactions in water (Klassen and Ross 1991, 1997, 2002). Impurities present in water act as scavengers for reactive species created during the radiolysis of water and this process may lead to a distortion of the energy balance which is then expressed as a non-zero heat defect. If all impurities can be consumed as calorimeter irradiation progresses, the system may tend to a steady state situation with zero heat defect. In general, however, for unknown levels of organic impurities, a non-zero heat defect exists that is dependent on the accumulated dose, dose rate and temporal history of the irradiations applied to the calorimeter. A water calorimeter may typically be run in a zero-heat defect mode achieved by saturating pure water with N_2, Ar or H_2 before operation. Once a zero heat-defect steady state has been reached, the calorimeter response becomes independent of the irradiation history; however, trace impurities may affect this steady state and prevent a zero-heat defect from being established.

A second mode of operation with a non-zero heat defect can be achieved when known amounts of known impurities are introduced to cause a predictable heat defect which is then estimated using a numerical calculation. Typically, different systems are created that exhibit a different, but a numerically predicable heat defect and the ensemble of the different systems is compared with model calculations. For example, the H_2/O_2 (50/50) system has been shown to produce a very stable −2.4% heat defect for photon and electron beams. Note that since there is a non-zero heat defect, the value depends on the radiation beam (linear energy transfer (LET), energy) and on all details of how the calorimeter is run, including operating temperature since the heat defect is dose rate dependent and varies as a function of time which leads to an observable change in temperature drift curves and extrapolation to mid-run (Klassen and Ross 1991, 1997, 2002). A third approach combines the two former approaches and has been used to track the behaviour of a system prepared with well-known initial impurities. The typical example is the H_2 system with trace impurities of O_2 in which the response evolves through a predictable and very sharp exothermic peak with accumulated dose as the trace amounts of O_2 are consumed. The latter system will achieve a zero-heat defect after the characteristic oxygen consumption exothermicity peak has been observed (Krauss and Roos 1998). A fourth, and elegant solution has been the completely sealed vessel in which water quality, once established, can be preserved perpetually and this calorimeter thus produces a zero-heat defect that remains stable over time. The uncertainty on the heat defect is estimated based on an assessment of agreement between relative experimental behaviour of the calorimeter response for different systems and what is predicted by model calculations. In this way, Krauss (2006a) determined a ($k = 1$) uncertainty estimate

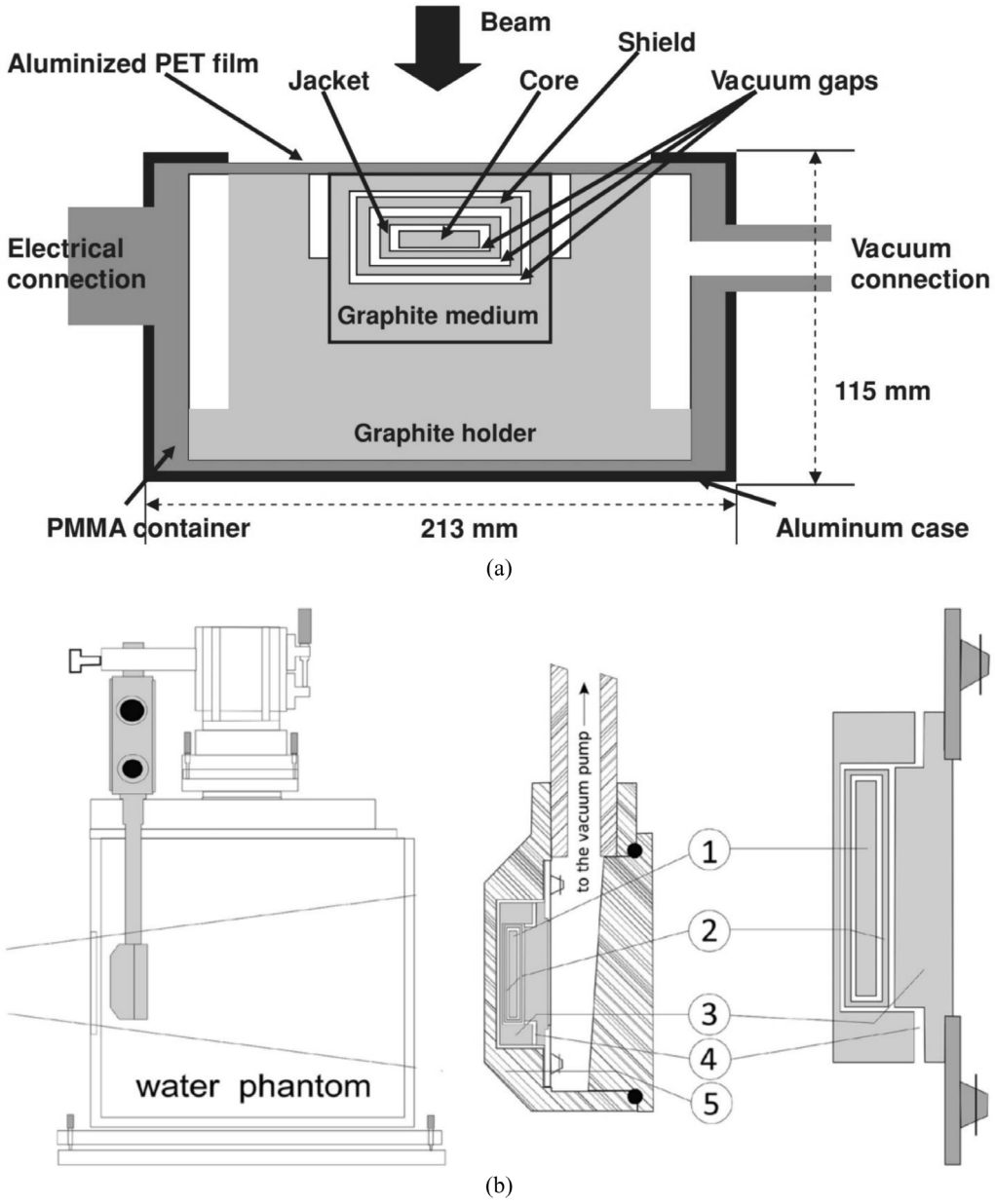

Figure 1. Schematic diagrams of the (a) NIRS portable graphite calorimeter (Reproduced from Sakama *et al* (2009), 2009 Institute of Physics and Engineering in Medicine. All rights reserved.), and (b) the ENEA-INMRI in-water-phantom graphite calorimeter (Reproduced from Pinto *et al* (2016), © 2016 Institute of Physics and Engineering in Medicine. All rights reserved.) depicting the (1) core, (2) jacket, (3) shield, (4) vacuum gaps, (5) PMMA envelope. Having different absorbed dose calorimeter designs reduces the number of common physical parameters, and therefore increases the confidence in the accuracy of respective designs during inter-comparisons.

of 0.14%; similar sub-percent uncertainty values are obtained in other PSDLs (Seuntjens and Duane 2009) for Co-60 and high energy photon beams.

The profile uniformity correction factor, k_{dd}, corrects for the effect of the difference in dose measured by the calorimeter versus the dose at the reference point. For water calorimetry, the measured dose is at the points of measurement of the thermistor probes, while for graphite calorimetry, this is taken as an average dose evaluated over the extent of the core volume. Both the correction and its uncertainty are often small in radiation therapy, as uniform dose distributions can be achieved.

For both water and graphite calorimeters, the signal measured at the location of the thermistor probes is affected by the presence of non-water and non-graphite materials, respectively (e.g. vacuum/air/aerogel gaps, glass vessel, vessel support structure, etc), both directly through radiation interactions and indirectly (i.e. thermally) because of the different heat capacities and conductivities contributing to the heat transfer in the sensitive volume. The normally small perturbation effect can be accounted for in water calorimetry by measurements using small detectors in the presence and absence of these items compared with MC calculations. In high energy photon beams this correction is generally on the order of 0.1%–0.2% with an uncertainty below 0.1% by design. Due to the fixed nature of the core within most graphite calorimeters, the influence of non-graphite materials

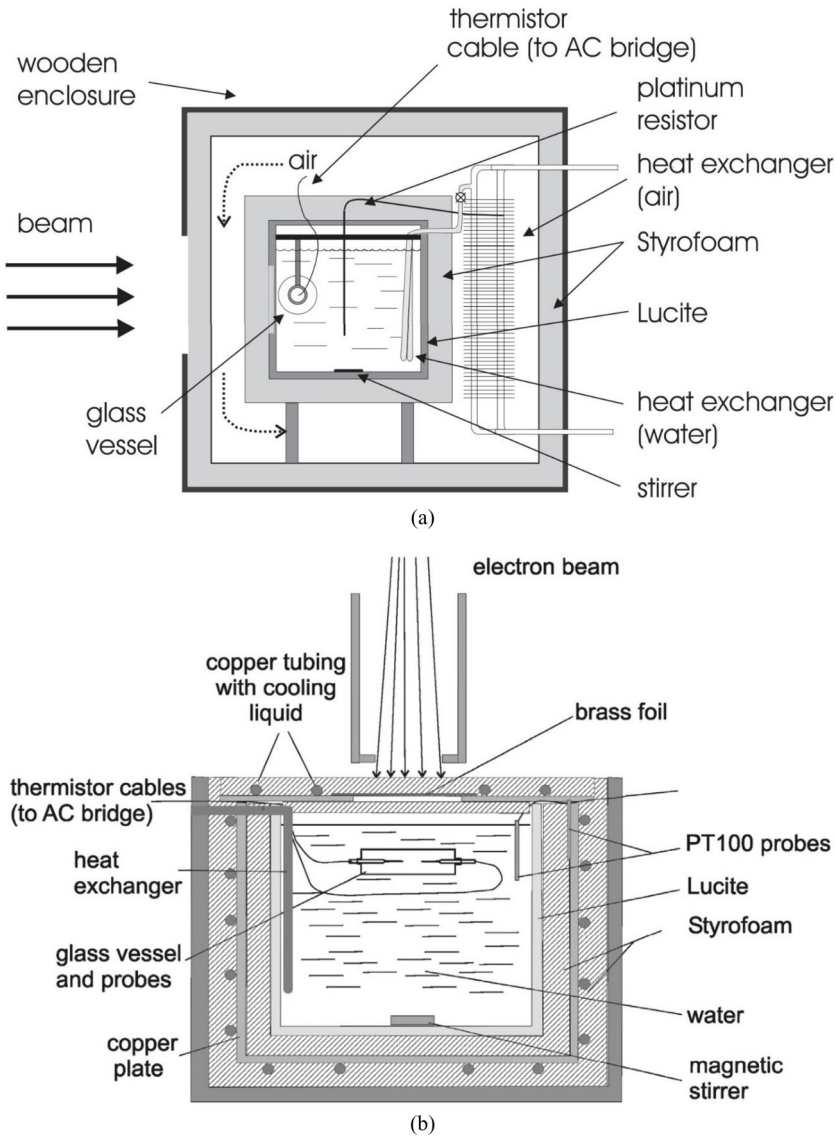

Figure 2. Schematic diagrams of the (a) NRC primary standard water calorimeter enclosure (adapted from Seuntjens *et al* (1999). © IOP Publishing Ltd. All rights reserved.), and (b) the electron sealed water calorimeter (ESWcal; reproduced with permission from Sarfehnia *et al* (2010a), John Wiley & Sons. © 2010 American Association of Physicists in Medicine.). These are examples of two typical water calorimeter enclosure designs which differ primarily in their cooling systems (air circulation-based versus liquid-cooled).

(often referred to as impurities) is not directly measurable. The impurities are also often impractically small to include in an accurate MC model (e.g. thermistor beads, wire, silk thread, etc). Thus, the mass impurity correction, k_i, must be estimated based on cavity theory using MC-generated photon and electron spectra to estimate the mean energy absorption coefficients and mean mass stopping powers. This contributes a type B uncertainty of typically 0.1% (Delaunay *et al* 2014).

Finally, for water calorimeters operated at 4 °C, the difference in water density between the operation temperature and the temperature at which the dosimeter is calibrated (typically room temperature) gives rise to a minor, slightly depth-dependent correction factor, k_ρ. For instance, for a depth of measurement of 8 cm, the density effect amounts to about 0.2 mm when comparing water at 4 °C and 22 °C. This correction can be avoided by determining the depth of measurement in terms of mass thickness (g cm^{-2}).

For graphite calorimeters, the conversion of dose to graphite to dose to water is commonly accomplished in one of three ways. All methods generally represent the largest source of uncertainty on the determination of absorbed dose to water, with a typical assignment ranging between 0.3%–0.4% for photon and electron beams (0.25% for Co-60; Delaunay *et al* 2014), and 1% for proton and carbon ion beams. The first technique is the photon fluence scaling method (Pruitt and Loevinger 1982), where the dose to graphite is simply converted to dose to water by calculating the water-graphite dose ratio at the reference depth. The relation between absorbed dose and electronic kerma is often used to calculate this factor. This approach typically requires additional corrections to account for differences in air attenuation and the finite source size, among other minor effects.

Table 1. Main characteristics and performance of recent high-energy photon water calorimeters reported in the literature.

Study	PTB (Krauss and Kapsch 2014)	VSL (de Prez *et al* 2016)	VSL (de Prez *et al* 2018)
Vessel type	Parallel plate	cylindrical	Cylindrical
Vessel material	Glass	glass	glass
Vessel wall thickness	0.7 mm	(0.9–1.4) mm	(0.9–1.4) mm
Beam type and size	4 MV–25 MV ($TPR_{20,10}$ 0.64–0.80); $10 \times 10\,cm^2$ & $3 \times 3\,cm^2$	Co-60; 6 MV & 10 MV ($TPR_{20,10}$ 0.680 & 0.735) $10 \times 10\,cm^2$	C0-60; 6 MV WFF, 6 MV FFF, 10 MV WFF, 10 MV FFF ($TPR_{20,10}$ 0.675–0.735); $10 \times 10\,cm^2$
Depth of measurement	10 cm	10 cm	10 cm
Water system used and heat defect	H^2-saturated $h = 0.0$	Ar-saturated $h = -5 \times 10^{-4} \pm 2 \times 10^{-3}$	Ar-saturated $h = -5 \times 10^{-4} \pm 2 \times 10^{-3}$
Non-water radiation perturbation correction, k_p	1.000 ± 0.001 ($10 \times 10\,cm^2$); 0.9970–1.0024 ($3 \times 3\,cm^2$)	(1.001–1.002) ± 0.05%	(1.0006–1.0018) ± 0.05%
Excess heat perturbation correction	0.995–0.997 ($10 \times 10\,cm^2$); 0.970–0.986 ($3 \times 3\,cm^2$)	0.9949 & 0.9985 (6 MV & 10 MV) ± 0.18%	(0.9975–0.9995) ± 0.18%
Combined relative standard uncertainty on absorbed dose to water	0.31%	0.37%	0.37%

$$D_w = D_{gr} \cdot \left(\frac{D_w}{D_{gr}}\right)_{calc} = D_{gr} \cdot \left(\frac{K_{coll,w} \cdot \beta_w}{K_{coll,gr} \cdot \beta_{gr}}\right)_{calc} = D_{gr} \cdot \left[\left(\frac{\bar{\mu}_{en}}{\rho}\right)^{w}_{gr} \cdot \Psi^{w}_{gr} \cdot \beta^{w}_{gr}\right]_{calc}. \quad (7)$$

The second technique involves the use of a transfer instrument, typically a thin-walled ionization chamber (Picard *et al* 2010, Shimizu *et al* 2015). The chamber is first calibrated in a graphite phantom representation of the calorimeter and is subsequently used to measure absorbed dose at a reference point in a water phantom. The dose to water formulation becomes:

$$D_w = D_{gr} \cdot \left(\frac{D_w}{D_{gr}}\right)_{meas} = D_{gr} \cdot M^{w}_{gr} \cdot \left(\frac{\bar{L}_\Delta}{\rho}\right)^{w}_{gr} \cdot P^{w}_{gr} \quad (8)$$

where P^w_g is presented as shorthand for the ratio of the products of ionization chamber correction coefficients in water to graphite. More details on the dose conversion process for photon beams can be found in Nutbrown *et al* (2002).

The third and most recent technique is a direct MC calculation of the dose ratio, $\left(\frac{D_w}{D_{gr}}\right)_{MC}$, as shown in equation (7), based on an accurate modelling of the radiation source, be it Co-60 or a linac-based high-energy x-ray beam, of the experimental calorimeter geometry, and of a water phantom geometry under reference conditions (Lye *et al* 2013, Delaunay *et al* 2014). This approach promises a more accurate and arguably more straightforward means of dose conversion, as fewer assumptions about the interactions occurring inside the calorimeter and phantom, not to mention fewer measurements, are required to transfer dose to an arbitrary water phantom geometry. The downside is that it relies entirely on the accuracy of the modelling process, and thus requires considerable quality assurance effort to ensure the validity of the model output.

3. Co-60 and high-energy x-ray beams

Historically, absorbed dose calorimetry has been most widely applied to the standardization of absorbed dose to water in high-energy photon beams. For more than three decades, PSDLs have led the development of calorimetry-based absorbed dose standards for photons with the aim of disseminating absorbed dose to water in Co-60 teletherapy fields via absorbed dose to water calibration coefficients for clinical ionization chambers. More recently, this practice of dissemination has been extended by several PSDLs to include linac-based photon beams. Even among primary standards, absorbed dose calorimetry is considered the most direct and absolute method of measuring absorbed radiation dose since device calibration can be achieved in terms of radiation-independent quantities that are traceable to standards with relatively lower uncertainty (i.e. electrical- and temperature-based standards).

National absorbed dose to water standards contribute to the international network of PSDLs. The BIPM. RI(I)-K6 comparison for standards for absorbed dose to water in accelerator photon beams was adopted as the

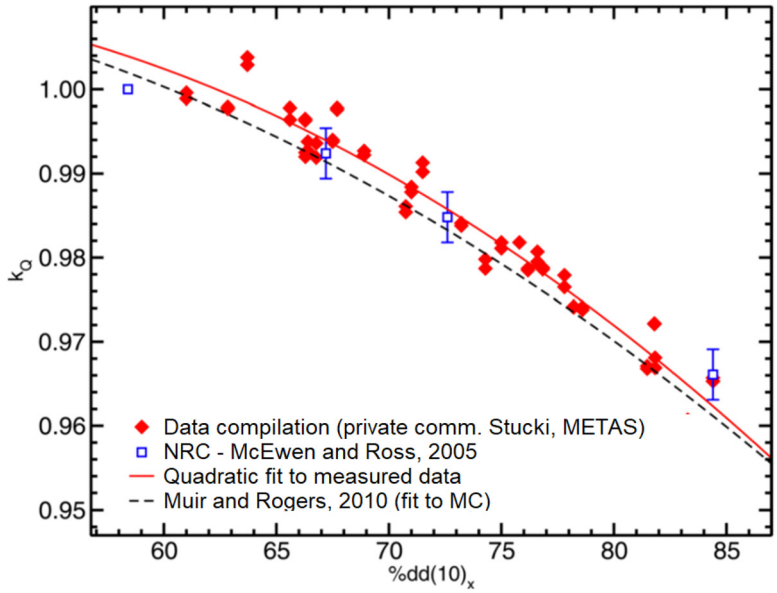

Figure 3. k_Q values for the NE2571 chamber determined by calorimetry techniques in primary standards dosimetry laboratories. The dashed line represents a fit to MC data by Muir and Rogers (2010). Reproduced with permission (Reproduced with permission from Muir *et al* (2011), John Wiley & Sons. © 2011 American Association of Physicists in Medicine.).

basis for the degree of equivalence of national primary standards by the Consultative Committee for Ionizing Radiation in May 2013. The degree of equivalence is defined by the pair of values, ($D_i = R_i - 1$; $U_i = 2u_i$) where R_i is the ratio of absorbed dose by lab i to the value at the BIPM, and u_i the combined standard uncertainty on the ratio R_i taking into account correlations. The results of the key comparison are maintained on the website kcdb.bipm.org, with data for ten PSDLs worldwide contributing to the database as of December 2018. The data shows typically a consistency significantly better than 0.5% on absorbed dose to water based on water calorimetry and graphite calorimetry.

3.1. Water calorimetry

Since the 1980s the primary focus of water calorimetry development has been with the application of high-energy photon beams in mind and the absorbed dose to water calibration chain nowadays is heavily based on the dissemination of absorbed dose to water using water calorimeters. At present, PSDLs in six countries (Canada, Germany, Netherlands, Russia, Switzerland, United States) have established water calorimetry as a primary standard for Co-60 teletherapy and/or linac-based high-energy x-ray beams. Table 1 summarizes the main characteristics and performance of recent high-energy photon water calorimeters, as reported in the literature. Historical data now suggests that, in general, sealed vessel calorimeters are stable at the ±0.25% level on the timescale of decades (Cojocaru *et al* 2016). The impact of water calorimetry has not been just in the primary standards but also in the experimental beam quality correction factor data that have been determined using water calorimetry and that have formed the experimental confirmation of data used in the absorbed dose calibration protocols such as (Almond *et al* 1999, McEwen *et al* 2014) and updates. Publications by authors from PSDLs report on detailed measurements of k_Q in high-energy photon beams and an exceptional consistency has been found in the measured data (Seuntjens *et al* 2000, McEwen 2010, Krauss 2010, Krauss and Kapsch 2014, Wright *et al* 2015, de Prez *et al* 2018). Figure 3 illustrates this assertion for the NE2571 chamber (adapted from Muir *et al* (2011)). Muir *et al* (2011) analyzed the difference between MC-calculated values of k_Q and calorimeter-determined values by McEwen (2010) and found that the deviation is less than the combined standard uncertainty on both studies but a systematic difference between the two data sets, with the MC-calculated values being lower on average than the experimentally determined values at high energy. Since MC values of $\underline{k}_Q$ do not consider a variable $(W/e)_{air}$, the comparison was used to establish an upper limit on a possible variation on $(W/e)_{air}$ between Co-60 and 25 MV which was found to be at most 0.29% (68% confidence). Muir and Rogers (2010) then used this information to assign an uncertainty on the assumption of a constant $(W/e)_{air}$ in MC-determined k_Q factors to arrive at uncertainties of 0.40% and 0.49% for graphite walled and A150-walled chambers, respectively. Along these same lines, Burns *et al* (2014) found no evidence for a variation in W_{air} at the 0.2% level, taking into account the mean excitation value, I, dependency, using a combination of graphite calorimetry, absolute ionometry, and MC calculations. As summarized in ICRU Report 90, measurements of W_{air} at energies above ~10 keV are based on equating the energy deposited, as measured by some technique (often calorimeter-based), with a charge deposition measurement, though the equivalency of this approach to a direct measurement has not been tested.

Based on a meta-analysis of historical measurements of W_{air}, the ICRU has concluded that no significant energy dependence exists for electron energies well above 10 keV, and recommends, based on a weighted mean of the available data, a value of 33.97 ± 0.12 eV.

3.2. Graphite calorimetry

To date, graphite calorimetry has been established as a primary absorbed dose standard for Co-60 teletherapy and/or linac-based high-energy x-ray beams by PSDLs in eight countries worldwide (Australia, Austria, France, Hungary, Italy, Japan, Russia, and the UK). This figure is expected to gradually increase, as considerable effort has been made by several active groups over the last decade to design, fabricate, and experimentally validate new graphite calorimeters, as well as improve upon and technologically-update older, well established systems. Table 2 summarizes the main characteristics and performance of recent high-energy photon graphite calorimeters, as reported in the literature. A notable example of such work has been the development of the GR series of graphite calorimeters at the LNE-LNHB. The so-called GR-08 is a Domen-type calorimeter that was built in 1984 and operated as a primary dose standard for over 20 years. As reported by Daures and Ostrowsky (2007), a successor, referred to as the GR-09, was built and first tested in 2007 to ensure the continuity of the standard. With a cylindrical core 3 mm thick and 16 mm in diameter, the internal structure of the GR-09, consisting of three concentric bodies each suspended by silk threads and separated by a 1 mm evacuated gap, was designed to be nearly identical to the GR-08. The GR09 was successfully compared to its predecessor through a combination of measurements and MC, with agreement being demonstrated at the level of 0.2% in MV photon beams. In 2011, Delaunay *et al* 2011 first described the GR-10, a calorimeter with a relatively smaller core cross section (6 mm thick, and 6 mm in diameter), built to fulfill the need to perform dosimetry in 2 × 2 cm^2 radiation fields. Initially, the height of the core was to be 3 mm, but the design was amended to reduce the dosimetric perturbations of all non-graphite materials to less than 1%. Like the GR-09, the GR-10 relies on a vacuum-based approach to establish thermal stability against which the radiation induced signals can be measured. The LNE-LNHB group successfully compared the GR-10 to the GR-9 in both Co-60 and a 12 MV accelerator-based photon beam (Daures *et al* 2012). Agreement between the two calorimeters was demonstrated to better than 0.05%. To extend the dose reference traceability to fields smaller than 2 × 2 cm^2, Dufreneix *et al* (2016a) of the LNE-LNHB designed and built a graphite calorimeter (GR-11) with a relatively large, 3 cm-wide, sensitive volume for dose-area product (DAP; see section 8 for further details) measurements. Other examples of recently developed graphite calorimeter systems include: (i) a unique design by Picard *et al* (2009) of the Bureau International des Poids et Mesures (BIPM) featuring a jacket that can be disassembled and made to house either the 45 mm diameter graphite core or a parallel-plate transfer ionization chamber, (ii) a Domen-type calorimeter with a 20 mm wide, 2 mm thick core constructed by Morishita *et al* (2012) of the NMIJ as a new Co-60 absorbed dose rate to water standard, and (iii) a duplicate of the GR-09 calorimeter (Kim *et al* 2017) built for use in linac-based x-rays by the Korea Research Institute of Standards and Science (KRISS). Outside of the NMIs, the probe-format calorimeter (referred to as Aerrow) built at McGill University by Renaud *et al* (2013, 2018), which resembles calorimeter probes constructed by Sundara Rao and Naik (1980) and Duane *et al* (2012), is the first such system being developed specifically for widespread use by clinicians (figure 13). Its relatively small form factor was chosen to resemble a Farmer-type ionization chamber to ensure minimal disruption to the clinical workflow. It has also been designed to be used directly in water or water-equivalent phantoms, the two mediums most likely encountered in the clinical setting. In contrast to all other graphite calorimeters, the McGill probe incorporates an aerogel-based material as opposed to vacuum to achieve thermal isolation from the surrounding environment (Bancheri *et al* 2019). The feasibility of using the McGill probe to perform absolute dosimetry in standard megavoltage photon beams to within an accuracy of 1% has been shown.

3.3. Other calorimetric techniques

Dombeck (2003) analyzed the theoretical use of conductivity, instead of temperature, to measure absorbed dose. The concept was based on the idea that radiation interaction-induced long-lived ions could result in a measurable change in the conductivity of the absorbing medium. The authors acknowledged that, experimentally, these measurements may be challenging. Malyarenko *et al* (2006, 2010) and Chen-Mayer *et al* (2007) proposed measuring minute radiation-induced temperature changes in water by monitoring the changes in the speed of ultrasound waves propagating in the medium. The μK-resolution ultrasonic thermometer was shown to be able to measure temperature changes of as little as 10 μK reliably in Co-60. Chen-Mayer and Tosh (2008) proposed performing water calorimetry at room temperature. Constant stirring of water outside the calorimeter vessel resulted in a forced convection and overall complex heat transfer patterns, which were studied numerically using finite element method simulations (Chen-Mayer and Tosh 2006). This group also explored the idea of analyzing the frequency component of the calorimetric signals in the Fourier domain to better differentiate random white noise and effects of heat loss from radiation-induced signals (Tosh and Chen-Mayer 2007). Hao *et al* (2006) of NPL reported on various microwave resonance-based calorimeter design, which when operated at

Table 2. Main characteristics and performance of recent high-energy photon graphite calorimeters reported in the literature.

Study	NPL (Duane *et al* 2012)	NMIJ (Morishita *et al* 2012)	ARPANSA (Ramanathan *et al* 2014)	McGill University (Renaud *et al* 2018)
Core shape and size	Spherical; radius = 2.50 mm	Cylindrical; radius = 10 mm, thickness = 2 mm	Cylindrical; radius = 10 mm, thickness = 2.75 mm	Cylindrical; radius = 3.05 mm, thickness 10 mm
Gap size	1 mm	1 mm	0.5 mm	0.7 mm
Phantom material and size	30 cm cube of water equivalent material (WT1)	150 × 150 × 100 mm^3 PMMA	Variable; graphite plates can be added in front and behind calorimeter assembly	30 × 30 × 20 cm^3 water
Beam type	6 MV ($TPR_{20,10}$ of 0.681); 10 × 10 cm^2 and seven-field head and neck step and shoot IMRT plan (collapsed to gantry zero)	Co-60 (~11 cm diameter)	Co-60; 6 MV, 10 MV, 18 MV ($TPR_{20,10}$ of 0.673–0.777)	6 MV (%$dd(10)_x$ = 66.4)
Depth of measurement	5 cm	Water equivalent depth of 5 g•cm^{-2}	Water equivalent depth of 10 g·cm^{-2}	5 cm
Radiation perturbation correction due to gaps, k_{gap}	Not reported	0.9961% ± 0.1%	1.0087 (6 MV), 1.0055 (10 MV), 1.0041 (18 MV)	Not reported; included in the graphite-to-water conversion factor
Excess heat perturbation correction	Not reported	Assumed to be unity; operated in isothermal mode	Assumed to be unity; included in electrical calibration (quasi-adiabatic) and assumed to be negligible (isothermal)	1.002 ± 0.002
Graphite-to-water conversion factor	Not reported	1.075% ± 0.3%	1.040 (6 MV), 1.063 (10 MV), 1.081 (18 MV)	1.117 ± 0.004 (Co-60) to 1.136 ± 0.004 (24 MV, %$dd(10)_x$ = 86.8)
Combined relative standard uncertainty on absorbed dose to water	Not reported; repeatability of 0.6% in 10 × 10 cm^2 field	0.37%	0.40% (Co-60); 0.44%–0.49% (6–18) MV	0.9% (for quasi-adiabatic & isothermal)

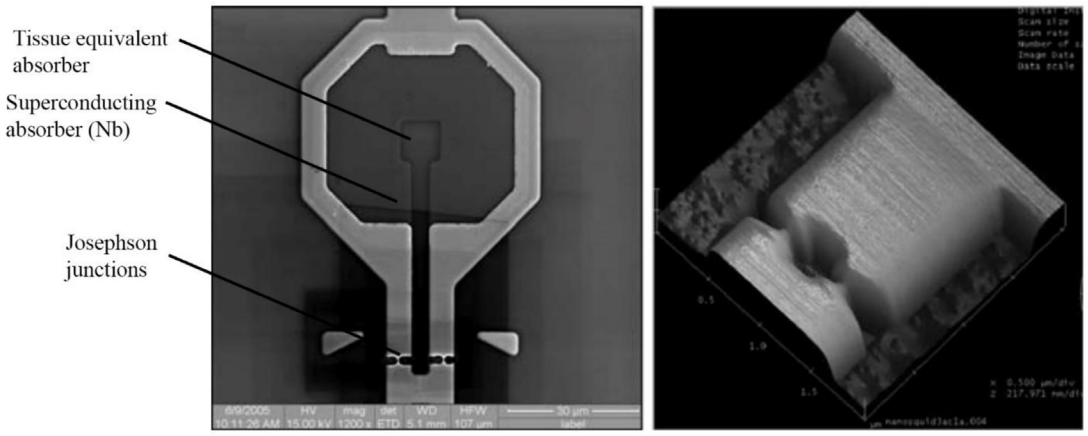

Figure 4. (Right) A scanning electron microscopy image of a 50 μm SQUID with Nb superconducting absorber within the square ring. (Left) An atomic force microscopy image of a nano-SQUID, highlighting the size of the microbridge junctions that are typically 60–80 nm in width and length (adapted with permission from Galer *et al* (2010), copyright © 2010, Oxford University Press).

cryogenic temperatures could offer considerable increases in sensitivity relative to conventional absorbed dose calorimeters. In their estimation, a design based on a microwave rutile resonator operating at 4.2 K could be expected to sense temperature rises on the order of 25 nK and energy rates of 1.5 fJ s^{-1}. Flores-Martinez *et al* (2016) proposed a water calorimeter based on an optical detection technique where the temperature dependence of the refractive index of water is used to determine a temperature rise. Since the interferometer determines the interference path difference across the width of a full calorimeter phantom, the resulting signal is proportional to the line integrated dose. The authors describe a method to convert the integrated dose to dose at a point, but their study shows a precision of the order of 10%. The application of digital holographic interferometry to radiation dosimetry has also been studied by Nicolau *et al* (1999), Ackerly *et al* (2011), Beigzadeh *et al* (2017), and Hubley *et al* (2019). Building off a design concept first proposed by Galer *et al* (2010) and Fathi *et al* (2016, 2017) described a novel micro-calorimeter technique based on the principles of a DC superconducting quantum interference device (SQUID; figure 4). This technology allows for direct measurement of LET of incident beams and may be important to the study of medium/high LET particles. The enabling technology behind the micro-calorimeter is an inductive superconductive transition edge detector (ISTED; Gallop *et al* 2015). Energy imparted to the radiation absorbing element, located within a superconducting loop, causes Cooper pairs to break into normal state electrons. The resulting change in the inductance is measured by the SQUID, thus providing an extremely sensitive measure of the energy deposition at the μm-scale (EURAMET 2017). Silicon photonics is another promising avenue that could lead to micro-scale calorimetry (Pazos 2017). Researchers at NIST are presently investigating the feasibility of using chip-based micro-loop resonators and Bragg waveguides to determine radiation-induced temperature rises based on the change in the measured resonance peak wavelength. Tosh and Bateman (2019) recently presented the results of irradiating such chips with a 1.8 MeV Van de Graaff-based electron beam at nominal dose rates on the order of (10 to 100) Gy s^{-1}. Promisingly, the device response was observed to be linear with beam current, although further analysis is required to convert these preliminary results to absorbed dose.

4. High-energy electron beams

As for high-energy photons, clinical reference dosimetry of megavoltage electron beams is traceable to absorbed dose to water standards. Unlike photons, however, efforts to develop dedicated electron absorbed dose standards, calorimetry included, have been limited to a handful of institutions. This is likely in part due to the relatively infrequent use of electrons (likely less than 10% of all cancer treatments), combined with the practical challenges associated with electron beam dosimetry. As a result, most electron beam dose measurements are based on Co-60-calibrated ionization chambers and calculated photon–electron and electron beam quality conversion factors, k_{ecal} and $k'_{R_{50}}$, respectively (AAPM TG-51), or beam quality correction factors, $k_{Q\,\mathrm{cross}}$ and $k_{Q,Q\,\mathrm{cross}}$ (IAEA TRS-398). Nevertheless, new applications of calorimetry to develop primary electron beam absorbed dose standards have been documented since McEwen and DuSautoy reviewed the status of the field back in 2009. Most of these studies have focused on the use of water calorimetry at the NRC, PTB, and McGill University, either as a stand-alone or in combination with a Fricke-based dosimetry system, while both the NRC and NPL have published work pertaining to graphite calorimetry in the last decade. It is noteworthy to mention that although there is only one electron beam standard based on water calorimetry in current operation (NRC), it is anticipated that as many as five PSDLs will have established such a standard in the near future. Most recently, McEwen *et al*

(2015) have reported on a trial comparison of three national standards for electron beams, including the NRC water calorimeter standard.

The biggest difficulties to contend with in electron dosimetry are the relatively short ranges and high dose gradients. For therapeutic energies (4 MeV to 20 MeV), the electron range varies from approximately 2 cm to 10 cm, within which dose gradients can exceed 5% per millimetre at the lowest energies. These physical constraints impact the measurement uncertainties associated with the positioning of the instrument, as well as with the determination of corrections for the heat transfer and radiation field perturbation. Another, more subtle challenge is the characteristic depth-dependent charge deposition. Charge build-up is a concern for calorimeters with extremely sensitive AC- or DC-based Wheatstone bridge circuits that can be successfully managed with adequate grounding. This phenomenon is less of a problem for other types of dosimetry systems, but nonetheless can affect the result of measurement if neglected.

4.1. Water calorimetry

Over the last ten years, the application of absorbed dose water calorimetry to the dosimetry of high-energy electron beams has been centred around the activities of the Ionizing Radiation Standards group at the NRC, the Department of Dosimetry for Radiotherapy at PTB, and the calorimetry research group at McGill University. Table 3 summarizes the main characteristics and performance of these high-energy electron water calorimeters, as reported in the literature. Though their calorimeter phantom designs may appear vastly different at first glance, they have many commonalities, and in certain respects (e.g. thermistor construction), are virtually identical. Arguably, the biggest difference between the three groups is their choice of vessel design, though the McGill vessels have been fabricated by the NRC. Variations of the plane parallel (pp)-type vessel have most commonly been used for electron beam measurements, although the Domen-type cylindrical vessel, which has historically been reserved for high-energy photon beams, has also been successfully used at higher energies.

The NRC primary standard water calorimeter was first applied to the dosimetry of electrons by McEwen and Ross (2007) with the aim of obtaining absorbed dose calibration coefficients for the following ionization chambers in clinical 12 MeV, 18 MeV, and 22 MeV beams: NE2571, PTW Roos, and NACP-02. Two pp vessels were constructed with a diameter of 100 mm, a thickness of 40 mm, a front window thickness of 1.05 mm, a rear window thickness of 1.9 mm, and side wall thickness of 2.7 mm. The two vessels differed only in the angle at which the thermistor probes were designed to be inserted (i.e. normal to the side wall, or angled towards the front window). Radiation field perturbation corrections accounting for the presence of the glass vessel were experimentally determined using a small ionization chamber or diode contained with a dummy vessel. Excellent agreement (within 0.2%) was observed between the standard pp and cylindrical vessels at 22 MeV, as well as between the standard pp and angled-probe pp at 18 MeV. The result of this study was the direct calibration of the three types of ionization chambers with an associated uncertainty of about 0.4%, a figure very much in line with analogous photon beam calibrations. This methodology was carried forward at the NRC and has recently culminated in the work published by Muir *et al* (2017). In their report, the same water calorimeter setup is used to repeat the calibration of the NE2571 chamber more than 10 year later, as well as calibrate an additional NE2571 and a PTW 30013 chamber in clinical 18 MeV and 22 MeV electron beams. The absorbed dose to water calibration coefficients obtained in 2006 and 2016 were found to agree to within 0.21% and 0.04% for the 22 MeV and 18 MeV beams, respectively. Using these calibrated chambers as secondary standards, Muir *et al* measured the beam quality conversion factors of eight plane-parallel and six cylindrical ionization chambers to an accuracy of about 0.4%.

For electron beam energies down to 4 MeV, Cojocaru *et al* (2010) of the NRC have successfully measured the electron beam quality conversion factors of a PTW Roos chamber using a Fricke dosimetry system calibrated against a water calorimeter in a high-energy electron beam ($\geqslant$18 MeV). Building on techniques first developed at METAS, the Fricke solution is contained within custom polyethylene bags of a size and shape tailored to the application of interest. This approach eliminates the perturbation of the container wall. Cojocaru *et al* compared the Fricke response to the NRC primary standard water calorimeter and secondary standard ionization chambers to develop response calibration curves in the range of 7 Gy to 50 Gy in 4 MeV, 8 MeV, 12 MeV, 18 MeV, and 22 MeV clinical electron beams. The accuracy and precision of the Fricke system was found to be very dependent on solution preparation and contaminants affection the readout. Despite these challenges, the standard uncertainty in the determination of absorbed to water using the Fricke system was estimated to be 0.6%.

Krauss and Kapsch (2018) applied the PTB transportable water calorimeter (Krauss *et al* 2012) in 6 MeV to 20 MeV electron beams to determine k_Q factors for several types of cylindrical and plane-parallel ionization chambers (NE 2561, NE 2571, FC65-G, TM34001). While the relative electron energy dependence of k_Q factors that they measured above 8 MeV were found to be in good agreement with literature, large (up to 2%) discrepancies were observed in the lower energy range for all chambers studied (an example dataset comparison is shown in figure 5). The reasons for the discrepancies remain open and suggests that further development of calorim-

Table 3. Main characteristics and performance of recent high-energy electron water calorimeters reported in the literature.

Study	McGill University (Renaud *et al* 2015)	McGill University (Renaud *et al* 2016)	NRC (Muir *et al* 2017)	PTB (Krauss and Kapsch 2018)
Vessel type	Parallel plate	Parallel plate	Parallel plate and cylindrical	Parallel plate
Vessel material	Glass	Glass	Glass	Glass
Vessel wall thickness	1.12 mm	1.12 mm	1.05 mm (parallel plate) and 1 mm (cylindrical)	0.7 mm
Electron energies	(6, 9, 12, 16, 20) MeV	(6 and 8) MeV	(18 and 22) MeV	(6, 8, 10, 12, 15, 18, 20) MeV
Depth of measurement	1.25 cm–4.86 cm (6 MeV–20 MeV)	10.8 mm	4.20 cm (18 MeV) and 5.26 cm (22 MeV)	1.03 cm–4.37 cm (6 MeV–20 MeV)
Water system used and heat defect	H_2-saturated $h = 0.0$	H_2-saturated $h = 0.0$	H_2- and N_2-saturated $h = 0.0$	H_2-saturated $h = 0.0$
Non-water radiation perturbation correction, k_p	1.009 ± 0.006 (6 MeV); 1.000 ± 0.003 (9 MeV–20 MeV)	Not reported; accounted for by mock vessel	Not reported; accounted for by mock vessels	1.0083 (6 MeV); 1.0048 (8 MeV); 1.0010 ± 0.0010 (10–20) MeV
Excess heat perturbation correction	1.014 ± 0.003 (6 MeV); 1.005–1.008 (9 MeV–20 MeV)	$1.042 \pm 0.2\%$ (6 MeV) and $1.049 \pm 0.2\%$ (8 MeV)	Not reported; assigned a 0.10% uncertainty	0.956–1.010 (6–8) MeV; 0.996–1.006 (10–20) MeV
Combined relative standard uncertainty on absorbed dose to water	1.0% (6 MeV) and 0.5% (9–20) MeV	0.6%	0.35% (18 MeV) and 0.37% (22 MeV)	0.68% (6 MeV); 0.47% (20 MeV)

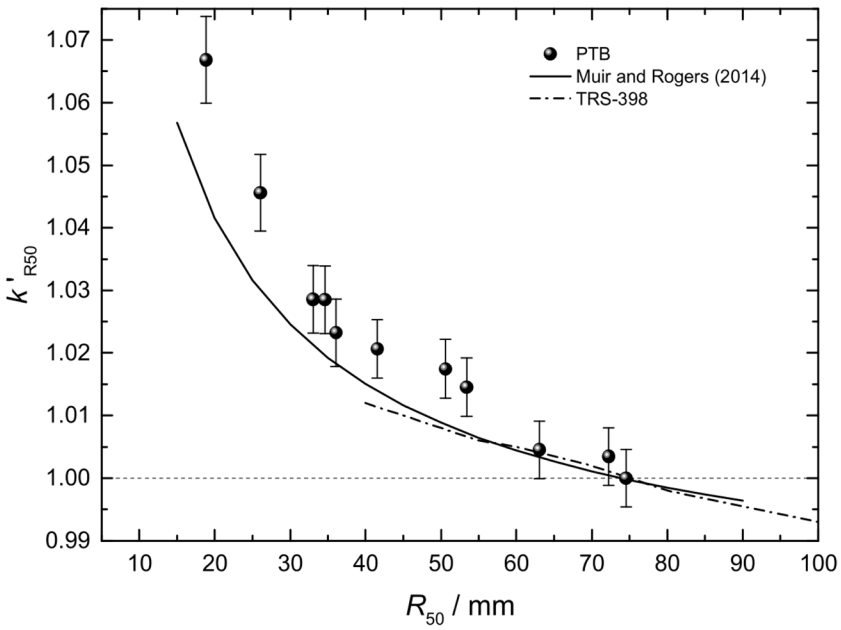

Figure 5. Relative energy dependence $k'_{R_{50}}$ of the electron beam quality conversion factor for the cylindrical FC65-G chamber in comparison to MC-calculated values obtained by Muir and Rogers (2014) and values taken from TRS 398 ($k_{Q,Q\text{int}}$) are also shown. Error bars represent the standard uncertainty of the data (reproduced from Krauss and Kapsch (2018), © 2018 Institute of Physics and Engineering in Medicine. All rights reserved.).

etry-based systems for the measurement of electron beam quality conversion factors in the low energy range is needed to improve the accuracy of these datasets.

At McGill University, the development of a sealed water calorimetry system specifically designed to operate in, and directly calibration ionization chambers across a wide range of clinical electron beams, was first reported on by Stewart in 2007. The calorimeter, referred to as the ESWcal, shares design aspects with the NRC primary standard water calorimeter and the Nederlands Meetinstitut (NMi). In contrast to nearly all other water calorimeters, the ESWcal was designed to operate under a vertical beam arrangement to contend with the range of electron beams down to 6 MeV. A pp vessel considerably smaller than the standard NRC pp vessel was constructed with a diameter of 79 mm, a thickness of 24 mm, a front and back window thickness of 1.12 mm, and a side wall thickness of 2.0 mm. In contrast to the NRC calorimeter, which uses a circulating air-based temperature control system, the ESWcal has 5 mm layers of copper arranged to encompass the water phantom and provide a quasi-isothermal shield. As a result, the overall size of the ESWcal is about two-thirds that of the NRC calorimeter, albeit considerably heavier. In 2015, Renaud *et al* used the ESWcal system to derive the electron beam quality conversion factors of an Exradin A12 and PTW Roos ionization chamber in clinical accelerator-based 6 MeV, 9 MeV, 12 MeV, 16 MeV, and 20 MeV electron beams. In contrast to the work of McEwen and Ross (2007), the radiation field perturbation due to the presence of the glass vessel was calculated using MC. The combined standard uncertainty on the measured dose to water was estimated to be 0.5% for the 9 MeV to 20 MeV beams and 1.0% for the 6 MeV beam, with predominant contributions from the positioning and perturbation correction.

Another unique water calorimeter design out of McGill University was reported by Renaud *et al* (2016). Referred to as the SHort-RangE Water calorimeter (SHREWcal), the calorimeter was built to measure absorbed doses in non-standard radiation fields (e.g. protons and carbon-ion beams) with reference depths in the range of 6 mm to 20 mm. The system was developed to be lightweight and transportable to operate at the user's facility and to calibrate ionization chambers *in situ*. In contrast to nearly all other water calorimeters, the SHREWcal was designed to operate without a large (typically on the order of $30 \times 30 \times 30\,\text{cm}^3$) water phantom. This was done to help reduce the minimum measurable reference depth, as well as to maintain a practical size and weight for ease of setup and transport. The SHREWcal was initially tested in a clinical 6 MeV and 8 MeV electron beam using the same vessel as the ESWcal to evaluate signal variation, thermal drifts, repeatability and the heat transfer modelling. The combined standard uncertainty on the measured doses to water were estimated to be 0.6%, with heat transfer corrections greater than 4% (see figure 7). It was concluded that, for such a calorimeter design, *a priori* calculation of the heat transfer correction would be necessary to determine the optimal thermistor position to minimize the uncertainties due to the heat transfer correction sensitivity, perturbation, and positioning.

4.2. Graphite calorimetry

The Institute of Physics and Engineering in Medicine (IPEM 2003) code of practice governing therapeutic electron beam dosimetry in the UK requires that a designated ionization chamber hold a calibration traceable to

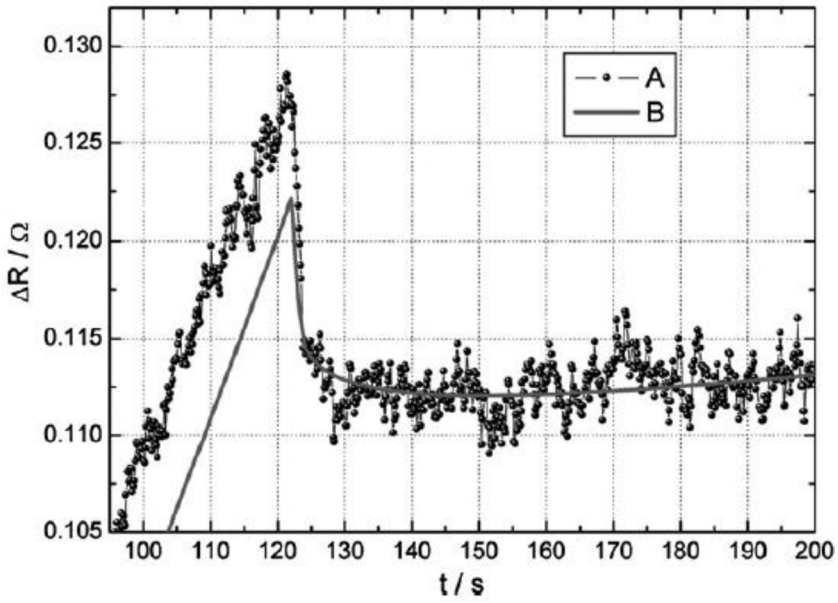

Figure 6. Enlarged view of the end of an irradiation run and the beginning of a post-drift showing a detail of the calculated excess temperature curve (B) together with the experimental data (A) for a 122 s irradiation with 150 kV x-rays. The calculated excess temperature curve is based on a detailed simulation of the vessel and probe geometry and normalized to the measurements using the data in the slope of the experimental drift curve during irradiation (reproduced from Krauss *et al* (2012), © 2012 Institute of Physics and Engineering in Medicine. All rights reserved.).

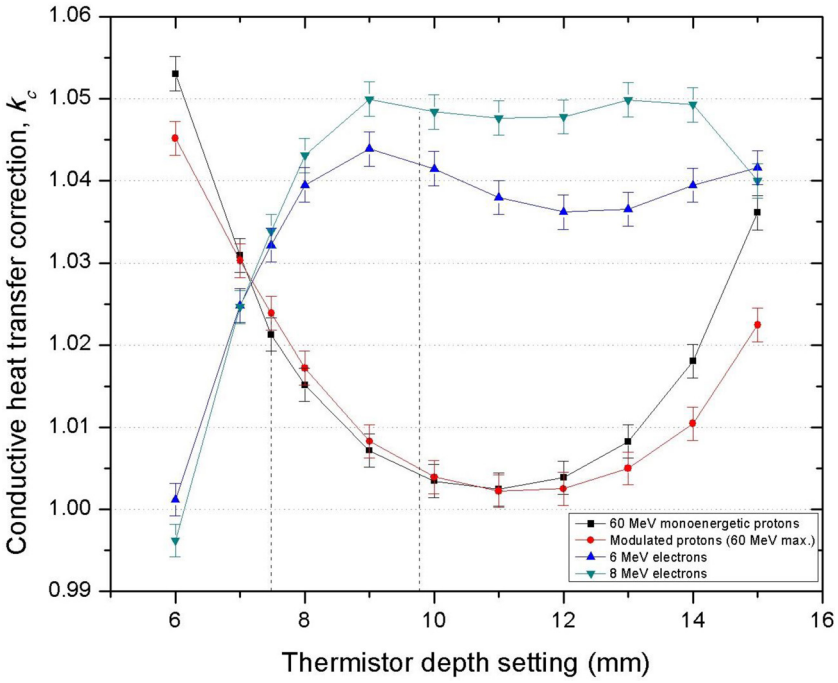

Figure 7. Heat conduction correction in the SHREWcal water calorimeter developed by Renaud *et al* (2016) for low-energy charged particle beams obtained by finite element modelling. The range of water-equivalent depths from 6 mm–15 mm corresponds with the possible positions of the thermistors while the vertical dashed line indicates the points of measurement used in the experiments (reproduced from Renaud *et al* (2016), © 2016 Institute of Physics and Engineering in Medicine. All rights reserved.).

the electron absorbed dose to water standard at NPL. The NPL electron absorbed dose calibration service is based on a primary standard graphite calorimeter and yields a direct calibration of an ionization chamber in terms of absorbed dose to water in a two-step process (McEwen *et al* 1998, 2001): (i) reference chambers are calibrated against the calorimeter in a graphite phantom, and (ii) user's chambers are then compared with calibrated reference chambers in a water phantom. Bass *et al* (2009) summarized the results of these types of calibrations for parallel-plate chambers (NACP-02 and PTW Roos-type 34001 chambers). Among the results, it was seen that chamber calibrations were repeatable to within 0.2% over a period of 2 to 3 years, and that calibration coefficient sensitivity across chambers of the same type varied between 1.1% for the Roos and 5.8% for the NACP-02. Bailey

and Shipley (2010) reported on the measurement and modelling of clinical linac-based electron beam profiles used in the determination of the graphite calorimeter gap corrections as well as ion chamber wall perturbation factors.

At the NRC, Bourgouin *et al* (2019) and Bourgouin and McEwen (2019) are actively investigating the possible energy dependence of W_{air} in the clinical energy range by performing graphite and aluminium calorimetry measurements in high energy electron beams. By combining ionometric and calorimetric measurements taken at the same point and using the same detector material for both chamber and calorimeter, W_{air} is derived using a MC-calculated dose conversion factor. Measurements were performed in 20 MeV and 35 MeV incident beams at seven different depths in graphite using a parallel-plate chamber and a calorimeter of similar dimension. The heat-loss corrected results yielded a value of 33.77 $\pm$ 0.13 eV for W_{air}, 0.6% lower than the recommended value from ICRU Report 90, though no energy dependence was observed, consistent with the Muir and Rogers (2010) investigation.

5. Low- and medium-energy x-ray beams

Low and medium energy x-rays are used clinically for the treatment of superficial lesions and national and international codes of practice based on air kerma standards have been published to standardize clinical reference dosimetry for these beams (Andreo *et al* 1997, Grimbergen *et al* 1997, Andreo *et al* 2000, Ma *et al* 2001, Aukett *et al* 2005). Low and medium energy x-rays can be defined as photon beams with tube potentials of 50 kV to 300 kV, with a somewhat artificial separation between low and medium energy x-rays at around 70–100 kV (~4 mm Al HVL).

Goodwin and Adair (1963) described total absorption measurements using a calorimeter for the determination of 'intensity of the beam directly in ergs per square centimeter' (i.e. energy fluence as a function of x-ray qualities) ranging from 50 kV (0.2 mm Cu) to 250 kV (4 mm Cu). By comparing the total absorbed energy corrected for backscattering, side scattering and beam attenuation with exposure at the same point in air, measured using ionometric methods, they came up with measured 'röntgen-to-rad' conversion factors. Goodwin (1960) used this methodology to determine absorption in different tissue equivalent plastics and directly determined the ratio of bone-to-tissue absorption ratios. A similar methodology using a dual core calorimeter was used in the Ph.D. thesis work of Redpath (1967) but in this case the goal was to determine the *W*-value of Ar, the gas used in the ionization chamber and this work was done for different spectra below 30 kV. The calorimeters in this era had absorbers made from a variety of materials including Al, Au, or Pb, depending on the goal of the experiment and the energy of the beam. With the advent of high energy radiation therapy, the emphasis on accurate dose determination in low and medium energy x-ray beams diminished and so did the literature around calorimetric measurements for these energies until the period leading up to the publication of absorbed dose standards-based dosimetry protocols.

5.1. Water calorimetry

Absorbed dose to water using water calorimetry has been used successfully for the measurement of absorbed dose to water in medium energy x-ray beams (tube potential of 70 kV and higher). One can distinguish roughly three generations in water calorimetry measurements for these beams. The first generation of measurements were carried out with open water calorimeters (Mattsson 1985, Kubo 1985, Seuntjens *et al* 1988) operated at room temperature. Although these studies showed that performing measurements at low dose rates was feasible with water calorimeters, there were several problems with these that limited accuracy to no better than around $\pm$5%. These problems included insufficient sensitivity, poor control of water quality leading to uncertainties in chemical heat defect (Klassen and Ross 2002) and heat loss specifically at room temperature where convective motion was shown to severely affect the accuracy of dose determination in open water calorimeters (Seuntjens *et al* 2000b).

The second generation of measurements were those based on a water calorimeter with a vessel system. Seuntjens (1991) and Seuntjens *et al* (1993) established a water calorimeter where purified N_2-bubbled water was contained in a Lucite vessel (4 cm diameter and 0.5 mm wall thickness), suspended in a 30 $\times$ 30 $\times$ 30 cm^3 water phantom which was stabilized at 25.8 °C. Numerical simulations were used to establish the heat loss correction factors for the Lucite vessel, whereas no heat loss correction was determined for the thermistor probes. Expressed as a correction on the mid-run extrapolated signal, the heat-loss corrections ranged between 0.997 and 1.000 for radiation qualities ranging from 100 kV (4.81 mm Al) to Co-60. The correction for perturbation of the radiation field by vessel and probe was determined using MC simulations and found to vary between 0.998 and unity for radiation qualities ranging from 100 kV (4.54 mm Al) to Co-60. Although the limited magnitude of these correction factors was a distinct advantage in the design of the Seuntjens *et al* (1993) calorimeter compared to later designs, a significant problem was the control of the water purity in the Lucite vessel. Seuntjens *et al* (1993) made assumptions on the heat defect based on comparative measurements in Co-60 against the PTB standard

Table 4. Main characteristics and performance of recent kV x-ray water calorimeters reported in the literature.

Study	VSL (de Prez *et al* 2008)	PTB (Krauss *et al* 2012)	LNE-LNHB (Rapp *et al* 2013)
Vessel type	Cylindrical	Parallel plate	Parallel plate
Vessel material	Glass	Glass	Quartz
Vessel wall thickness	0.8 mm	0.6 mm–0.7 mm	0.8 mm
Depth of measurement	3.6 g cm^{-2} (not clear how scaled)	50 mm between inner surface of water phantom and thermistor probes	0.8 mm quartz + 19.2 mm water
Water system used and heat defect	Ar-saturated $h = 0.0$	H_2-saturated $h = 0.0$	N_2-saturated $h = 0.0$
Non-water radiation perturbation correction, k_p	Between 1.055 and 1.001 for 100 kV (0.16 mm Cu) and 250 kV (2.48 mm Cu)	Between 1.084 and 1.005 for 70 kV (0.11 mm Cu) and 280 kV (3.38 mm Cu)	Between 1.064 and 1.015 for 80 kV (3.01 mm Al) and 300 kV (3.40 mm Cu)[a]
Excess heat perturbation correction	Between 1.061 and 1.024 for 100 kV (0.16 mm Cu) and 250 kV (2.48 mm Cu)	Between 0.964 and 0.988 for 70 kV (0.11 mm Cu) and 280 kV (3.38 mm Cu)	Between 1.041 and 1.006 for 80 kV (3.01 mm Al) and 300 kV (3.40 mm Cu)
Combined relative standard uncertainty on absorbed dose to water	Between 1.4% and 1% for 100 kV (0.16 mm Cu) and 250 kV (2.48 mm Cu)	Between 0.98% and 0.45% for 70 kV (0.11 mm Cu) and 280 kV (3.38 mm Cu)	Between 0.72% and 0.55% for 80 kV (3.01 mm Al) and 300 kV (3.40 mm Cu)

[a] Note: In the LNE calorimeter, most of the perturbation effect appears to be from attenuation in the beam path due to the window and the extruded polystyrene used as insulation.

of absorbed dose to water at that energy. The same vessel system, water fill and N_2 saturation of the calorimeter was used in the Co-60 and x-ray measurements and the response of the system as a function of accumulated dose in both Co-60 and the 250 kV (2.52 mm Cu) was carefully monitored. Using numerical simulations, it was also demonstrated that the heat defect, if any, would not be modified due to differences in LET between Co-60 and kV x-ray beams for the doses and dose rates used in the measurements. The absorbed doses measured in kV beams using the calorimeter were then corrected for a 1.5% ± 1.4% absorbed dose difference observed at Co-60 between water calorimeter and PTB absorbed dose to water standard. The overall $k = 1$ uncertainty on the absorbed dose to water reported in this work varied between 2.1% (100 kV 4.54 mm Al) and 1.5% (280 kV, 3.41 mm Cu). The absorbed dose measurements using the water calorimeter were then used to determine correction factors for on air kerma calibrated ionization chambers in medium energy x-rays. These corrections were involved in an update to the IAEA TRS-277 code of practice for medium energy x-rays (Andreo *et al* 1997).

In a third generation of papers on water calorimetry in kV beams calorimeter-based primary standards developed specifically for calibration of instruments in terms of absorbed dose to water in kV beams, have been discussed (de Prez *et al* 2008, Krauss *et al* 2012, Rapp *et al* 2013). These water calorimeters are typically compact versions of high-energy photon beam calorimeters in which dimensions are used that allow for measurements at shallower depths typically in horizontal beam configurations. Table 4 summarizes some of the parameters of these studies. The calorimeter setups differ from the Seuntjens *et al* (1993) configuration in two aspects: (i) the vessel containing the pure water is glass or quartz; (ii) the more recent calorimeters are operated at 4°C. Vessels employed in the VSL and PTB calorimeters have wall thicknesses of 0.7 mm–0.8 mm. All of the systems reported operate with a zero-heat defect, hence, the LET dependence question on heat defect that was raised in the Seuntjens *et al* (1993) study is no longer relevant in the more recent studies.

One of the challenges with glass vessels in kV beams is radiation absorption and perturbation. In the calorimeter studies this is taken into account by making subsidiary ionization measurements and MC calculations. For all studies the perturbation effect of vessel and other non-water materials in the beam path varies between 8.4% for the lowest energy studied and 0.5% for the highest energy, depending on the vessel and thermal enclosure material. Despite these large effects, the uncertainties on this correction factor are generally well below 0.5%. A second challenge is the excess heat generated by glass and quartz vessels in kV beams due to the mass energy absorption coefficients and their substantially lower specific heat capacity relative to water. This effect is generally modeled by heat conduction simulations, similarly as in Seuntjens and Palmans (1999) and depends on the individual vessel and calorimeter setup. In addition, when a single correction factor on the extrapolated signal is determined, it varies from run to run, and depends strongly on the timing used in the extrapolation of the drift curves. For this reason, corrections reported in different calorimeter setups cannot be directly compared. Table 4 shows that the combined standard uncertainty ($k = 1$) in the recent kV calorimeters is superior to that

of Seuntjens *et al* (1993) and generally sub-percent. The kV water calorimeters have been used in the determination of correction factors for Farmer-type ionization chambers for reference dosimetry in kV beams (e.g. see Perichon *et al* (2013) and Krauss *et al* (2012)) and will allow the data specified in the codes of practice for kV dosimetry to be updated.

Of special note is the effect noticed in the calorimeter signal trace at onset and end of irradiation (see figure 6). This effect had been observed in calorimeter studies in kV beams throughout times (Seuntjens *et al* 1988, de Prez *et al* 2008, Krauss *et al* 2012) and not in MV beams and had been attributed prima facie to excess heat effects due to direct energy absorption in the thermistors and leads. It had also been assumed that the effect at onset and at the end of the irradiation compensate each other and the overall effect on a dose determination could be ignored. Using detailed modeling of the components in the thermistor probes, Krauss *et al* (2012) confirmed this assumption and demonstrated that the effect was due to a combination of effects of the leads and a radiation induced current in the leads.

5.2. Graphite calorimetry

Recently, Pinto *et al* (2016) described a graphite-in-water calorimeter system not unlike the probe-format graphite calorimeter of Renaud *et al* (2013) or Sundara Rao and Naik (1980) but now applied to the determination of absorbed dose to water in medium energy x-rays in comparison with air kerma-based dose to water determination. The calorimeter is composed of three bodies with a disc-shaped core of 21 mm diameter and 2 mm thickness weighing 1.134 g, sealed in a PMMA waterproof envelope with air-evacuated gaps. The measured signal is converted into absorbed dose to graphite by taking into account heat loss and foreign mass effects. In kV beams, the latter are particularly sensitive to small amounts of non-graphite materials used in the calorimeter and amounted to corrections of 1.115 (0.5%) and 1.066(0.5%) for radiation qualities of 180 kV (HVL 1.0 mm Cu) and 250 kV (HVL 2.5 mm Cu), respectively. Absorbed dose to graphite was converted into absorbed dose to water using a MC-calculated dose conversion factor. The authors indicate that in-water-phantom graphite calorimetry poses increasing challenges with lower photon energies. The overall standard uncertainty on absorbed dose to water using this system was 1.9% ($k = 1$) and was mainly due to signal reproducibility, foreign mass correction and the conversion of dose to graphite into dose to water.

6. Proton beams

The adoption of proton therapy has been relatively slow in comparison to high-energy photon-based modalities though at least 81 facilities are in clinical operation, with another 40 under construction as of April 2019 (Particle Therapy Co-Operative Group, PTOCOG 2019). This section summarizes to some extent, but also expands on, previous reviews on the topic of the use of calorimeters in proton beams given in Palmans *et al* (2009), Karger *et al* (2010), Palmans (2011), Palmans and Vatnitsky (2015), Palmans (2017), Palmans (2018a, 2018b) and Giordanengo and Palmans (2018). The section reviews water, graphite and tissue-equivalent calorimetry and discusses the main aspects that are different for proton beams as compared to previously discussed general issues. Table 5 summarizes the main characteristics and performance of recent proton and carbon-ion water calorimeters, as reported in the literature.

6.1. Water calorimetry

At least three distinct types of water calorimeters have been used for reference dosimetry in proton beams. The first type was used by Schulz *et al* (1992), Siebers *et al* (1995), Vatnitksy *et al* (1996) and Hashemian *et al* (2003) and consist of a glass water phantom containing high-purity water in which the thermistor probes are embedded at a fixed position and which is thermally controlled by water flowing in a mantle around the phantom. A second type is based on the sealed water calorimeter concept of Domen (1994) and was used in protons by Seuntjens *et al* (1994), Palmans *et al* (1996), Medin *et al* (2006), Medin (2010), Sarfehnia *et al* (2010) and Gagnebin *et al* (2010). These consist of a sealed PMMA or glass vessel with a cylindrical or pancake shape containing high-purity water in which the thermistor probes are positioned and that is suspended in a larger water phantom with water of lower purity. A variation of this with a vessel which was not suspended in water was used by Renaud *et al* (2016) for measurements in a low-energy proton beam. A third type of water calorimeter was use by Brede *et al* (2006) and Giesen and Beck (2014) and consists of a gilded aluminium container with high-purity water which is suspended in vacuum.

Heat defect in proton beams is not very well known, as the production of primary species is LET dependent. Elliot (1994) and Ross and Klassen (1996) have comprehensively compiled data chemical yields as a function of LET and numerous investigations have been performed to calculate the chemical heat defect of aqueous systems in protons (Seuntjens *et al* 1994, Palmans *et al* 1996, Brede *et al* 1997, Sassowsky and Pedroni 2005, Medin *et al* 2006, Brede *et al* 2006). Those investigations have resulted in the following observations:

Table 5. Main characteristics and performance of recent proton and carbon-ion water calorimeters reported in the literature.

Study	PTB (Brede *et al* 2006)	Lund University (Medin 2010)	METAS (Gagnebin *et al* 2010)	McGill University (Sarfehnia *et al* 2010)	McGill University (Renaud *et al* 2016)	PTB (Osinga-Blattermann *et al* 2017)
Vessel type	Parallel plate	Cylindrical	Parallel plate	Parallel plate	Parallel plate	Parallel plate
Vessel material	Gilded aluminum	Glass	Glass	Glass	Glass	Glass
Vessel wall thickness	0.3 mm	1 mm average	1 mm	1.12 mm	1.12 mm	0.7 mm
Beam type	Protons (scattered) 32 MeV; protons (scattered) 182 MeV; carbon-ions (scanned) 430 MeV/u	Protons (scanned) 180 MeV	Protons (scanned) 250 MeV	Protons (scattered & scanned) 235 MeV	Protons (monoenergetic & scattered) 60 MeV	Carbon-ions (scanned) 429 MeV/u
Depth of measurement	20 mm	Water equivalent depth of 6.0 cm	16.8 cm	Water equivalent depth of 12.6 cm	Water equivalent depth of 11 mm	50 mm
Water system used and heat defect	Described in Brede (2004); $h = 0.4\% \pm 0.3\%$ (protons, 32 MeV); $h = 0.3\% \pm 0.3\%$ (protons, 182 MeV); $h = 1.0 \pm 0.5$ (carbon ions, 430 MeV/u)	N_2-saturated $h = 0.001 \pm 0.003$	N_2-saturated $h = 0.0$	H_2-saturated; $h = 0.0$	H_2-saturated $h = 0.0$	H_2-saturated $h = 0.0$
Non-water radiation perturbation correction, k_p	Not reported	$1.0009 \pm 0.05\%$	Not reported	less than 0.1%	Not reported; accounted for by mock vessel	$1.0021 \pm 0.21\%$
Excess heat perturbation correction	Described in Brede *et al* (2000)	$0.999\% \pm 0.1\%$	Not reported	$0.996 \pm 0.2\%$ (scattered beam); $0.953 \pm 0.5\%$ (scanned beam)	$1.021\% \pm 0.4\%$ (monoenergetic beam); $1.024 \pm 0.3\%$ (scattered beam)	$1.0177\% \pm 0.5\%$
Combined relative standard uncertainty on absorbed dose to water	1.5% (protons, 32 MeV); 1.4% (protons, 182 MeV); 1.8% (carbon-ions, 430 MeV/u)	0.5%	on the order of 5%	0.4% (scattered beam); 0.6% (scanned beam)	0.6% (monoenergetic beam); 0.7% (scattered beam)	0.7%

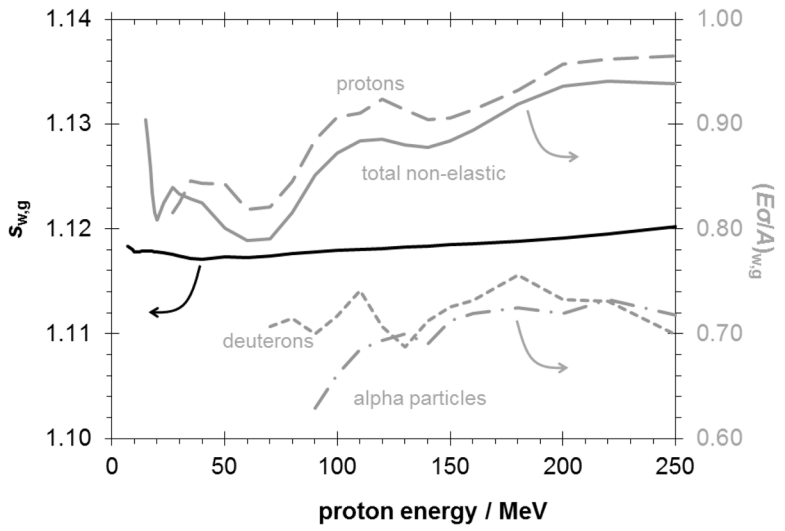

Figure 8. Water-to-graphite stopping power ratio as a function of proton energy from ICRU Report 90 and ratios of energy transferred per unit mass in non-elastic nuclear interactions (total and to the production of protons, deuterons and alpha particles) from ICRU (2000).

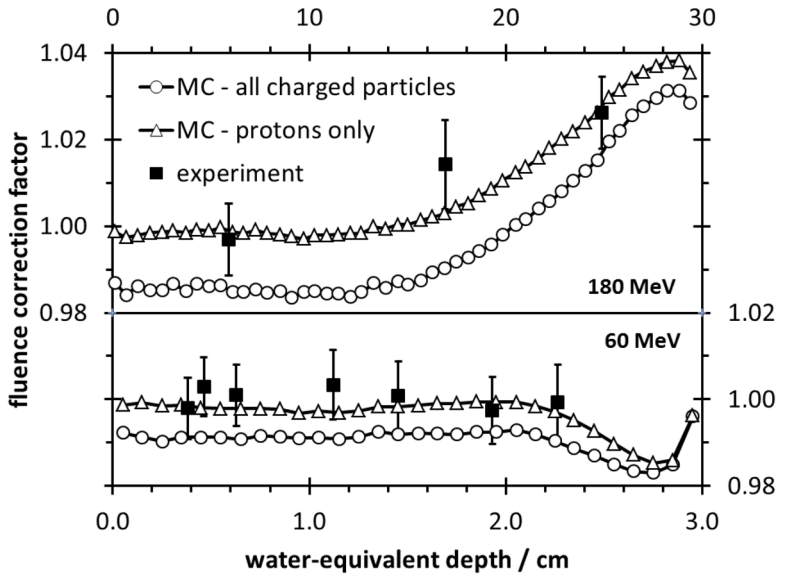

Figure 9. Fluence correction factors for the conversion of dose to graphite to dose to water using graphite to water mass stopping power ratios for two pristine proton beam energies calculated using FLUKA MC simulations and determined experimentally using plane-parallel ionization chambers (data extracted from Lourenço *et al* (2016)). Results are shown for small charged particles but also considering only protons to show that the contributions by the latter are in better agreement with experiments. This can be explained by the short range of heavier secondary particles with insufficient energy to penetrate the wall of the ionization chambers and thus their in-phantom dose contributions are not detected.

- For low-LET protons, pure water saturated with a chemically inert gas such as Ar or N_2 exhibits a small (sub-promille) initial chemical heat defect reaching a steady state after a modest accumulated radiation dose, similarly as in photon beams (Seuntjens *et al* 1994, Palmans *et al* 1996). For high-LET protons, on the other hand, the net production of hydrogen peroxide results in a steady increase of the chemical energy in the aqueous system resulting in a non-zero endothermic chemical heat defect (Sassowsky and Pedroni 2005).
- For the entire proton LET-range, pure water saturated with H_2 results in a zero chemical heat defect due to the enhanced decomposition of hydrogen peroxide as compared to the pure water system saturated with argon or nitrogen (Seuntjens *et al* 1994, Palmans *et al* 1996, Medin *et al* 2006). However, as discussed for photon beams, when initial trace oxygen concentrations are present, pure water saturated with hydrogen exhibits an initial exothermic chemical heat defect that increases to very substantial values until oxygen becomes depleted after which the chemical heat defect drops rapidly to zero (Seuntjens *et al* 1994, Palmans *et al* 1996, Sarfehnia *et al* 2010). This makes it an attractive system since this marked time dependence

provides a way of monitoring at what cumulative dose the steady-state zero chemical heat defect condition is reached.

- For a mixed LET proton field (in the spread-out Bragg peak (SOBP) of a modulated proton beam) it was shown that water with a known quantity of sodium formate as a deliberate impurity saturated with oxygen exhibits an exothermic heat defect about half in size of that in a Co-60 beam with the same average dose rate (Seuntjens *et al* 1994, Palmans *et al* 1996). This was explained by the variation of the chemical yields as a function of LET combined with the detailed time structure of the production of chemical species due to the beam modulation.

The experiments that have contributed to the validation of these theoretical results can be separated in two categories:

1. Total absorption experiments comparing irradiation heating in water with that in a metal (Roos *et al* 1992). The same number of protons is totally absorbed in either the water component or the metal component of a dual water/metal absorber that forms a single thermal body. From the difference in the temperature rise observed in both irradiations the chemical heat defect of water can be derived under the assumption that the chemical heat defect in the metal is zero. Using aluminium as a metal in such a dual absorber system Brede *et al* (1997) demonstrated that the chemical heat defect of pure water irradiated by protons is slightly endothermic but within experimental uncertainties not significantly different from zero.
2. Relative determinations of the chemical heat defect of pairs of water systems by comparing their relative response to a given dose. In this manner, the initial exothermicity of the hydrogen system in the presence of trace oxygen concentrations was demonstrated for protons as well as the relative agreement of the steady state responses of the hydrogen-saturated water system with the nitrogen- or argon-saturated water system (Seuntjens *et al* 1994, Palmans *et al* 1996). Also, the lower chemical heat defect of the oxygen-saturated sodium formate aqueous solution under modulated proton irradiation as compared to photon irradiation was demonstrated experimentally in the same work.

Since heat conduction bears no relation with the source of temperature differences, the same considerations as for photon beams apply. For irradiations lasting not more than a few minutes, heat losses are in general small when the distance from the measurement point to regions with high thermal gradient is at least 3 cm. In addition to adequate distance from the penumbrae, the measurement point should also be sufficiently far away from the Bragg peak or the distal edge of the SOBP. In narrow low-energy proton beams (e.g. as used for treatment of eye melanoma), these conditions cannot be achieved, however, and corrections must be applied contributing also larger uncertainties to the absorbed dose to water (Renaud *et al* 2016). Also, the need to keep the high-purity water containing glass vessel small for such low-energy beams results in heat transfer correction factors that are very sensitive to the exact position of the thermistor within the glass vessel as shown in figure 7; over a range of depths spanning not more than 10 mm, the correction factor varies by almost 6%. The increases at the extremes of the range are dominated by excess heat from the front and back glass walls of the vessel, while the difference between pristine and modulated beams at the larger depths is due to the extra excess heat from the Bragg peak in the pristine beam.

Upon first impression, it may appear that scanned proton beams introduce another level of complication to the heat transfer problem since large and time-dependent gradients will be present when the pencil beam passes the measurement point. However, it has been demonstrated theoretically (Sassowsky and Pedroni 2005) and confirmed experimentally (Sarfehnia 2010, Sarfehnia *et al* 2010) that if the painting of a target volume takes no more than 2 min–3 min, the correction for heat conduction and its uncertainty are very similar as for a passively scattered broad proton beam irradiation of a similar target volume for the same duration. Also, the excess heat in scanned beams due to the presence of non-water materials (e.g. glass vessels and thermistors probes) has been found to be similar as for passively scattered beams (Sarfehnia *et al* 2010).

The non-uniformity correction often requires special consideration in proton beams. The main non-uniformity correction to account for in a sealed-water calorimeter is due to the vessels used to contain the high-purity water needed to control the chemical heat defect. One way around this is to compare the calorimeter response with that of an ionization chamber in the same position as the thermistors within the vessel or within a mock vessel that creates the same attenuation and scatter as the one used in the calorimeter as was for example demonstrated by Renaud *et al* (2016). But for practical reasons, ionization chamber dosimetry is usually performed in the calorimeter phantom in absence of the vessel and any perturbation of the fluence at the point of measurement by the vessel thus must be corrected for. Palmans (2013) used two independent MC codes to calculate the correction factor, k_{vessel}, for glass vessels of 1 mm thickness in the entrance region of pristine proton beams as the ratio of dose to water in a small volume around the measurement point in the absence and in the

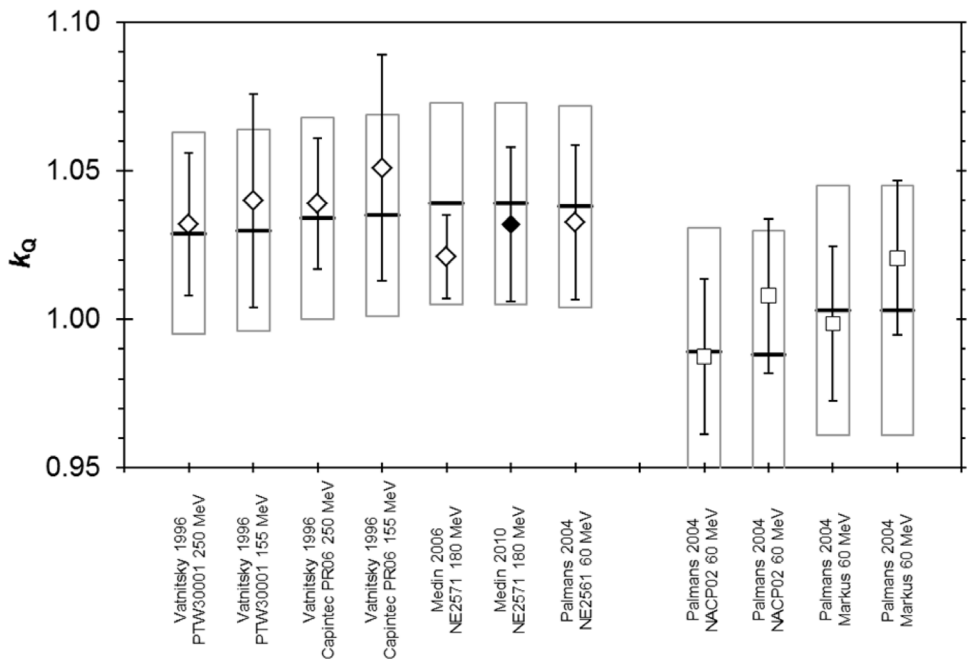

Figure 10. Experimental k_Q values for proton beams obtained from comparing ionization chambers with calorimeters compared with theoretical k_Q values in from TRS-398 (horizontal lines with boxes as uncertainty intervals) for reference-class cylindrical ionization chambers (left group of data) and plane-parallel chambers (right group of data). All hollow data points were obtained in scattered beams while the filled diamond data point was obtained in a scanned beam. Uncertainties are expressed at 95% confidence level based on the information given in the publications.

presence of the vessel. Assuming that the correction varies linearly with the vessel wall thickness, the results can be summarized using the following expression:

$$k_{\text{vessel}} = 1 - 0.18 \cdot t \cdot \left(1 - \frac{1}{1 + 0.3 \cdot R_{\text{res}}^{-1.45}}\right) \tag{9}$$

where t is the thickness (in mm) of the vessel wall along the beam direction, regardless of its shape (typically cylindrical or pancake) and R_{res} is he residual range (in cm), the distance from the measurement point to the 10% dose level distal to the Bragg peak. The maximum vessel thickness and minimum residual range for which this expression was obtained were 1.1 mm and 1 cm, respectively. Some researchers have also measured this correction by measuring the response of a small ionization chamber at the measurement point in the vessel in the absence and in the presence of the vessel (e.g. Medin *et al* (2006)) and those experimental results are in good agreement with expression 10. For measurements in an SOBP, the correction is found to be negligible.

Typical relative standard uncertainties on absorbed dose to water with water calorimeters amount to 0.4% to 1%, dominated by contributions from the chemical heat defect, heat conduction and thermistor calibration (Palmans *et al* 1996, Sassowsky and Pedroni 2005, Medin *et al* 2006, Medin 2010, Sarfehnia *et al* 2010, Renaud *et al* 2016).

6.2. Graphite and tissue-equivalent calorimetry

Solid calorimeters used for reference dosimetry in proton beams are all similar in concept to the Domen and Lamperti (1974) design consisting of a thin plane-parallel cylindrical core separated from the environment by one or more air-filled or vacuum gaps (Delacroix *et al* 1997, Palmans *et al* 2004, Petrie 2016, Thomas *et al* 2019).

In graphite calorimeters, a physical heat defect results from the changes in lattice energy due to the creation and annihilation of interstitial defects. This physical heat defect is generally assumed to be small but given the higher probability of a sufficient energy transfer to a recoil nucleus it will be larger in proton beams than in photon beams. This physical heat defect has been demonstrated experimentally for graphite moderators in nuclear reactors after receiving a dose of the order 100 Gy. When a sample of such highly exposed graphite is heated to temperatures above 250 °C, a measurable excess heat, amounting to 0.2% of the total energy deposited by radiation, is observed in the sample due to the release of the so-called Wigner energy resulting from the annealing of lattice defects (IAEA 2000). It is not clear, however, how these results translate to radiotherapeutic dose levels (Ramanathan 2008). Schulz *et al* (1990) designed an experiment of a similar principle as the dual-absorber experiment of Brede *et al* (1997). In a dual graphite/aluminium absorber, the rise in temperature due the same number of protons totally absorbed either in the graphite or in the aluminum part of the absorber forming a

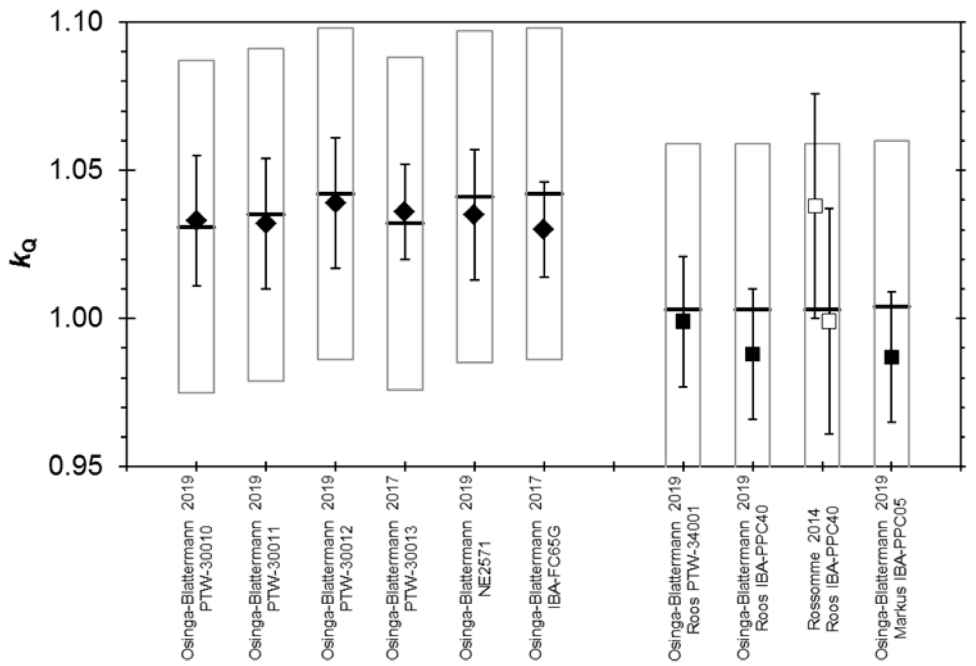

Figure 11. Experimental k_Q values for carbon ions obtained from comparing ionization chambers with calorimeters compared with theoretical k_Q values in from TRS-398 (horizontal lines with boxes as uncertainty intervals) for Farmer type cylindrical ionization chambers (left group of data) and plane-parallel chambers (right group of data). The full symbols represent data points obtained in scanned beams while the two hollow symbols represent two data points obtained during different measurement sessions in a scattered beam. Uncertainties are expressed at 95% confidence level based on the information given in the publications.

single thermal mass was measured and compared. Assuming the heat defect of aluminium to be zero, an endothermic heat defect of 0.4% with a standard uncertainty of 0.3% was observed for graphite indicating that the physical heat defect in graphite must be limited to a few tenths of a percent, and thus of similar magnitude as in the annealing experiment described above.

Graphite calorimeters can also exhibit a chemical heat defect. One mechanism that has been suggested is the reaction of graphite with oxygen present in the grain boundaries resulting in an exothermic heat defect. Bewley and Page (1972) observed an initial over response of 2% of a graphite calorimeter that disappears after sufficient pre-irradiation with the calorimeter operated in vacuum and ascribed the effect to reaction of graphite with oxygen diffused into the calorimeter grain boundaries. A similar mechanism of a reaction of the calorimeter medium with dissolved oxygen has been suggested to explain an initial chemical heat defect of 10% that disappears after irradiation observed in calorimeters made of tissue-equivalent plastic A-150 (Bewley *et al* 1972), which used to be designed for neutron dosimetry, but have also been applied to the dosimetry of proton beams (Verhey *et al* 1979, Delacroix *et al* 1997). In A-150, another suggested mechanism for a chemical heat defect is the dissociation of polymers which can explain the endothermic heat defect of about 4% observed in similar total absorption experiments as described above using dual A150/aluminium absorbers (Fleming and Glass 1969, MacDonald and Goodman 1982, Schulz *et al* 1990).

Ideally, temperature profiles within a small irradiated sample of graphite re-distribute within a time interval much shorter than the irradiation time itself. However, due to the Bragg peak and the sharp distal edge, it is more difficult to achieve the quasi-adiabatic condition in proton beams, since steep temperature gradients often cannot be kept far enough away from the core, especially in low-energy proton beams. Shielding the influence of those steep gradients can be achieved by inducing more vacuum gaps. Another strategy that has been used is to match the size of graphite parts beyond the core such that the energy deposited per unit mass in those parts equals the absorbed dose in the core (Palmans *et al* 2004).

For scanned proton beams, the interplay between the rapidly varying and steep instantaneous dose distributions combined with the high thermal diffusivity of graphite and the much slower radiative heat transfer may lead to a very complex pattern of heat transfer between the core and the surrounding medium. Petrie (2016) studied the heat transfer in a graphite calorimeter, first for static narrow beams and then for a full scanned beam in passive mode (similar to quasi-adiabatic mode without active temperature control of the inner components but given the varying temperature difference between core and jacket it cannot be called quasi-adiabatic during irradiation). In the first study, different parts of the calorimeter (core, first jacket, second jacket and body) were exposed to static narrow proton beams and the heating in other components measured and it was shown that the experimental observations could be modelled accurately by heat transfer simulations. Subsequent experiments

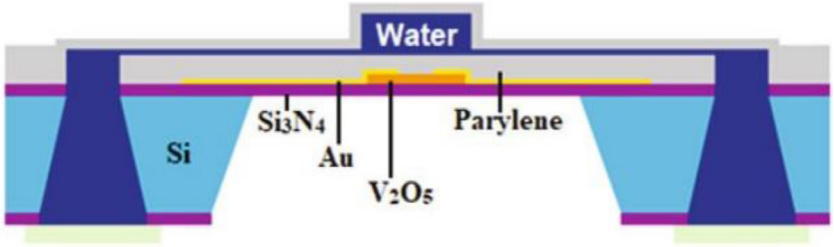

Figure 12. Cross-sectional schematic view of the MFC detector prototype (not to scale). Each of the Si_3N_4, Au, and V_2O_5 layers is several hundred nm thick (Reproduced with permission from Schaarschmidt *et al* (2019) , reprinted by permission from Springer Nature, Journal of the Korean Physical Society, Schaarschmidt *et al* 2019, © The Korean Physical Society 2019.).

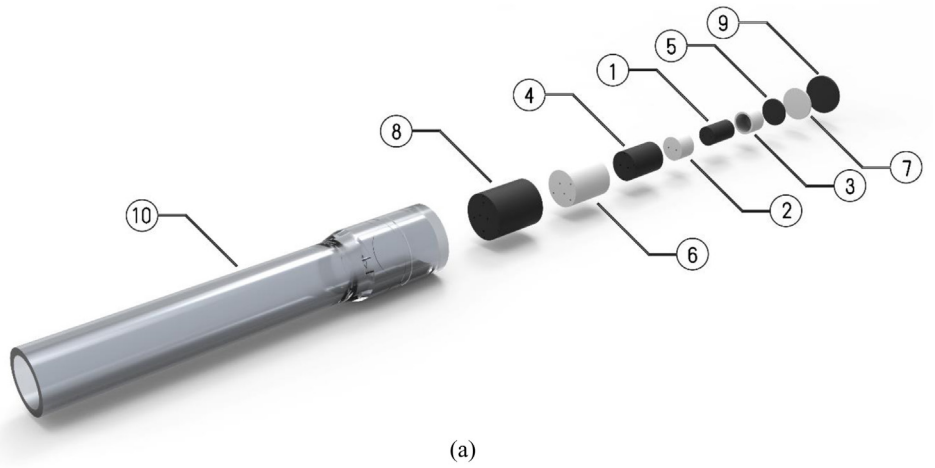

(a)

(b)

Figure 13. Examples of probe format calorimeters developed by (a) McGill University, and (b) NPL. The blown-up schematic of the McGill probe (i.e. Aerrow) depicts the constituent graphite and aerogel components (by number, they are: (1) the graphite core, 6.1 mm wide, 10 mm long; (2) and (3) the two halves of the inner aerogel layer, both 0.7 mm thick; (4) the graphite jacket and (5) jacket cap, both 0.7 mm thick; (6) the outer aerogel layer and (7) aerogel cap, each 1.0 mm thick; (8) the graphite shield and (9) shield cap, both 1.0 mm thick; and (10) the acrylic (PMMA) stem to envelop and waterproof the calorimeter assembly). The NPL IMRT differs in that it has a spherical core (5 mm diameter) and only one surrounding graphite layer (reproduced from Duane *et al* (2012), © 2012 BIPM & IOP Publishing Ltd. All rights reserved.).

and simulations of fully scanned high-energy proton beam delivery sequences showed that, similarly as in water calorimeters, the net heat transfer in graphite calorimeters exposed to a scanned box field is very comparable with that in a broad beam uniform dose distribution with the same total irradiation time. Practical experience with isothermal operation mode in scanned beams has shown that this mode presents a considerable challenge for the typical, rather slow, control systems used in graphite calorimeters (Petrie 2016).

For graphite calorimeters in charged particle beams, an important source of uncertainty is the conversion of dose to the graphite to dose to water (Palmans *et al* 2013). The simplest conversion model assumes that the charged particle spectra at equivalent depths in water and graphite (scaled by the CSDA ranges of both materials) are identical so that the ratio of dose to water in water and dose to graphite in graphite equals the water-to-graphite mass stopping power ratio for the charged particle spectrum. Figure 8 shows that the variation of the water-to-graphite stopping power ratio with energy is small and can for most applications in clinical proton beams be assigned a constant value of 1.118. However, the assumption that the particle spectra are identical at equivalent depths is only approximately fulfilled. Deviations result from differences in the absorption of primary protons by non-elastic nuclear interactions and in the production of secondary charged particles in water and graphite. Figure 8 also presents ratios of energy transferred in nuclear interactions per unit of mass showing that they are very different from the stopping power ratios. Palmans *et al* (2013) have formally defined a fluence correction factor, k_{fl}, that must be factored in the conversion formula:

$$D_w = D_g \cdot s_{w,g} \cdot k_{\mathrm{fl}} \tag{10}$$

where k_{fl} can be calculated as:

$$k_{\mathrm{fl}} = \frac{\sum_i \left[\int_0^{E_{\max,i}} \Phi_{E,w,i} \cdot (S/\rho)_{g,i} \cdot dE\right]}{\sum_i \left[\int_0^{E_{\max,i}} \Phi_{E,g,i} \cdot (S/\rho)_{g,i} \cdot dE\right]} \tag{11}$$

where $\Phi_{E,w,i}$ and $\Phi_{E,g,i}$ are the spectra, differential in energy, of charged particle species, i, at equivalent depths in water and graphite.

Several studies have quantified the fluence correction factor for graphite by MC simulations in which the integrals in equation (11) were either calculated in-line or derived retrospectively from calculated spectra. For low-energy proton beams (e.g. 60 MeV), Palmans *et al* (2013) and Lourenço *et al* (2016) calculated with a range of different MC codes that k_{fl} is not more than 1% different from unity, while for high-energy protons Lourenço *et al* (2016) found substantially larger fluence corrections of up to 4%, depending on depth (but limited to 2% for depths up to ¾ of the range). Experiments using ionization chambers have confirmed these MC calculated values to the extent that the observed corrections coincide with the contribution of primary beam attenuation and energetic secondary protons to the fluence correction factor. Non-negligible contributions by short-range alpha particles or heavier fragments generated in water or graphite that cannot reach the cavity of the ionization chamber are not included in the experimentally determined fluence correction factors as shown in figure 9. For A-150 tissue-equivalent plastic, Al-Sulaiti *et al* (2010) and Lourenço *et al* (2017a) showed by MC simulations that the fluence correction factors are close to unity.

As for non-uniformity and volume averaging corrections, no experimental data has been reported and the only information comes from MC simulations. Gap corrections can be assessed by calculating the ratio of the average dose over the core with all gaps substitute by graphite and the average absorbed dose in the presence of the gaps. This approach is called the substituted gap scheme but usually gap corrections are evaluated in a compensated gap scheme in which components are first shifted along the beam axis so that there are no gaps upstream of any component; the gaps downstream are consequently expanded and filled up with graphite material in the simulation. Palmans *et al* (2004) were the first to report MC-simulated gap corrections for a small-body calorimeter used in a 3 cm diameter low-energy proton beam; compensated gap corrections were found to be negligible but substituted gap corrections at shallow depth in a 60 MeV proton beam were found to be 2% and increasing with depth due to the substantial depth dose gradient in such low-energy beams. This indicates that it is very advantageous to account for the graphite material effectively present upstream the core to determine the depth of measurement rather than the physical distance between the surface and the centre of the core. More recent simulations (Petrie *et al* 2017) show that for narrow beams of 3 cm diameter, the compensated gap correction increases with energy and amounts to about 1% for the highest clinical proton beams at 2 cm depth due to a reduced production of secondary protons by the presence of the gaps. For broad beams the corrections are again much smaller (Romano *et al* 2019). Volume averaging corrections are also found to be negligible in most situations and only in pristine beams at residual ranges less than 0.5 cm, which would in most cases not be a suitable condition for reference dosimetry, the correction for a 2 mm thick core becomes larger than 0.5% (Palmans 2013).

Typical relative standard uncertainties on absorbed dose to water with graphite calorimeters amount to 1% to 2% dominated by contributions from the water-to-medium mass stopping power ratio, fluence corrections factors, electrical calibration and heat transfer (Palmans *et al* 2004). For A-150 calorimeters, in addition, the chemical heat defect contributes substantially to the uncertainty and overall uncertainties are 2% to 3% (Schulz *et al* 1990, Delacroix *et al* 1997, ICRU 1998).

Table 6. Main characteristics and performance of recent Ir-192 HDR brachytherapy water calorimeters reported in the literature.

Study	PTB (Bambynek *et al* 2009)	McGill University (Sarfehnia *et al* 2010)	VSL (de Prez and de Pooter 2012)
Vessel type	Parallel plate	Parallel plate	Cylindrical with a cavity along its major axis
Number of thermistors	2	2	4
Source-detector distance	(24.5–48.37) mm	(25–70) mm	20 mm
Irradiation time	60 s, 90 s, and 120 s	(200–300) s	60 s
Non-water radiation perturbation correction, k_p	1.005 ± 0.002	1.003 ± 0.001	1.4% accounting for the presence of aluminum heat sink
Excess heat perturbation correction	0.978–1.082 depending on the position, irradiation time, and analysis method	Nominally 0.96% with convection considered	1.5%
Combined relative standard uncertainty on absorbed dose to water	0.9%	1.9%	2%

Table 7. Main characteristics and performance of recent Ir-192 HDR brachytherapy graphite calorimeters reported in the literature.

Study	ENEA-INMRI (Guerra *et al* 2012)	NPL (Sander *et al* 2012)
Core geometry and size	Ring-shaped (diameter = 50 cm, with a rectangular cross-section of 2 mm × 5 mm)	Ring-shaped (inner & outer radius = 24 mm & 26 mm; height = 5 mm)
Gap size	0.75 mm	1 mm
Source-detector distance	2.5 cm	2.5 cm
Graphite phantom dimensions	Height = 30 cm; diameter = 30 cm	Height = 14 cm; diameter = 20 cm
Radiation perturbation correction due to gaps, k_{gap}	0.998 ± 0.002	0.9992 ± 0.0004 & 0.9987 ± 0.0006 as calculated with EGSnrc & FLUKA
Correction for source self-heating	0.997 for irradiation of 120 s	Not reported
Graphite-to-water conversion factor	6.890 ± 0.013	6.90 ± 0.02 and 6.92 ± 0.03 as calculated with EGSnrc and FLUKA, respectively
Combined relative standard uncertainty on absorbed dose to water	1.38% (quasi-adiabatic mode)	1.02% for quasi-adiabatic mode operation and 0.68% for quasi-isothermal mode

6.3. Review of measured k_Q data

Numerous comparisons of water calorimeters (Schultz *et al* 1992, Seuntjens *et al* 1994, Siebers *et al* 1995, Palmans *et al* 1996, Medin *et al* 2006, Medin 2010, Sarfehnia *et al* 2010, Gagnebin *et al* 2010), graphite calorimeters (Palmans *et al* 2004) and A150-calorimeters (Delacroix *et al* 1997) with ionization chambers have been reported that have contributed to evaluations of the mean energy required to produce an ion pair in dry air, W_{air} (Jones 2006, Palmans and Vatnitsky 2016a) confirming the value of 34.2 eV that has been used in IAEA TRS-398 (Andreo *et al* 2000) for the calculation of beam quality correction factors, k_Q. For example, from a comparison of a water calorimeter with an ionization chamber in a proton beam with beam quality, Q, and comparison of the same two instruments in a Co-60 calibration beam, the value of $(W_{air})_Q$ for the proton beam can be derived as:

$$(W_{air})_Q = \frac{D^{cal}_{w,Q}}{D^{cal}_{w,Co\text{-}60}} \frac{M_{Co\text{-}60}}{M_Q} \frac{(W_{air})_{Co\text{-}60} \cdot (s_{w,air})_{Co\text{-}60} \cdot p_{Co\text{-}60}}{(s_{w,air})_Q \cdot p_Q} \quad (12)$$

where $D^{cal}_{w,Q}$ and $D^{cal}_{w,Co\text{-}60}$ are the absorbed dose to water determined by the water calorimeter in the proton beam and the Co-60 beam, respectively, M_Q and $M_{Co\text{-}60}$ are the ionization chamber readings, corrected for influence quantities in the proton beam and the Co-60 beam, respectively, $(W_{air})_{Co\text{-}60}$ is the mean energy required to produce an ion pair in dry air in Co-60, $(s_{w,air})_Q$ and $(s_{w,air})_{Co\text{-}60}$ are the Spencer-Attix stopping power ratio for the charged particle spectrum at the measurement point in the proton beam and the Co-60 beam, respectively, and p_Q and $p_{Co\text{-}60}$ are the fluence perturbations by the presence of the ionization chamber in water in the proton beam and the Co-60 beam, respectively. A number of papers have also reported directly measured beam quality correction factors (Vatnitsky *et al* 1995, Palmans *et al* 2004, Medin *et al* 2006, Medin 2010, Sarfehnia *et al* 2010). Figure 10 shows k_Q-values obtained by comparing ionization chambers with water and graphite calorimeters both in passively scattered proton beams and in scanned proton beams for a number of reference-class ionization

chambers. These data are either obtained by comparing the response of the ionization chamber with that of the calorimeter in both the proton beam as in the calibration beam or by comparing the response of an ionization chamber, calibrated in terms of absorbed dose to water in a standards laboratory, with that of the calorimeter in the proton beam only. As can be observed in figure 10, all the results are within uncertainties in agreement with the theoretical values from IAEA TRS-398. The good agreement between results in scattered and scanned beams for the same chamber type also indicates that those different beam delivery modes do not affect the beam quality correction factors, the same conclusion as was reached by Sorriaux *et al* (2017) based on MC simulations.

7. Carbon ion beams

7.1. Water calorimetry

According to PTGOC, there are presently 13 carbon-ion therapy facilities in operation in five countries (Austria, China, Germany, Italy, Japan), with another 5 facilities under construction (PTCOG 2019). Two types of water calorimeters have been used for reference dosimetry in carbon beams. Holm *et al* (2019) and Osinga-Blattermann *et al* (2017) used a sealed water calorimeter according to the concept of Domen (1994) which was similar as the primary standard calorimeter of PTB described by Krauss (2006a). Brede *et al* (2006) used a water calorimeter consisting of a gilded aluminium container with high-purity water which is suspended in vacuum.

Using the same dual-component total-absorption calorimeter as for protons (see section 6.1) Brede *et al* (1997, 2006) showed that the endothermic heat defect in pure water increases with LET saturating to a value of about +4% for 100 keV μm^{-1} alpha particles. Palmans (2011, 2018b) proposed an exponential function as an adequate fit to those data with corresponding uncertainty estimates on the fit parameters:

$$h = (0.041 \pm 0.004) \cdot \left(e^{-(0.035 \ \pm \ 0.010) \cdot LET} - (1.000 \pm 0.001)\right) \tag{13}$$

where the LET is expressed in keV μm^{-1}.

Since the dose distributions in which reference dosimetry for carbon ions is performed are generally very similar to those in proton beams and the delivery modes are generally very similar (scattered or scanned), the behaviour of heat conduction is also similar. Osinga-Blattermann *et al* (2017) calculated the heat conduction correction for a scanned carbon ion beam and found it to be limited to 0.2%.

7.2. Graphite calorimetry

Sakama *et al* (2008, 2009) performed graphite calorimetry but did not go into the conversion from absorbed dose to graphite to absorbed dose to water. The core used was 20 mm diameter and 2 mm thick and surrounded by two jackets (the outer one denoted as shield). An impurity correction smaller than 0.1% was estimated and no other perturbation corrections were accounted for. Rossomme *et al* (2014a) performed graphite calorimetry in an 80 MeV per nucleon unmodulated carbon ion beam. The measurements were performed in a nuclear physics accelerator centre rather than in a clinical environment. The calorimeter core had a diameter of 16 mm closely coinciding with the collecting electrode diameter of a Roos chamber and a thickness of 2 mm. No corrections for gaps and non-graphite impurities were applied.

Regarding heat defect, no information is available, but it should be expected that the heat defect due to the formation of lattice defects is higher for carbon ions as for protons. Corrections accounting for heat conduction is treated the same as in proton beams, with the only difference being that the depth dose distribution in the SOBP is not necessary uniform. Given that the gradient remains approximately constant, this may not be an issue, but it warrants further investigation.

For the calculation of stopping power ratios as a function of depth for ion beams, Lühr *et al* (2011a) proposed and validated the following approximation:

$$s_{w,g}(z_w) = \frac{\left(\frac{Z}{A}\right)_w \cdot \ln\left(\frac{E_0}{I_w}\right) + 0.58824 \cdot \ln\left(1 - \frac{z_w}{R_p}\right) - 6.1291}{\left(\frac{Z}{A}\right)_g \cdot \ln\left(\frac{E_0}{I_g}\right) + 0.58824 \cdot \ln\left(1 - \frac{z_w}{R_p}\right) - 6.1291} \tag{14}$$

where z_w is the depth in water, Z/A is the ratio of the atomic number and atomic weight of the material, E_0 is the incident ion beam energy, I is the mean excitation energy and R_p is the practical range in water. For clinical beam energies and residual ranges above 1 cm, the water to graphite stopping power ratio has an almost constant value of 1.120 (deviations not more than 0.2%) using the most recent recommendations of ICRU Report 90 (ICRU 2016).

Fluence correction factors for the conversion from dose to graphite in a graphite (calorimeter) phantom to dose to water in water are defined in the same way as for protons. Lühr *et al* (2011b) were the first to quantify this fluence correction factor by MC simulations for carbon ions obtaining corrections of less than 0.5% for low-energy beams but that could increase with depth to 2% for higher clinical energies. Rossomme *et al* (2013) studied this both by MC simulations and experiment in a low-energy (80 MeV per nucleon) carbon ion beam

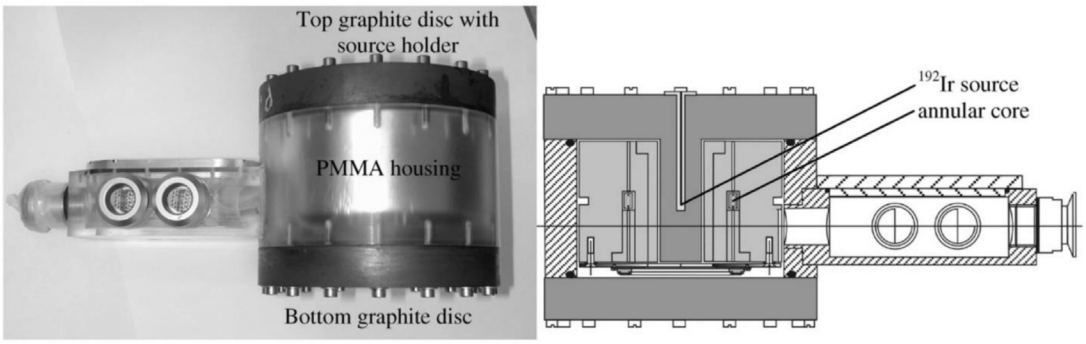

Figure 14. (Left) Lateral view and (right) schematic section of the ENEA-INMRI HDR graphite calorimeter. The ring-shaped core is 50 mm in diameter and the external PMMA housing is 130 mm in diameter and 105 mm in height (reproduced from Guerra *et al* (2012), © 2012 BIPM & IOP Publishing Ltd. All rights reserved.).

and found also that corrections were limited to 0.5%. Lourenço *et al* (2017b) performed a similar experimental and MC study (using FLUKA) in a higher-energy carbon ion beam (290 MeV per nucleon) with both methods consistently resulting in small corrections at shallow depth that increase to 2% at depths in the vicinity of the Bragg peak but the corrections were in the opposite direction as those found by Lühr *et al* (2011b) using a different MC code (SHIELD-HIT).

7.3. Review of measured k_Q data

Sakama *et al* (2009) compared two Farmer-type ionization chambers and three plane-parallel ionization chambers with the calorimeter. All analysis was performed in terms of dose to graphite, while no information was given on the dose conversion. The W_{air} value derived was on average 3.5% higher than in TRS-398. Figure 11 shows k_Q-values obtained by comparing ionization chambers with water calorimeters in scanned carbon ion beams. For two chamber types (PTW-30013 and IBA-FC65G) these data are obtained by directly comparing the response of the ionization chamber with that of the calorimeter in both the carbon ion beam and in the calibration beam. For the other chambers the data are obtained by indirectly comparing the response of the ionization chamber with that of the directly calibrated ionization chambers.

8. Non-standard fields

Nonstandard reference photon beams and small photon beams have been the subject of significant investigation over the past decade due to the introduction of new machines that cannot realize the standard reference fields and that are clinically used mostly in treatments involving small photon beams. The IAEA TRS-483 (Palmans *et al* 2017, 2018) covers recommendations on the determination of absorbed dose in nonstandard static fields (termed machine specific reference fields or *msr* fields) as well as on the determination of small photon field output factors. One possible calibration route in TRS-483 is the provision of the clinical user with calibration coefficients directly in the *msr* field. To enable this, some standards dosimetry laboratories and dosimetry research labs have been in the process of developing standards for absorbed dose to water in nonstandard and small fields.

Amongst the calorimetric methodologies discussed in this review both water and graphite calorimeter techniques can be adjusted to determine absorbed dose to water in nonstandard and small fields, although graphite calorimeters have distinct advantages over water calorimeters for fields of $3 \times 3\,cm^2$ and smaller. For water calorimetry in small fields, conductive heat-loss eventually becomes a correction with a significant uncertainty (de Prez 2010). Krauss (2007) investigated the application of water calorimetry on the calibration of reference ionization chambers in $5 \times 5\,cm^2$ and $10 \times 10\,cm^2$ with the conclusion that calibration and measurement of beam quality correction factors can be accurately determined for these field sizes. Krauss and Kapsch (2014) extended this work to fields of $3 \times 3\,cm^2$ with heat-loss corrections that became of the order of several percent and led to a slightly increased uncertainty on the absorbed dose to water. de Prez *et al* (2016, 2019a), Nusrat *et al* (2018), Krauss *et al* (2019) and D'Souza *et al* (2019) have constructed and successfully operated water calorimeters for MR-guided radiation therapy fields, paving the way for direct determination of ionization chamber calibrations in MR-guided radiation beams (de Prez 2019b). In a wholly numerical study, Schaarschmidt *et al* (2019) investigated the feasibility of using a water-based microfluidic calorimeter (MFC) for absolute dosimetry of small and composite high-energy photon fields by examining the water-equivalence and angular dependence of their design using a GEANT4 MC model. The proposed MFC detector prototype (figure 12) is composed of a vanadium oxide thin film thermistor with gold contacts situated on a silicon substrate with Si_3N_4 coating and covered by a 1 μm thick parylene layer. A water block with a total active volume of $500 \times 500 \times 100\,\mu m^3$ sits on top of the parylene layer.

Lye *et al* (2016) developed a graphite calorimeter-based absolute dosimetry technique in a dynamically scanned synchrotron radiotherapy beam in comparison with ionization chambers. Aside from these types of very specialized applications of graphite calorimetry, research on the application of graphite calorimetry to absorbed dose determination in nonstandard and small photon fields has been carried out following two approaches, (i) dose-area product (DAP)-based approach and (ii) probe calorimeter-based approach.

The DAP approach (Duane *et al* 2010, Ostrowsky *et al* 2010, Dufreneix *et al* 2016a, 2016b) is based on the measurement of absorbed dose in a graphite calorimeter, the disk-shaped core of which is significantly larger in size than the radiation field size. Although a DAP could be disseminated directly and allow direct calibration of DAP in small fields, this would require a reference dosimetry protocol by itself and the development of a transfer ionization chamber compatible with the calorimeter core size (Palmans and Vatnitsky 2016b). Therefore, the most practical dissemination method would be to determine absorbed dose to water at a point in a small field from the DAP standard by applying a profile correction factor. This methodology was also discussed in Sanchez-Doblado *et al* (2007); however, Dufreneix *et al* (2016b) found that a precise determination of a profile correction factor for a surface larger than the beam cross section still poses some challenges. Another issue for disseminating this quantity by calibrating large-area chambers is that their response is not laterally uniform (Kuess *et al* 2017).

Probe calorimeters represent the opposite approach in addressing the challenges of small field absolute dosimetry. Probe calorimeters are developed with the same functionality as small field ionization chambers. In this vein, relatively small calorimeters, such as the IMRT calorimeters relying on vacuum pump systems to minimize conductive and convective heat transfer, have been developed by Duane *et al* (2012) and Daures *et al* (2012). Renaud *et al* (2013, 2018) developed a more clinically-oriented version of a probe calorimeter called Aerrow by using aerogel insulation instead of vacuum gaps (see figure 13) and by performing isothermally operated signal measurements of the probe inserted in a water or solid phantom. Although the original version of Aerrow is not suitable for measurements in fields smaller than $2 \times 2\,\mathrm{cm}^2$, smaller versions of the calorimeter are under development and can be optimized to provide a small field absolute detector for field sizes smaller than $1 \times 1\,\mathrm{cm}^2$ (Côté *et al* 2019). Aerrow has also been demonstrated to provide accurate doses in 1.5 T MR fields in both liquid and solid phantoms (Renaud *et al* 2019).

9. Brachytherapy

Brachytherapy is the 'near' administration of radiation to a target whereby the radiation source (radionuclide or electronic radiation sources) is placed in proximity to the region of interest. This can be accomplished through interstitial, intracavitary, intraluminar, intravascular, intraoperative placement, or simply by surface application. Brachytherapy treatments are often categorized based on dose rate of the radiation source used: Low dose rate (LDR) brachytherapy uses sources with nominal dose rates of 0.4–2 Gy hr^{-1} at the dose specification point, while medium dose rate (MDR) brachytherapy uses sources with dose rates between 2–12 Gy hr^{-1}, and high dose rate (HDR) sources have a nominal dose rate exceeding 12 Gy hr^{-1} (clinical HDR sources typically have dose rates much greater than this). Currently, most brachytherapy treatments are carried out with HDR sources (Ir-192 being the most commonly used, followed by Co-60). The use of LDR sources (e.g. I-125, Pd-103, Au-198) is also common. Electronic brachytherapy with x-ray energies less than 300 kV generating potentials have also been used clinically (Rivard *et al* 2004, 2006).

With the advent of absorbed dose calorimetry in brachytherapy, current air kerma strength reference dosimetry protocols may perhaps one day be replaced by absorbed dose to water standards. At the very least, calorimetry can provide measured confirmation of and reduced uncertainty on the dose rate constants currently used in present air kerma strength standards. Often, this crucial parameter is based on MC calculation alone (Bovi *et al* 2009) or measurements with non-primary dosimeters. Tables 6 and 7 summarize the main characteristics and performance of recent Ir-192 HDR brachytherapy water and graphite calorimeters, respectively, as reported in the literature.

9.1. Water calorimetry

Given the dominance of Ir-192 HDR brachytherapy, most calorimetry work performed in HDR has been focused on this source. The first successful application of absorbed dose calorimetry in this area of study was published by Sarfehnia *et al* (2007). A 4 °C stagnant portable water calorimeter developed for external beam radiotherapy with a plane parallel vessel (Stewart 2007, Sarfehnia and Seuntjens 2010) was modified with the aim to demonstrate the feasibility of HDR brachytherapy water calorimetry. The results showed that although feasible, HDR brachytherapy water calorimetry presents several unique challenges. The choice of separation between the HDR source and the point of measurement (i.e. the thermistors) was shown to be a relatively important parameter to consider. Smaller separations result in larger signal to noise ratios, while also resulting in large relative positioning uncertainty. Furthermore, the heat generated inside the brachytherapy source due to self-attenuation of the radiation decay energy (i.e. source self-heating) is another major challenge in brachytherapy calorimetry. Here,

the source self-heating, which is often orders of magnitude greater than the radiation-induced temperature rises of interest, can reach the point of measurement through heat transfer and perturb the signal acquisition. Incorporation of specially designed heat sinks, and/or active cooling of the source can mitigate this issue.

Sarfehnia *et al* (2010b) demonstrated the feasibility of absolute dose rate measurement for Ir-192 HDR brachytherapy sources with water calorimetry with a combined standard uncertainty of 1.9% ($k = 1$). The dominant source of uncertainty (1.5%) was the non-linear temperature drifts that need to be accounted for analytically. The relatively large thermal drifts present inside the calorimeter were mostly due to source self-heating and sharp dose gradients. Under these conditions, despite the calorimeter being operated at 4 °C, convection was thought to play an important role in the overall heat transfer of the system, unlike in most external beam radiotherapy calorimetry. It was surmised that, provided enough time between successive measurements, the temperature gradients would equilibrate, thus reducing the magnitude of the heat transfer correction and the dominant source of uncertainty on the dose determination. At an estimated 0.85%, the next largest source of uncertainty was the source-to-detector positioning. With the source catheter kept under tension using a spring-loaded mechanism inside a stainless-steel tube, a 0.4% type A standard error on the mean was assigned based on more than 80 repeated calorimetric measurements.

In 2008, within the framework of the European Metrology Research Programme (EMRP), a three-year project towards 'Increasing cancer treatment efficacy using 3D brachytherapy' was established. This initiative resulted in a mandate towards the establishment of absorbed dose calorimetry-based standards for brachytherapy across several European standard laboratories (Ankerhold and Toni 2012). Bambynek *et al* (2009) of PTB performed HDR Ir-192 water calorimetry using a design akin to their high-energy photon standard. Source positioning accuracy was maintained using a stainless-steel needle that could be positioned at ±24 mm, +48 mm, and +60 mm from the thermistors contained within a parallel plate vessel (the effects of the needle were accounted for with MC calculations). Large non-linear temperature drifts were measured following irradiation, qualitatively similar to those recorded by the Sarfehnia group. These were somewhat minimized, however, by cooling the HDR source inside of a temperature-controlled lead block prior to insertion within the 4 °C stagnant water calorimeter phantom. With this setup, the absorbed dose to water was determined with a combined standard uncertainty of 0.9% after 100 repeated runs.

Most recently, de Pooter and de Prez (2010, 2012) reported on VSL's fully redesigned glass calorimetry vessel that was constructed to address the issues surrounding self-heating and positioning observed by Sarfehnia *et al* and Bambynek *et al* In their design, the source travels through the centre of the large vessel and is surrounding by aluminum heat sinks that help to remove the source self-heat. By positioning four thermistors on opposite sides of the source, the sensitivity of the system to source-to-detector positioning is greatly reduced. These two design features were incorporated to achieve an uncertainty of 2% at a source distance of 20 mm with fewer measurements than required by previous groups.

9.2. Graphite calorimetry

From the EMRP project mentioned in section 9.1, two ring-shaped graphite calorimeters were developed by NPL and the Italian National Agency for New Technologies, Energy and Sustainable Economic Development (ENEA). The ring-shaped cores in these systems reduce the uncertainty associated with distance positioning by an order of magnitude. These relatively new systems have since been used to experimentally determine HDR brachytherapy source dose rate constants with associated standard uncertainties of less than 2.5% (Selbach *et al* 2012).

In 2012, Guerra *et al* of the ENEA-INMRI presented their development of a primary standard-level graphite calorimeter designed to measure absorbed dose rate to graphite at 2.5 cm due to an Ir-192 HRD brachytherapy source (figure 14). The design consisted of three axially-symmetric graphite rings, each with rectangular cross sections and the source axis at the centre. The $2 \times 5\,\text{mm}^2$ core ring was built to be 50 mm in diameter. Surrounding the core are two layers of graphite, each of which are thermally insulated from one another by a 0.75 mm vacuum gap. The graphite ring assembly is housed in an acrylic cylinder, the top and bottom of which are sealed with vacuum-proof graphite discs. The graphite disc sealing the top contains a 2-mm diameter borehole extending to the centre of the graphite rings. The borehole is meant to accommodate the insertion of an Ir-192 source encased in an afterloading catheter. The entire graphite-acrylic assembly is designed to be embedded in a much larger graphite phantom to provide full scatter. Functionally, the calorimeter may be run either quasi-adiabatically or isothermally. Dose rate to water at 1 cm is determined from the corrected absorbed dose rate to the core, which is converted using a MC-calculated factor. With this setup, the relative combined standard uncertainty on the dose rate to water at 1 cm was estimated to be 1.4%, a marked improvement over the achievable accuracy of the reference air kerma rate methodology.

A similar graphite calorimetry system was developed at NPL by Sander *et al* (2012) as an absorbed dose to water standard for HDR brachytherapy sources. Like the ENEA calorimeter, the NPL HDR calorimeter was designed to measure the absorbed dose rate to a graphite core at 2.5 cm from the source. This quantity is then converted to a dose rate to water at 1 cm with the aid of a MC-calculated factor (Sander *et al* 2019). The NPL

system consists of a ring-shaped core, which is surrounded by a 1 mm vacuum gap and four cylindrical graphite bodies: two between the centrally-located source and the core, and two outer cylindrical blocks. Each graphite component can be thermally controlled to operate the system quasi adiabatically or isothermally. Both modes have been used to determine dose rate to water at 1 cm due to an Ir-192 source with a combined standard uncertainty of 1% or better. As is typically the case for primary standard-level graphite calorimeters, the dominant source of uncertainty comes from the calculation of the graphite-to—water dose conversion factor.

9.3. Other calorimetric techniques

The use of digital holographic interferometry to detect radiation-induced temperature changes affecting the refractive index of water was investigated by Cavan and Meyer (2014). They successfully showed the feasibility of interferometry for absorbed dose measurement in HDR brachytherapy with 30 μm spatial resolution and a standard deviation on the measurements of around 2%. Building on the work by Stump *et al* (2005) and Malin *et al* (2014, 2016) proposed a novel cryogenic calorimeter for measurement of emitted power from LDR brachytherapy sources. The measurements had an uncertainty ranging between 2.6% to 4.5% ($k = 1$).

10. Outlook

Calorimetry cemented itself as a critical measurement technique for the determination of absorbed dose in the metrology laboratories nearly half a century ago. In the early days, its development followed that of thermometry, manufacturing, radiochemistry, and digital technologies. As calorimetry has matured, greater strides have been made on the numerical side, driven by new radiation transport codes, finite element analysis software packages, and computer-aided design. While the core operating principles remain largely unchanged, the field has seen a relatively rapid rise and diversification of calorimeter designs in the past decade and a half, partly in response to the rise of new and varied radiotherapy modalities. This trend towards developing absorbed dose calorimeters purpose-built for use in user's clinical beam in a more agile manner is unlikely to end any time soon, as it is infeasible for NMIs to possess, or even have local access to every specialized and non-conventional radiotherapy delivery machine brought to market. In the long run, it will be more practical to perform at least some dose calibrations in the clinical environment using transfer standards, eliminating the uncertainty in the beam qualities used by NMIs and those used for clinical practice in hospitals. Absorbed dose calorimeter designs of tomorrow could therefore make use of emerging technologies aimed to reduce the overall footprint, operating complexity, and turnaround time of present systems; technologies such as printable electronics and non-contact sensors (e.g. micrometer-wide thermistors, Balčytis *et al* 2018; cleaved silica microspheres for interferometric temperature measurement, Gomes *et al* 2018), carbon allotrope and/or aerogel-based additive manufacturing (e.g. Tang *et al* (2018) and Campbell *et al* (2019)), and 3D micro-structuring techniques (e.g. spark assisted chemical engraving for the sub-millimeter machining of glass, Hof 2019). The trend of increasing clinical dose rates (e.g. FLASH-RT, Lempart *et al* 2019) will steadily ease the often-limiting sensitivity issue of absorbed dose calorimeters, and in fact, may one day replace conventional ion chambers in linac output monitoring systems given a lack of dose rate dependence. Continued development of absorbed dose calorimeters will see an increased industrial participation, some possibly by entrepreneurs, and interaction between NMIs and cross-disciplinary academic institutions (e.g. computer science, radiobiology, electrical and mechanical engineering), as well as high-tech manufacturing facilities ensuring the overall economic viability, scientific relevancy through diversification, and clinical impact of such endeavours.

Acknowledgments

We acknowledge partial support by the CREATE Medical Physics Research Training Network grant of the Natural Sciences and Engineering Research Council (NSERC) (#432290). This work was partially supported by NSERC (#RGPIN-2014-06475) and Canadian Institutes of Health Research (CIHR), grant FDN #333254.

References

Ackerly T, Crosbie J C, Fouras A, Sheard G J, Higgins S and Lewis R A 2011 High resolution optical calorimetry for synchrotron microbeam radiation therapy *J. Instrum.* **6** P03003

Alfonso R *et al*2008 A new formalism for reference dosimetry of small and nonstandard fields *Med. Phys.* **35** 5179–86

Almond P R, Biggs P J, Coursey B M, Hanson W F, Saiful Huq M, Nath R and Rogers D W O 1999 AAPM's TG-51 protocol for clinical reference dosimetry of high-energy photon and electron beams *Med. Phys.* **26** 1847–70

Al-Sulaiti L, Shipley D, Thomas R, Kacperek A, Regan P and Palmans H 2010 Water equivalence of various materials for clinical proton dosimetry by experiment and Monte Carlo simulation *Nucl. Instrum. Methods Phys. Res.* A **619** 344–7

Andreo P, Burns D T, Hohlfeld K, Huq M S, Kanai T, Laitano F, Smyth V and Vynckier S 2000 Absorbed dose determination in external beam radiotherapy: an international code of practice for dosimetry based on standards of absorbed dose to water *IAEA Technical Report Series* No. 398 (Vienna: IAEA)

Andreo P, Cunningham J C, Svensson H and Hohlfeld K 1997 *Absorbed Dose Determination in Photon and Electron Beams: an International Code of Practice IAEA TRS-277* 2nd edn (Vienna: International Atomic Energy Agency)
Andreo P, Cunningham J R, Hohlfeld K and Svensson H 1987 Absorbed dose determination in photon and electron beams: an international code of practice *IAEA Technical Report Series* 277 (Vienna: IAEA)
Ankerhold U and Toni M P 2012 European research projects for metrology in Brachytherapy and External Beam Cancer Therapy *Metrologia* **49** S167
Aukett R J, Burns J E, Greener A G, Harrison R M, Moretti C, Nahum A E and Rosser K E 2005 Addendum to the IPEMB code of practice for the determination of absorbed dose for x-rays below 300 kV generating potential (0.035 mm Al–4 mm Cu HVL) *Phys. Med. Biol.* **50** 2739–48
Bailey M and Shipley D R 2010 Measurement and modelling of electron beam profiles and calculation of graphite calorimeter gap corrections and ion chamber wall perturbation factors for the NPL Elekta Synergy linear accelerator *E2-CN-182 IDOS (Vienna, 9–12 November)*
Balčytis A, Ryu M, Juodkazis S and Morikawa J 2018 Micro-thermocouple on nano-membrane: thermometer for nanoscale measurements *Sci. Rep.* **8** 6324
Bambynek M, Krauss A and Selbach H J 2009 Calorimetric determination of absorbed dose to water for an ^{192}Ir HDR brachytherapy source in near-field geometry *IFMBE Proc. 25/XIII on Medical Physics and Biomedical Engineering* ed R Magjarevic (IUPESM: Munich) pp 89–92
Bancheri J, Seuntjens J, Sarfehnia A and Renaud J 2019 Density effects of silica aerogel insulation on the performance of a graphite probe calorimeter *Med. Phys.* **46** 1874–82
Bass G, Thomas R and Pearce J 2009 The calibration of parallel-plate electron ionization chambers at NPL for use with the IPEM 2003 code of practice: summary data *Phys. Med. Biol.* **54** N115–24
Baumgartner A, Steurer A, Tiefenböck W, Gabris F, Maringer F J, Kapsch R P and Stucki G 2010 Re-evaluation of correction factors of a primary standard graphite calorimeter in 60Co gamma ray beams as a basis for the appointment of the BEV absorbed dose rate to water reference value *Radiat. Protec. Dosi.* **145** 3–12
Becker J A, Green C B and Pearson G L 1946 Properties and uses of thermistors—thermally sensitive resistors *Elec. Eng. Transac.* **65** 711–25
Beigzadeh A M, Rashidian Vaziri M R and Ziaie F 2017 Modelling of a holographic interferometry-based calorimeter for radiation dosimetry *Nucl. Instrum. Methods Phys. Res.* A **864** 40–9
Berland V, Bregadze Y U, Vainberg S, Epiphanov L, Ermakov I, Isaev B, Kvasov V, Lutova N and Stavitsky R 1990 Determination of the absorbed dose of photon (1–50 MeV) and electron beams (5–50 MeV) in external radiation therapy National Code of Practice (in Russian) Izdatelstvo standartov: RD-50-691-89 (Moscow)
Berlyand V A and Bregadze Y I 1985 The national standard of the unit of absorbed dose rate of photon ionizing radiation *Izmeritel'naya Tekhnika* **4** 5–7 (in Russian)
Bernier J P, Skarsgard L D, Cormack D V and Johns H E 1956 A calorimetric determination of the energy required to produce an ion pair in air for cobalt-60 gamma-rays *Radiat. Res. Soc.* **5** 613–33
Bewley D K 1963 The measurement of locally absorbed dose of megavoltage x rays by means of a carbon calorimeter *Br. J. Radiol.* **36** 865–78
Bewley D K and Page B C 1972 Heat defect in carbon calorimeters for radiation dosimetry *Phys. Med. Biol.* **17** 584–5
Bewley D K, McCullough E C, Page B C and Sakata S 1972 Heat defect in tissue-equivalent radiation calorimeters *Phys. Med. Biol.* **17** 95–6
BIPM 2018 *Calibration and Measurement Capabilities Ionizing Radiation Dosimetry Branch* (Sèvres: BIPM) (cited 23 March 2018) (https://kcdb.bipm.org/AppendixC/search.asp?reload=1&branch=1)
Bourgouin A and McEwen M 2019 Determination of W_{air} in high-energy clinical electron beams using aluminium detectors No. *IAEA-CN—273* (Vienna: IDOS) (18–21 June)
Bourgouin A, Cojocaru C, Ross C and McEwen M 2019 Determination of Wair in high energy electron beams using graphite detectors *Med. Phys.* **46** 5195–5208
Boutillon M 1989 Gap correction for the calorimetric measurement of absorbed dose in graphite with a ^{60}Co beam *Phys. Med. Biol.* **34** 1809–21
Boutillon M, Coursey B M, Hohlfeld K, Owen B and Rogers D W O 1994 Comparison of primary water absorbed dose standards *Measurement Assurance in Dosimetry (Proc. Symp. Vienna)* p IAEA-SM-330/48
Bovi M *et al* 2009 Traceability to absorbed-dose-to-water primary standards in dosimetry of brachytherapy sources used for radiotherapy *Proc. XIX IMEKO World Congress Fundamental and Applied Metrology* pp 1674–9
Bradshaw A L 1965 Calorimetric measurement of absorbed dose with 15 MeV electrons *Phys. Med. Biol.* **10** 355–64
Brahme A 1984 Dosimetric precision requirements in radiation therapy *Acta Radiol. Oncol.* **23** 379–91
Brede H J 2004 *Darstellung der Wasserenergiedosis im kollimierten, gemischten Neutronen-Photonenfeld der PTB* (Braunschweig: PTB)
Brede H J, Greif K D, Hecker O, Heeg P, Heese J, Jones D T L, Kluge H and Schardt D 2006 Absorbed dose to water determination with ionization chamber dosimetry and calorimetry in restricted neutron, photon, proton, and heavy-ion radiation fields *Phys. Med. Biol.* **51** 3667–82
Brede H J, Hecker O and Hollnagel R 1997 Measurement of the heat defect in water and A-150 plastic for high-energy protons, deuterons and α-particles *Radiat. Prot. Dosim.* **70** 505–8
Brede H J, Hecker O and Hollnagel R 2000 An absorbed dose to water calorimeter for collimated radiation fields *Nucl. Instrum. Methods* A **455** 721–32
Burns D T, Picard S, Kessler C and Roger P 2014 Use of the BIPM calorimetric and ionometric standards in megavoltage photon beams to determine W_{air} and I_c *Phys. Med. Biol.* **59** 1353–65
Burns J E, Dale J W G, DuSautoy A R, Owen B and Pritchard D H 1988 New calibration service for high energy x-radiation at NPL (IAEA-SM-298/56) *Dosimetry in Radiotherapy* vol 2 (Vienna: IAEA) pp 125–32
Callendar H L 1910 The radio-balance. A thermoelectric balance for the absolute measurement of radiation, with applications to radium and its emanation *Proc. Phys. Soc. London* **23** 1–34
Campbell P, Baumann T F, Biener J, Chandrasekaran S, Oakdale J S and Worsley M A 2019 Conversion of additively manufactured organic polymer parts to substantially pure carbon *U.S. Patent Application* 10/196,270
Cavan A and Meyer J 2014 Digital holographic interferometry: a novel optical calorimetry technique for radiation dosimetry *Med. Phys.* **41** 022102
Chen-Mayer H and Tosh R 2006 SU-FF-T-392: simulating absorbed dose: finite element modeling of a stirred water calorimeter *Med. Phys.* **33** 2136
Chen-Mayer H and Tosh R 2008 NIST water calorimeter update: measured dose rate as a function of exposure time *Med. Phys.* **35** 2781–2
Chen-Mayer H, Tosh R and Malyarenko E 2007 Experimental observations of convection in an ultrasound thermometer for measuring absorbed dose to water *Med. Phys.* **34** 2453

Choi Y, Jeon K J, Park Y and Hyun S 2019 Numerical simulation of heat-loss compensated calorimeter *Int. J. Comput. Methods Exp. Meas.* **7** 285–96
Cojocaru C D, Stucki G, McEwen M R and Ross C K 2010 Determination of absorbed dose to water in megavoltage electron beams using a calorimeter-Fricke hybrid system No. *IAEA-CN—182 (Vienna: IDOS) (9–12 November)*
Cojocaru C, Muir B, McEwen M, Ross C, Klassen N and Marchington D 2016 Sci-Sat AM: radiation dosimetry and practical therapy solutions—09: stability of a water calorimetry system as a primary standard for absorbed dose to water *Med. Phys.* **43** 4960–1
Cole A, Almond P and Sinclair W K 1962 Calorimetric determination of absorbed dose *Symp. on Cobalt 60 Beam Therapy in Malignant Disease* ed S Krishnamurthi and V Shante (Madras: Associated Printers)
Côté B, Seuntjens J, Sarfehnia A and Renaud J 2019 Aerrow-mini: a probe-format graphite calorimeter for absolute dosimetry of small high-energy photon fields *CN-273 (18–21 June)* (Vienna: IDOS) Paper No 280
Csete I *et al* 2010 Comparison of air kerma and absorbed dose to water measurements of Co-60 radiation beams for radiotherapy *EUROMET Report* no 813 (EUROMET. RI (I)-K1 and EUROMET. RI (I)-K4) (Braunschweig: EUROMET)
Curie M 1904 Recherches sur les substances radioactives (2e éd.) *Doctorate Thesis* École Polytechnique, Paris
Curie P and Laborde A 1903 Sur la chaleur degagée spontanément par les sels de Radium *Comput. Rend. Acad. Sci.* **136** 673
D'Souza M, Nusrat H, Renaud J, Peterson G, Entezari N and Sarfehnia A 2019 Design and performance of an MR-compatible calorimeter *CN-273 (18–21 June)* (Vienna: IDOS) Paper No 287
Daures J and Ostrowsky A 2005 New constant-temperature mode for graphite calorimeter at LNE-LNHB *Phys. Med. Biol.* **50** 4035
Daures J and Ostrowsky A 2007 Test of the new GR9 graphite calorimeter Comparison with GR8 *Workshop on Absorbed Dose and Air Kerma Primary Standards (Paris, France, 9–11 May)*
Daures J, Ostrowsky A and Rapp B 2012 Small section graphite calorimeter (GR-10) at LNE-LNHB for measurements in small beams for IMRT *Metrologia* **49** S174–8
de Lavoisier A L and Laplace P S 1920 *Mémoire sur la Chaleur* (Paris: Gauthier-Villars)
de Pooter J L and de Prez L A 2010 Development of a water calorimeter as a primary standard for absorbed dose to water measurements for HDR brachytherapy sources *Proc. Int. Symp. on Standards, Applications and Quality Assurance in Medical Radiation Dosimetry No. IAEA-CN-182* p S25
de Prez L A 2010 Small field dosimetry in high energy photon beams based on water calorimetry *E2-CN-182 (9–12 November)* (Vienna: IDOS) Paper No 168
de Prez L A and de Pooter J A 2008 The new NMi orthovoltage x-rays absorbed dose to water primary standard based on water calorimetry *Phys. Med. Biol.* **53** 3531–42
de Prez L A and de Pooter J A 2012 Development of a water calorimeter as a primary standard for absorbed dose to water for HDR brachytherapy sources *Radiother. Oncol.* **103** S25
de Prez L, de Pooter J, Jansen B and Aalbers T 2016 A water calorimeter for on-site absorbed dose to water calibrations in ^{60}Co and MV-photon beams including MRI incorporated treatment equipment *Phys. Med. Biol.* **61** 5051–76
de Prez L, de Pooter J, Jansen B, Perik T and Wittkämper F 2018 Comparison of kQ factors measured with a water calorimeter in flattening filter free (FFF) and conventional flattening filter (cFF) photon beams *Phys. Med. Biol.* **63** 045023
de Prez L, de Pooter J, Jansen B, Woodings S, Wolthaus J, van Asselen B, van Soest T, Kok J and Raaymakers B 2019a Commissioning of a water calorimeter as a primary standard for absorbed dose to water in magnetic fields *Phys. Med. Biol.* **64** 035013
de Prez L, Woodings S, de Pooter J, van Asselen B, Wolthaus J, Jansen B and Raaymakers B 2019b Direct measurement of ion chamber correction factors k_Q and k_B in a 7 MV MRI-linac *Phys. Med. Biol.* **64** 105025
Delacroix S, Bridier A, Mazal A, Daures J, Ostrowsky A, Nauraye C, Kacperek A, Vynkier S, Brassard N and Habrand J L 1997 Proton dosimetry comparison involving ionometry and calorimetry *Int. J. Radiat. Oncol. Biol. Phys.* **37** 711–8
Delaunay F *et al* 2011 LNE-LNHB realization of the unit of the absorbed dose to water under IMRT conditions *Proc. PTB-Dos-56 (Braunschweig) Advanced Metrology for Cancer Therapy* p 12
Delaunay F, Gouriou J, Daures J, Le Roy M, Ostrowsky A, Rapp B and Sorel S 2014 New standards of absorbed dose to water under reference conditions by graphite calorimetry for ^{60}Co and high-energy x-rays and LNE-LNHB *Metrologia* **51** 552–62
Dewar J 1905 Studies with the liquid hydrogen and air calorimeters *Proc. R. Soc.* A **76** 325–33
Dewar J and Curie P 1904 Examen des gaz occlus ou dégagés par le bromure de radium *J. Phys. Theor. Appl.* **3** 193–4
Dombeck T W 2003 A possible water calorimeter based on radiation-induced conductivity *IEEE Trans. Nucl. Sci.* **50** 1153–60
Domen S R 1980 Absorbed dose water calorimeter *Med. Phys.* **7** 157–9
Domen S R 1982 An absorbed dose water calorimeter: theory, design and performance *J. Res. NBS* **87** 211–35
Domen S R 1987 Advances in calorimetry for radiation dosimetry *The Dosimetry of Ionizing Radiation* vol II, ed K R Kase *et al* (Orlando, FL: Academic) pp 245–320
Domen S R 1988 The role of water purity, convection and heat conduction in a new water calorimeter design *Proc. NRC Workshop on Water Calorimetry (NRC Report 29637)* ed C K Ross and N V Klassen (Ottawa: NRC) pp 85–91
Domen S R 1994 A sealed water calorimeter for measuring absorbed dose *NIST J. Res.* **99** 121–41
Domen S R and Lamperti P J 1974 A heat-loss-compensated calorimeter: theory, design, and performance *J. Res. Natl Bur. Stand. A Phys. Chem.* **78A** 595–610
Duane S, Aldehaybes M, Bailey M, Lee N D, Thomas C G and Palmans H 2012 An absorbed dose calorimeter for IMRT dosimetry *Metrologia* **49** S168–73
Duane S, Graber F and Thomas R A S 2010 Application of dose area product and DAP ratio to dosimetry in IMRT and small field external beam radiotherapy *E2-CN-182 (9–12 November)* (Vienna: IDOS) Paper No 222
Dufreneix S, Ostrowsky A, Le Roy M, Sommier L, Gouriou J, Delaunay F, Rapp B, Daures J and Bordy J-M 2016A Using a dose-area product for absolute measurements in small fields: a feasibility study *Phys. Med. Biol.* **61** 650–62
Dufreneix S, Ostrowsky A, Rapp B, Daures J and Bordy J M 2016B Accuracy of a dose-area product compared to an absorbed dose to water at a point in a 2 cm diameter field *Med. Phys.* **43** 4085–92
DuSautoy A R 1995 The UK primary standard calorimeter for photon-beam absorbed dose measurement *Phys. Med. Biol.* **41** 137–51
DuSautoy A R 1996 The UK primary standard calorimeter for photon-beam absorbed dose measurement *Phys. Med. Biol.* **41** 13
Elliot A J 1994 *Rate Constants and G-Values for the Simulation of the Radiolysis of Light Water over 0 °C–300 °C Range AECL* 11073 (Chalk River, ON: AECL)
Ellis C D and Wooster W A 1927 The average energy of disintegration of radium E *Proc. R. Soc.* A **117** 109–23
EURAMET 2017 *Biologically Weighted Quantities in Radiotherapy (BioQuaRT) SIB06 V2.1* (Braunschweig: PTB) (www.ptb.de/emrp/bioquart.html)
Fathi K 2016 Optimisation of a novel micro-calorimeter through Monte Carlo simulations and thermal analysis for use in particle therapy *PhD Thesis* University of Surrey, Guildford

Fathi K, Galer S, Kirkby K J, Palmans H and Nisbet A 2017 Coupling Monte Carlo simulations with thermal analysis for correcting microdosimetric spectra from a novel micro-calorimeter *Radiat. Phys. Chem.* **140** 406–11
Fleming D M and Glass W A 1969 Endothermic processes in tissue-equivalent plastic *Radiat. Res.* **37** 316–22
Flores-Martinez E, Malin M J and DeWerd L A 2016 Development and characterization of an interferometer for calorimeter-based absorbed dose to water measurements in a medical linear accelerator *Rev. Sci. Instrum.* **87** 114301
Gagnebin S, Twerenbold D, Pedroni E, Meer D, Zenklusen S and Bula C 2010 Experimental determination of the absorbed dose to water in a scanned proton beam using a water calorimeter and an ionization chamber *Nucl. Instrum. Methods Phys. Res.* B **268** 524–8
Galer S, Hao L, Gallop J, Palmans H, Kirkby K and Nisbet A 2010 Design concept for a novel SQUID-based microdosimeter *Radiat. Protect. Dosi.* **143** 427–31
Gallop J, Cox D and Hao L 2015 Nanobridge SQUIDs as calorimetric inductive particle detectors *Supercond. Sci. Technol.* **28** 084002
Geisselsoder J, Koepke K and Laughlin J S 1963 Calorimetric determination of absorbed dose and G_{Fe+++} of the Fricke dosimeter with 10 MeV and 20 MeV electrons *Radiat. Res.* **20** 423
Genna S and Laughlin J S 1955 Absolute calibration of a cobalt-60 gamma-ray beam *Radiology* **65** 394407
Genna S, Jaeger R G, Sanielevici A and Nagl J 1963 Quasi-adiabatic calorimeter for the direct determination of radiation dose in rads *At. Energy Rev.* **1** 239
Giesen U and Beck J 2014 New measurements of W-values for protons and alpha particles *Radiat. Prot. Dosim.* **161** 23–6
Giordanengo S and Palmans H 2018 Particle therapy: dose detectors, sensors and their applications *Med. Phys.* **45** e1051–72
Gomes A D, Silveira B, Dellith J, Becker M, Rothhard M, Bartelt H and Frazao O 2018 Cleaved silica microsphere for temperature measurement *IEEE Photonics Technol. Lett.* **30** 797–800
Goodwin P 1959 Calorimetric measurements on a cesium-137 teletherapy unit *Radiat. Res.* **10** 6
Goodwin P N 1960 Calorimetric measurements of bone/tissue absorption ratios *Radiology* **75** 112–5
Goodwin P N and Adair H W 1963 Calorimetric measurements of absorbed dose for low- and medium-kilovoltage x-rays *Radiology* **81** 320–3
Grimbergen T W M, Aalbers A H L, Mijneer B J, Seuntjens J, Thierens H, Van Dam J, Wittkamper F W and Zoetelief J 1997 Dosimetry of low and medium energy x-rays *NCS Report* 10 Nederlands Commission on Radiation Dosimetry, Task Group Uniformity Dosimetry Protocols, Delft
Guerra A S, Loreti S, Pimpinella M, Quini M, D'Arienzo M, Astefanoaei I, Caporali C, Bolzan C and Pagliari M 2012 A standard graphite calorimeter for dosimetry in brachytherapy with high dose rate 192-Ir sources *Metrologia* **49** S179
Gunn S R 1976 Radiometric calorimetry: a review *Nucl. Instrum. Methods* **135** 251–65
Hao L, Gallop J, MacFarlane J, Palmans H, Sander T and Duane S 2006 Low temperature calorimetry for ionising radiation dosimetry *NPL Report DEM TQD* 008 National Physical Laboratory, UK
Hashemian R, Foster C C, Murray K M, Landolt R L, Shaw S M and Bloch C 2003 Measurement of W/e for protons in air *39th Meeting of the Particle Therapy Co-Operative Group (San Francisco, CA)*
Henry W H 1977 The NRC absorbed dose to water calibration service *NRC Flyer* (Ottawa: NRC)
Hochanadel C J and Ghormley J A 1953 A calorimetric calibration of gamma-ray actinometers *J. Chem. Phys.* **21** 880–5
Hof L A 2019 High-precision micro-machining of glass for mass-personalization *Doctoral Thesis* Concordia University, Montreal
Hofmeester G H 1980 Calorimetric determination of absorbed dose in water for 1–25 MeV x-rays *Biomedical Dosimetry: Physical Aspects, Instrumentation, Calibration (Paris, France, 27–31 October)* (IAEA & WHO, IAEA-SM-249/56) pp 235–59
Hohlfeld K 1988 The standard DIN 6800: procedures for absorbed dose determination in radiology by the ionization method (IAEA-SM-298/31) *Dosimetry in Radiotherapy* vol **1** (Vienna: IAEA) pp 13–22
Holm K, Weber U, Simeonov Y, Brons S, Jäkel O, Ankerhold U, Greilich S and Krauss A 2019 Absorbed dose to water measurements in the SOBP of a clinical carbon ion beam using water calorimetry *CN-273 (18–21 June)* (Vienna: IDOS) Paper No 48
Hubley L, Roberts J, Meyer J, Moggré A and Marsh S 2019 Optical-radiation-calorimeter refinement by virtual-sensitivity analysis *Sensors* **19** 1167
Huntley R B, Wise K N and Boas J F 1999 The Australian standard of absorbed dose *Recent Advances in Calorimetric Absorbed Dose Standards (Proc. Workshop Teddington, UK, 1999) Rep. CIRM* vol **42** pp 37–46
Huq M S and Andreo P 2004 Advances in the determination of absorbed dose to water in clinical high-energy photon and electron beams using ionization chambers *Phys. Med. Biol.* **49** R49–104
IAEA 2000 Stored energy and the thermo-physical properties of graphite. In Irradiation damage in graphite due to fast neutrons in fission and fusion systems *IAEA Technical Document* 1154 International Atomic Energy Agency, Vienna, Austria
ICRU 1954 Recommendations of the International Commission of Radiological Units (ICRU) Seventh International Congress of Radiology, Copenhagen, July, 1953 *Br. J. Radiol.* **27** 243–5
ICRU 1998 Clinical proton dosimetry Part I: Beam production, beam delivery and measurement of absorbed dose *ICRU Report No* 59 International Commission on Radiation Units and Measurements, Bethesda MD
ICRU 2000 Nuclear data for neutron and proton radiotherapy and for radiation protection *ICRU Report* 63 ICRU, Bethesda, MD
ICRU 2007 Prescribing, recording, and reporting proton-beam therapy *ICRU Report No* 78 ICRU, Bethesda, MD
ICRU 2014 Prescribing, recording, and reporting of stereotactic treatments with small photon beams *ICRU Report* 91 ICRU, Bethesda, MD
ICRU 2016 Key data for ionizing-radiation dosimetry: Measurement standards and applications *ICRU Report No* 90 Oxford University Press, Oxford, UK
IPEM 2003 The IPEM code of practice for electron dosimetry for radiotherapy beams of initial energy from 4 to 25 MeV based on an absorbed dose to water calibration *Phys. Med. Biol.* **48** 2929–70
IPSM 1990 Code of Practice for high-energy photon therapy dosimetry based on the NPL absorbed dose calibration service *Phys. Med. Biol.* **35** 1355–60
Johns H E, Bernier J P and Cormack D V 1955 A direct measurement of the energy locally absorbed from a gamma-ray beam *Nature* **176** 560
Jones D T L 2006 The w-value in air for proton therapy beams *Rad. Phys. Chem.* **75** 541–50
Karger C P, Jäkel O, Palmans H and Kanai T 2010 Dosimetry for ion beam radiotherapy *Phys. Med. Biol.* **55** R193–234
Kase K R 1996 1975-present *A History of the Radiological Sciences—Radiation Physics* ed R A Gagliardi and P R Almond (Reston, VA: Radiology Centennial Inc.) pp 178–80
Kemp L A W E, Marsh A R S and Baker M J 1971 Pyrolitic graphite microcalorimeter for the measurement of x-ray absorbed dose *Nature* **230** 41–2
Kim I J, Kim B C, Kim J H, Chung J-P, Kim H M and Yi C-Y 2017 Building a graphite calorimetry system for dosimetry of therapeutic x-ray beams *Nucl. Eng. Technol.* **49** 810–6
Klassen N V and Ross C K 1991 Absorbed dose calorimetry using various aqueous solutions *Radiat. Phys. Chem.* **38** 95–104
Klassen N V and Ross C K 1997 Water calorimetry: The heat defect *J. Res. Natl Inst. Stand. Technol.* **102** 63–71

Klassen N V and Ross C K 2002 Water calorimetry: a correction to the heat defect calculations *J. Res. Natl Inst. Stand. Technol.* **107** 171–8
Krauss A 2006a The PTB water calorimeter for the absolute determination of absorbed dose to water in ^{60}Co radiation *Metrologia* **43** 259–72
Krauss A 2006b Heat conduction effects during the calorimetric determination of absorbed dose to water in radiotheray beams *Thermochim. Acta* **445** 126–32
Krauss A 2010 Calorimetric determination of k_Q factors for an NE2561 ionization chamber in 3 cm × 3 cm beams of 6 MV and 10 MV photons *No. IAEA-CN—182 (9–12 November)* (Vienna: IDOS)
Krauss A and Kapsch R P 2007 Calorimetric determination of *kQ* factors for NE 2561 and NE 2571 ionization chambers in 5 cm × 5 cm and 10 cm × 10 cm radiotherapy beams of 8 MV and 16 MV photons *Phys. Med. Biol.* **52** 6243
Krauss A and Kapsch R P 2014 Experimental determination of kQ factors for cylindrical ionization chambers in 10 cm × 10 cm and 3 cm × 3 cm photon beams from 4 MV to 25 MV *Phys. Med. Biol.* **59** 4227
Krauss A and Kapsch R-P 2018 Direct determination of kQ factors for cylindrical and plane-parallel ionization chambers in high-energy electron beams from 6 MeV to 20 MeV *Phys. Med. Biol.* **63** 035041
Krauss A and Roos M 1998 Heat conduction, convection and radiolysis of the H_2/O_2 system in the water absorbed dose calorimeter *Thermochin. acta* **310** 53–60
Krauss A, Ankerhold U, Spindeldreier K and Klüter S 2019 A water calorimeter for absorbed dose to water measurements in an MR-linac *CN-273 (18–21 June)* (Vienna: IDOS) Paper No 47
Krauss A, Büermann L, Kramer H M and Selbach H J 2012 Calorimetric determination of the absorbed dose to water for medium-energy x-rays with generating voltages from 70 to 280 kV *Phys. Med. Biol.* **57** 6245–68
Kubo H 1983 Absorbed dose determination with a water calorimeter in comparison with an ionization chamber *Phys. Med. Biol.* **28** 1391–9
Kubo H 1985 Water calorimetric determination of absorbed dose by a 280 kVp orthovoltage x-rays *Radiother. Oncol.* **4** 275–81
Kubo H and Brown D E 1984 Calorimeter dose determinations by direct voltage measurements on a Wheatstone-type bridge circuit *Phys. Med. Biol.* **29** 885–9
Kuess P, Böhlen T T, Lechner W, Elia A, Georg D and Palmans H 2017 Lateral response heterogeneity of Bragg peak ionization chambers for narrow-beam photon and proton dosimetry *Phys. Med. Biol.* **62** 9189–206
Laidler K J 1995 Thermodynamics *The World of Physical Chemistry* (Oxford: Oxford University Press)
Laughlin J S and Genna S 1956 Calorimetric methods *Radiation Dosimetry* ed G J Hine and G L Brownell (New York: Academic)pp 411–52
Lempart M, Blad B, Adrian G, Bäck S, Knöös T, Ceberg C and Petersson K 2019 Modifying a clinical linear accelerator for delivery of ultra-high dose rate irradiation *Radiother. Oncol.* **139** 40–5
Lourenço A *et al* 2017a Evaluation of the water-equivalence of plastic materials in low- and high-energy clinical proton beams *Phys. Med. Biol.* **62** 3883–901
Lourenço A, Thomas R, Bouchard H, Kacperek A, Vondracek V, Royle G and Palmans H 2016 Experimental and Monte Carlo studies of fluence corrections for graphite calorimetry in low- and high-energy clinical proton beams *Med. Phys.* **43** 4122–32
Lourenço A, Thomas R, Homer M, Bouchard H, Rossomme S, Renaud J, Kanai T, Royle G and Palmans H 2017b Fluence correction factor for graphite calorimetry in a clinical high-energy carbon-ion beam *Phys. Med. Biol.* **62** N134–46
Lühr A, Hansen D C, Jäkel O, Sobolevsky N and Bassler N 2011a Analytical expressions for water-to-air stopping-power ratios relevant for accurate dosimetry in particle therapy *Phys. Med. Biol.* **56** 2515–33
Lühr A, Hansen D C, Sobolevsky N, Palmans H, Rossomme S and Bassler N 2011b Fluence correction factors and stopping power ratios for clinical ion beams *Acta Oncol.* **50** 797–805
Lye E, Harty P D, Butler D J, Crosbie J C, Livingstone J, Poole C M, Ramanathan G, Wright T and Stevenson A W 2016 Absolute dosimetry on a dynamically scanned sample for synchrotron radiotherapy using graphite calorimetry and ionization chambers *Phys. Med. Biol.* **61** 4201–22
Lye J E, Butler D J, Franich R D, Harty P D, Oliver C P, Ramanathan G, Webb D V and Wright T 2013 Direct MC conversion of absorbed dose to graphite to absorbed dose to water for ^{60}Co radiation *Radiat. Protect. Dosi.* **155** 100–9
Ma C, Coffey C, Dewerd L A, Liu C, Nath R, Seltzer S and Seuntjens J 2001 AAPM protocol for 40–300 kV x-ray beam dosimetry in radiotherapy and radiobiology *Med. Phys.* **28** 868
MacDonald J C and Goodman L J 1982 Measurements of thermal defect for A-150 plastic *Phys. Med. Biol.* **27** 229–33
MacDonald J C, Laughlin J S and Freeman R E 1976 Portable tissue equivalent calorimeter *Med. Phys.* **3** 80–6
Malin M, Palmer B and DeWerd L 2014 WE-A-17A-02: BEST IN PHYSICS (THERAPY)—development of a calorimeter for the measurement of the power emitted from LDR brachytherapy sources *Med. Phys.* **41** 487
Malin M, Palmer B R and DeWerd L A 2016 Absolute measurement of LDR brachytherapy source emitted power: Instrument design and initial measurements *Med. Phys.* **43** 796–806
Malyarenko E V, Heyman J S, Chen-Mayer H H and Tosh R E 2010 Time-resolved radiation beam profiles in water obtained by ultrasonic tomography *Metrologia* **47** 208–18
Malyarenko E, Heyman J, Guy S, Chen-Mayer H and Tosh R 2006 Absorbed radiation dose measurement with a μK-resolution ultrasonic thermometer *Med. Phys.* **33** 2292
Mann W B 1954 Use of Callendar's 'radio-balance' for the measurement of the energy emission from radioactive sources *J. Res. Natl Bur. Stand.* **52** 177–84
Mattsson O 1984 Application of the water calorimeter, Fricke dosimeter and ionization chamber in clinical dosimetry *PhD Thesis* University of Goteburg
Mattsson O 1985 Comparison of water calorimetry and ionization chamber dosimetry in 100 and 200 kV x-ray beams CCEMRI (1)/85-15
McElhinney J, Zendle B and Domen S R 1957 Calorimetric determination of the power in a 1400 kv x-ray beam *Radiat. Res.* **67** 40
McEwen M 2010 Measurement of ionization chamber absorbed dose k_Q factors in megavoltage photon beams *Med. Phys.* **37** 2179–93
McEwen M 2015 Evaluation of alanine as a refrence dosimeter for therapy level dose comparisons in megavoltage electron beams *Metrologia* **52** 272–9
McEwen M R and Duane S 2000 A portable calorimeter for measuring absorbed dose in the radiotherapy clinic *Phys. Med. Biol.* **45** 3675–91
McEwen M R and DuSautoy A R 2009 Primary standards of absorbed dose for electron beams *Metrologia* **46** S59–79
McEwen M R and Ross C K 2007 Direct calibration of ionization chambers in linac electron beams *Proc. of Absorbed Dose and Air Kerma Primary Standards Workshop* (Paris: LNE-LNHB)
McEwen M R, DuSautoy A R and Williams A J 1998 The calibration of therapy level electron beam ionization chambers in terms of absorbed dose to water *Phys. Med. Biol.* **43** 2503–19
McEwen M R, Williams A J and DuSautoy A R 2001 Determination of absorbed dose calibration factors for therapy level electron beam ionization chambers *Phys. Med. Biol.* **46** 741–55
McEwen M, DeWerd L, Ibbott G, Followill D, Rogers D W, Seltzer S and Seuntjens J 2014 Addendum to the AAPM's TG-51 protocol for clinical reference dosimetry of high-energy photon beams *Med. Phys.* **41** 041501

Medin J 2010 Implementation of water calorimetry in a 180 MeV scanned pulsed proton beam including an experimental determination of k_Q for a Farmer chamber *Phys. Med. Biol.* **55** 3287–98
Medin J, Ross C K, Klassen N V, Palmans H, Grusell E and Grindborg J E 2006 Experimental determination of beam quality factors k_Q for two types of Farmer chambers in a 10 MV photon and 175 MeV proton beam *Phys. Med. Biol.* **51** 1503–21
Medin J, Ross C K, Stucki G, Klassen N V and Seuntjens J P 2004 Commissioning of an NRC-type sealed water calorimeter at METAS using ^{60}Co gamma-rays *Phys. Med. Biol.* **49** 4073
Milvy P, Barr N F, Geisselsoder J and Laughlin J S 1960 The calorimetric determination of absorbed dose *Trans. IX Congress of Radiology*, ed B Rajewsky (Stuttgart: Georg Thieme Verlag) pp 1348
Milvy P, Genna S, Barr N and Laughlin J S 1958 Calorimetric determination of local absorbed dose *Proc. Of the Second United National Int. Conf. on the Peaceful Uses of Atomic Energy (Geneva)* vol **21** pp 142–6
Morishita Y, Kato M, Takata N, Kurosawa T, Tanaka T and Saito N 2012 A standard for absorbed dose rate to water in a ^{60}Co field using a graphite calorimeter at the National Metrology Institute of Japan *Radiat. Protec. Dosimetry* **154** 331–9
Muir B and Rogers D W O 2010 Monte Carlo calculations of k_Q, the beam quality conversion factor *Med. Phys.* **37** 5939–50
Muir B R and Rogers D W O 2014 Monte Carlo calculations of electron beam quality conversion factors for several ion chamber types *Med. Phys.* **41** 111701
Muir B R, Cojocaru C D, McEwen M R and Ross C K 2017 Electron beam water calorimetry measurements to obtain beam quality conversion factors *Med. Phys.* **44** 5433–44
Muir B R, McEwen M R and Rogers D W O 2011 Measured and Monte Carlo calculated kQ factors: accuracy and comparison *Med. Phys.* **38** 4600–9
Myers I T, Le Blanc W H and Fleming D M 1961 Precision adiabatic gamma-ray calorimeter using thermistor thermometry *Rev. Sci. Instrum.* **32** 1013–5
Nicolau S, Sporea D G and Niculescu V I R 1999 Holographic interferometry in radiation dosimetry, microprocessor assisted *Proc. SPIE* **3745** 393–9
Nusrat H, Renaud J, Entezari N, Keller B, Seuntjens J and Sarfehnia A 2018 Absolute dosimetry using a novel portable water calorimeter design in MR-linac *Med. Phys.* **45** E629
Nutbrown R F, Duane S, Shipley D R and Thomas R A S 2002 Evaluation of factor to convert absorbed dose calibrations from graphite to water for the NPL high-energy photon calibration service *Phys. Med. Biol.* **47** 441
O'Brien D J, Roberts D A, Ibbott G S and Sawakuchi G O 2016 Reference dosimetry in magnetic fields: formalism and ionization chamber correction factors *Med. Phys.* **43** 4915–27
Osborne N S, Stimson H F and Ginnings D C 1939 Measurements of heat capacity and heat of vaporization of water in the range 0 °C to 100 °C *J. Res. Natl Bur. Stand.* **23** 197–259
Osinga-Blattermann J-M, Brons S, Greilich S, Jakel O and Krauss A 2017 Direct determination of k_Q for Farmer-type ionization chambers in a clinical scanned carbon ion beam using water calorimetry *Phys. Med. Biol.* **62** 2033–54
Ostrowsky A, Bordy J M, Daures J, de Carlan L and Delaunay F 2010 Dosimetry for small size beams such as IMRT and stereotactic radiotherapy: is the concept of the dose at a point still relevant? Proposal for a new methodology *E2-CN-182 (9–12 November)* (Vienna: IDOS) Paper No 264
Owen B and DuSautoy A R 1991 Correction for the effect of the gaps around the core of an absorbed dose graphite calorimeter in high energy photon radiation *Phys. Med. Biol.* **36** 1699–704
Palmans H 2011 *Dosimetry Proton Therapy Physics* ed H Paganetti (London: CRC Press) pp 191–219
Palmans H 2013 *Monte Carlo Calculations for Proton and Ion Beam Dosimetry Monte Carlo Applications in Radiation Therapy* ed F Verhaegen and J Seco (London: CRC Press) pp 185–99
Palmans H 2018a Dosimetry—detectors, relative dosimetry and microdosimetry *Proton Therapy Physics* 2nd edn, ed H Paganetti (London: CRC Press) pp 275–308
Palmans H 2018b Dosimetry—absolute and reference dosimetry *Proton Therapy Physics* 2nd edn, ed H Paganetti (London: CRC Press) pp 309–41
Palmans H and Vatnitsky S 2015 Dosimetry and beam calibration *Principles and Practice of Proton Beam Therapy* (*AAPM 2015 Summer School*) ed I J Das and H Paganetti (Madison, WI: Medical Physics Publishing) pp 317–51
Palmans H and Vatnitsky S 2016b Beam monitor calibration in scanned light-ion beams *Med. Phys.* **43** 5835–47
Palmans H and Vatnitsky S M 2016a Comment on 'Proton beam monitor chamber calibration' *Phys. Med. Biol.* **61** 6585–93
Palmans H, Al-Sulaiti L, Andreo P, Shipley D, Luhr A, Bassler N, Martinkovic J, Dobrovodsky J, Rossomme S and Thomas R A S 2013 Fluence correction factors for graphite calorimetry in a low-energy clinical proton beam: I. Analytical and Monte Carlo simulations *Phys. Med. Biol.* **58** 3481–99
Palmans H, Andreo P, Huq M S, Seuntjens J, Christaki K and Megzhefene A 2017 Dosimetry of small static fields used in external beam radiotherapy. An international code of practice for reference and relative dose determination *Technical Reports Series No.* 483 IAEA, Vienna
Palmans H, Andreo P, Huq M S, Seuntjens J, Christaki K and Megzhefene A 2018 Dosimetry of small static fields used in external photon beam radiotherapy: Summary of TRS-483, the IAEA–AAPM international Code of Practice for reference and relative dose determination *Med. Phys.* **45** e1123
Palmans H, Kacperek A and Jäkel O 2009 *Hadron dosimetry Clinical Dosimetry Measurements in Radiotherapy (AAPM 2009 Summer School)* ed W O Rogers and J Cygler (Madison, WI: Medical Physics Publishing)
Palmans H, Mondelaers W and Thierens H 1999 Absorbed dose beam quality correction factors k_Q for the NE2571 chamber in a 5 MV and a 10 MV photon beam *Phys. Med. Biol.* **44** 647
Palmans H, Seuntjens J, Verhaegen F, Denis J M, Vynckier S and Thierens H 1996 Water calorimetry and ionization chamber dosimetry in an 85 MeV clinical proton beam *Med. Phys.* **23** 643–50
Palmans H, Thomas R, Simon M, Duane S, Kacperek A, DuSautoy A and Verhaegen F 2004 A small-body portable graphite calorimeter for dosimetry in low-energy clinical proton beams *Phys. Med. Biol.* **49** 3737–49
Pazos I 2007 Chip-scale calorimetry for industrial dosimetry *Proc. 25th Annual CIRMS Conference: Past, Present, and Future* p 17
Perichon N, Rapp B, Denoziere M, Daures J, Ostrowsky A and Bordy J-M 2013 Comparison between absorbed dose to water standards established by water calorimetry at the LNE-LNHB and by application of international air-kerma based protocols for kilovoltage medium energy x-rays *Phys. Med. Biol.* **58** 2787–806
Petree B 1958 Absorbed dose calorimeters for high dose rate *Radiat. Res.* **2** 166
Petree B and Lamperti P 1967 A comparison of absorbed dose determinations in graphite by cavity ionization measurements and by calorimetry *J. Res. Natl Bur. Stand.* C **71** 19–27

Petree B and Ward B 1962 The construction of calorimeters for the measurement of absorbed dose *NBS Technical Note* 163 (Washington DC: National Bureau of Standards)
Petrie L M 2016 Characterisation of a graphite calorimeter in scanned proton beams *PhD Thesis* University of Surrey, Guildford
Petrie L M, Galer S, Shipley D and Palmans H 2017 Monte Carlo calculated correction factors for the NPL proton calorimeter *Radiat. Phys. Chem.* **140** 383–5
Picard S, Burns D T and Roger P 2007 Determination of the specific heat capacity of a graphite sample using absolute and differential methods *Metrologia* **44** 294
Picard S, Burns D T and Roger P 2009 Construction of an absorbed-dose graphite calorimeter *Report* (Sèvres: BIPM)
Picard S, Burns D T, Roger P, Allisy-Roberts P J, McEwen M R, Cojocaru C D and Ross C K 2010 Comparison of the standards for absorbed dose to water of the NRC and the BIPM for accelerator photon beams *Metrologia* **47** 1–22
Pieksma M W H, de Prez L A and Aalbers A H L 2002 The NMi water calorimeter *Proc. of the Int. Workshop on Recent Developments in Accurate Radiation Dosimetry (McGill University, Montreal), AAPM Proc. Series 13* (Madison, WI: Medical Physics Publishing) pp 108–19
Pinto M, Pimpinella M, Quini M, D'Arienzo M, Astefanoaei I, Loreti S and Guerra A S 2016 A graphite calorimeter for absolute measurements of absorbed dose to water: application in medium-energy x-ray filtered beams *Phys. Med. Biol.* **61** 1738
Pruit J S, Domen S R and Loevinger R 1981 The graphite calorimeter as a standard of absorbed dose for cobalt-60 gamma radiation *J. Res. NBS* **86** 495–502
Pruitt J S and Loevinger R 1982 The photon-fluence scaling theorem for Compton-scattered radiation *Med. Phys.* **9** 176–9
PTCOG 2019 *Particle Therapy Facilities in Clinical Operation* (Villigen: Particle Therapy Co-operative Group) (cited 16 April 2019) (www.ptcog.ch/index.php/facilities-in-operationsearch.asp?reload=1&branch=1)
Ramanathan G 2008 Possible heat defect in graphite *NPL Report AIR (RES)* 017 National Physical Laboratory, Teddington, UK
Ramanathan G, Harty P, Wright T, Lye J, Butler D, Webb D and Huntley R 2014 The Australian Primary Standard for absorbed dose to water (graphite calorimeter) *No.* TR—166 Australian Radiation Protection and Nuclear Safety Agency (ARPANSA)
Rapp B, Perichon N, Denoziere M, Daures J, Ostrowsky A and Bordy J M 2013 The LNE-LNHB water calorimeter for primary measurement of absorbed dose at low depth in water: application to medium-energy x-rays *Phys. Med. Biol.* **58** 2769–86
Redpath A T 1967 The dosimetry of low-energy x-rays *PhD Thesis* University of Edinburgh, Edinburgh
Reich H 1979 Choice of the measuring quantity for therapy-level dosemeters *Phys. Med. Biol.* **24** 895
Reid W B and Johns H E 1961 Measurement of absorbed dose with calorimeter and determination of W *Radiat. Res.* **14** 1
Renaud J, Marchington D, Seuntjens J and Sarfehnia A 2013 Development of a graphite probe calorimeter for absolute clinical dosimetry *Med. Phys.* **40** 020701
Renaud J, Rossomme S, Sarfehnia A, Vynckier S, Palmans H, Kacperek A and Seuntjens J 2016 Development and application of a water calorimeter for the absolute dosimetry of short-range particle beams *Phys. Med. Biol.* **61** 6602–19
Renaud J, Sarfehnia A, Bancheri J and Seuntjens J 2018 Aerrow: a probe-format graphite calorimeter for absolute dosimetry of high-energy photon beams in the clinical environment *Med. Phys.* **45** 414–28
Renaud J, Sarfehnia A, Bancheri J and Seuntjens J 2019 Calorimetry-based clinical reference dosimetry of a 1.5 T MRI-linac in water and solid phantoms using Aerrow *CN-273 (18–21 June)* (Vienna: IDOS) Paper No 229
Renaud J, Sarfehnia A, Marchant K, McEwen M, Ross C and Seuntjens J 2015 Direct measurement of electron beam quality conversion factors using water calorimetry *Med. Phys.* **42** 6357–68
Rivard M J, Coursey B M, DeWerd L A, Hanson W F, Saiful Huq M, Ibbott G S, Mitch M G, Nath R and Williamson J F 2004 Update of AAPM Task Group No. 43 Report: a revised AAPM protocol for brachytherapy dose calculations *Med. Phys.* **31** 633–74
Rivard M J, Davis S D, DeWerd L A, Rusch T W and Axelrod S 2006 Calculated and measured brachytherapy dosimetry parameters in water for the Xoft Axxent x-ray source: an electronic brachytherapy source *Med. Phys.* **33** 4020–32
Rogers D W O 1996 Fundamentals of dosimetry based on absorbed-dose standards *Teletherapy Physics, Present and Future* ed J R Palta and T R Mackie (Washington, DC: AAPM) pp 319–56
Romano F, Shipley D and Palmans H 2019 Monte Carlo correction factors for a proton calorimeter in clinical proton beams *CN-273 (18–21 June)* (Vienna: IDOS) Paper No 230
Roos M, Grosswendt B and Hohlfeld K 1992 An experimental method for determining the heat defect of water using total absorption of high-energy electrons *Metrologia* **29** 59–65
Ross C K and Klassen N V 1996 Water calorimetry for radiation dosimetry *Phys. Med. Biol.* **41** 1–29
Ross C K, Klassen N V and Smith G D 1984 The effects of various dissolved gases on the heat defect of water *Med. Phys.* **11** 653–8
Ross C K, Klassen N V, Shortt K R and Smith G D 1988 Water calorimetry, with emphasis on the heat defect *NRC Workshop on Water Calorimetry* (*NRC Report* 29637) ed C K Ross and N V Klassen (Ottawa: NRC) pp 69–75
Ross C K, McEwen M R and Klassen N V 2007 Vessel designs and correction factors for water calorimetry *Proc. of Absorbed Dose and Air Kerma Primary Standards Workshop* (Paris: LNE-LNHB)
Ross C K, Seuntjens J P, Klassen N V and Shortt K R 1999 The NRC sealed water calorimeter: correction factors and performance *Proc. of Workshop on Recent Advances in Calorimetric Absorbed Dose Standards, Report CIRM* vol 42 (Teddington, UK: NPL) pp 90–120
Rossomme S *et al* 2014a Reference dosimetry for light-ion beams based on graphite calorimetry *Radiat. Prot. Dosim.* **161** 92–5
Rossomme S, Palmans H, Shipley D, Thomas R, Lee N, Romano F, Cirrone P, Cuttone G, Bertrand D and Vynckier S 2013 Conversion from dose-to-graphite to dose-to-water in an 80 MeV A^{-1} carbon ion beam *Phys. Med. Biol.* **58** 5363–80
Rossomme S, Renaud J, Lee N, Thomas R, Sarfehnia A, Seuntjens J, Kacperek A, Bertrand D, Vynckier S and Palmans H 2014b SU-ET-408: determination of $k_{Q,Q0}$-factors from water and graphite calorimetry in a 60 MeV proton beam *Med. Phys.* **41** 319
Rump W 1927 Berichtigung zu der arbeit: Energiemessungen an Röntgenstrahlen *ZS. Phys.* **43** 254–95
Sakama M, Kanai T and Fukumura A 2008 Development of a portable graphite calorimeter for radiation dosimetry *Japan. J. Med. Phys.* **28** 1–14
Sakama M, Kanai T, Fukumura A and Abe K 2009 Evaluation of w values for carbon beams in air, using a graphite calorimeter *Phys. Med. Biol.* **54** 1111–30
Sanchez-Doblado F, Hartmann G H, Pena J, Rosello J V, Russiello G and Gonzalez-Castano D M 2007 A new method for output factor determination in MLC shaped narrow beams *Phys. Med.* **23** 58–66
Sander T, Duane S, Lee N D, Thomas C G, Owen P J, Bailey M and Palmans H 2012 NPL's new absorbed dose standard for the calibration of HDR 192Ir brachytherapy sources *Metrologia* **49** S184
Sander T, Subiel A and Galer S E 2019 Monte Carlo calculated conversion and correction factors for NPL's HDR ^{192}Ir brachytherapy absorbed dose standard and measured dose rate constant for the HDR ^{192}IR Flexisource *CN-273 (18–21 June)* (Vienna: IDOS) Paper No 104

Sarfehnia A 2010 Water calorimetry-based radiation dosimetry in iridium-192 brachytherapy and proton therapy *PhD Thesis* McGill University, Montreal
Sarfehnia A and Seuntjens J 2010 Development of a water calorimeter-based standard for absorbed dose to water in HDR ^{192}Ir brachytherapy *Med. Phys.* **37** 1914–23
Sarfehnia A, Clasie B, Chung E, Lu H M, Flanz J, Cascio E and Seuntjens J 2010a Direct absorbed dose to water determination based on water calorimetry in scanning proton beam delivery *Med. Phys.* **37** 3541–52
Sarfehnia A, Kawrakow I and Seuntjens J 2010b Direct measurement of absorbed dose to water in HDR ^{192}Ir brachytherapy: water calorimetry, ionization chamber, Gafchromic film, and TG-43 *Med. Phys.* **37** 1924–32
Sarfehnia A, Stewart K and Seuntjens J 2007 An absorbed dose to water standard for HDR Ir-192 brachytherapy sources based on water calorimetry: Numerical and experimental proof-of-principle *Med. Phys.* **34** 4957–61
Sassowsky M and Pedroni E 2005 On the feasibility of water calorimeter with scanner proton radiation *Phys. Med. Biol.* **50** 5381–400
Saul A and Wagner W 1989 A fundamental equation for water covering the range from the melting line to 1273 K at pressures up to 25 000 MPa *J. Phys. Chem. Ref. Data* **18** 1537–64
Schaarschmidt T, Kim Y K and Chung H T 2019 Feasibility study of a small field detector based on a microfluidic calorimeter *J. Korean Phys. Soc.* **74** 630–6
Schultz R J, Verhey L J, Saiful Huq M and Venkataramanan N 1992 Water calorimeter dosimetry for 160 MeV protons *Phys. Med. Biol.* **37** 947–53
Schulz R J and Venkataramanan N 1988 Measurement of the thermal defect of water exposed to protons in the range 0.9–40 MeV *Proc. NRC Workshop on Water Calorimetry NRC-29637* ed C K Ross and N V Klassen (Ottawa: NRC) pp 115–9
Schulz R J, Almond P R, Cunningham J R, Holt J G, Loevinger R, Suntharalingam N, Wright K A, Nath R and Lempert G D 1983 AAPM Task Group 21: a protocol for the determination of absorbed dose from high-energy photon and electron beams *Med. Phys.* **10** 741–71
Schulz R J, Venkataramanan N and Huq M S 1990 The thermal defect of A-150 plastic and graphite for low-energy protons *Phys. Med. Biol.* **35** 1563–74
Schulz R J, Wuu C S and Weinhous M S 1987 The direct determination of dose-to-water using a water calorimeter *Med. Phys.* **14** 790–6
Selbach H J, Bambynek M, Aubineau-Laniece I, Gabris F, Guerra A S, Toni M P, de Pooter J, Sander T and Schneider T 2012 Experimental determination of the dose rate constant for selected 125 I- and 192 Ir-brachytherapy sources *Metrologia* **49** S219
Seuntjens J 1991 Comparative study of ion chamber dosimetry and water calorimetry in medium energy x-ray beams *PhD Thesis* Gent University, Gent
Seuntjens J and Duane S 2009 Photon absorbed dose standards *Metrologia* **46** S39–58
Seuntjens J and Palmans H 1999 Correction factors and performance of a 4 C sealed water calorimeter *Phys. Med. Biol.* **44** 627–46
Seuntjens J P 1993 Correction factors for a cylindrical ionization chamber used in medium-energy x-ray beams *Phys. Med. Biol.* **38** 805–32
Seuntjens J P and DuSautoy A R 2003 Review of calorimeter-based absorbed dose to water standards *Standards and Codes of Practice in Medical Radiation Dosimetry: Proc. of an Int. Symp. IAEA-CN-96-3* (Vienna: IAEA)
Seuntjens J P, Ross C K, Shortt K R and Rogers D W O 2000a Absorbed-dose beam quality conversion factors for cylindrical chambers in high energy photon beams *Med. Phys.* **27** 2763–79
Seuntjens J, der Plaetsen A V, Laere K V and Thierens H 1994 Study of correction factors and the relative heat defect of a water calorimetric determination of absorbed dose to water *Proc. Int. Symp. On Measurement Assurance in Dosimetry (Vienna, Austria, 24–27 May)* (IAEA SM 330/6) pp 45–9
Seuntjens J, Kawrakow I and Ross C K 2000b Revisiting convective motion in stagnant water calorimeters operated at room temperature *Proc. of the NPL Workshop on Recent Advances in Calorimetric Absorbed Dose Standards* ed A J Williams and K E Rosser (Teddington: National Physical Laboratory) pp 103–19
Seuntjens J, Palmans H, Verhaegen F, Denis J-M, Vynckier S and Thierens H 1994 Water calorimetry for clinical proton beams *Proc. of a Calorimetry Workshop* (Teddington: National Physical Laboratory)
Seuntjens J, Thierens H, Poffijn A and Segaert O 1988 Water calorimetry in medium energy x-ray beams *Proc. NRC Workshop on Water Calorimetry (1988, Ottawa)* ed C K Ross and N V Klassen (Ottawa: NRC) pp 101–7
Shimizu M *et al* 2015 Comparison of the NMIJ and the ARPANSA stanards for absorbed dose to water in high-energy photon beams *Radiat. Protec. Dosi.* **164** 181–6
Shortt K R, Ross C K, Schneider M, Hohlfeld K, Roos M and Perroche A-M 1993 A comparison of absorbed dose standards for high-energy x-rays *Phys. Med. Biol.* **37** 1937–55
Siebers J V, Vatnitsky S M, Miller D W and Moyers M F 1995 Deduction of the air w value in a therapeutic proton beam *Phys. Med. Biol.* **40** 1339–56
Skarsgard L D, Bernier J P, Cormack D V and Johns H E 1957 Calorimetric determination of the ratio of energy absorption to ionization for 22 MeV X-rays *Radiat. Res.* **7** 217
Sorriaux J, Testa M, Paganetti H, Bertrand D, Lee J A, Palmans H, Vynckier S and Sterpin E 2017 Consistency in quality correction factors for ionization chamber dosimetry in scanned proton beam therapy *Med. Phys.* **44** 4919–27
Stahel E 1929 Bestimmung der bei Gamma- und Röntgenstrahlbehandlung vom gewebe absorbierten Energiemengen *Strahlentherapie* **33** 296–321
Stewart K J 2007 The development of new devices for accurate radiation dose measurement: a guarded liquid ionization chamber and an electron sealed water calorimeter *PhD Thesis* McGill University, Montreal (https://ui.adsabs.harvard.edu/#abs/2007PhDT.....416S/abstract)
Stump K E, DeWerd L A, Rudman D A and Schima S A 2005 Active radiometric calorimeter for absolute calibration of radioactive sources *Rev. Sci. Instrum.* **76** 033504
Rao S and Naik S B 1980 Graphite calorimeter in water phantom and calibration of ionization chambers in dose to water for ^{60}Co gamma radiation *Med. Phys.* **7** 196–201
Tang X, Zhou H, Cai Z, Cheng D, He P, Xie P, Zhang D and Fan T 2018 Generalized 3D printing of graphene-based mixed-dimensional hybrid aerogels *ACS Nano* **12** 3502–11
Thomas R, Lourenço A, Palmans H and Lee N 2019 Design, development and operation of a primary standard graphite calorimeter for proton beam dosimetry *CN-273 (18–21 June)* (Vienna: IDOS) Paper No 313
Tosh R and Bateman F 2019 Silicon photonic nanostructures for radiation calorimetry *Med. Phys.* **46** E433
Tosh R E and Chen-Mayer H H 2007 Frequency-domain characterization of heat conduction in sealed water calorimeters *Nucl. Instrum. Methods Phys. Res.* A **580** 594–7
Vatnitsky S M, Siebers J V and Miller D W 1995 Calorimetric determination of the absorbed dose-to-water beam quality correction factor k_Q for high-energy photon beams *Med. Phys.* **22** 1749–52

Verhey L J, Koehler A M, McDonald J C, Goitein M, Ma I C, Schneider R J and Wagner M 1979 The determination of absorbed dose in a proton beam for purposes of charged-particle radiation therapy *Radiat. Res.* **79** 34–54

Wang K, Jin S, Yang X, Zhang J, McEwen M, Cojocaru C and Ross C 2014 Development of a water calorimeter as the absorbed dose-to-water primary standard for China *Physica Medica* **30** e61

Witzani J, Duftschmid K E, Strachotinsky Ch and Leitner A 1984 A graphite absorbed-dose calorimeter in the quasi-isothermal mode of operation *Metrologia* **20** 73–9

Wright T, Lye J E, Ramanathan G, Harty P D, Oliver C, Webb D V and Butler D 2015 Direct calibration in megavoltage photon beams using Monte Carlo conversion factor: validation and clinical implementations *Phys. Med. Biol.* **60** 883–904